# DEVELOPMENT OF NOVEL BREAST CANCER-TARGETED SPECT IMAGING PEPTIDES BY PHAGE DISPLAY

---

A Dissertation Presented to the Faculty of the Graduate School
University of Missouri-Columbia

In Partial Fulfillment of the Requirements for the Degree
Doctor of Philosophy

---

by

BENJAMIN M. LARIMER

Dr. Susan L. Deutscher, Dissertation Supervisor

MAY 2014

# ACKNOWLEDGMENTS

I would like to begin by thanking my mentor, Sue. Sue has been instrumental in my development as a scientist, and I would not be the scientist I am today without her. She has generously shared her knowledge, patience and time, and for that I am truly grateful. I want to thank my committee for taking time to offer me advice and direction, and Dr. Jurisson in particular, who was kind enough to accept me as a trainee on her training grant.

Also I would like to thank everyone in the lab. Marie has not only provided me with advice and help in the lab, but she has also coached me through a marathon and is always there to give me advice in life. Jess has helped me critique all of my ideas and taught me useful skills in the lab, and even discussed a little friendly bit of politics. Mette has made the graduate student journey together with me and has provided great insight and shared in my graduate student frustrations.

I want to thank my family, especially my parents, for teaching me that hard work and perseverance pay off. They have never hesitated to do anything to help me, and I will never be able to repay them.

Most importantly, I want to thank my wife and best friend, Carissa. A common theme with me is that patience is required, and she has had endless patience. She knows when I need support and when I need to be pushed, and I can't thank her enough. I couldn't have asked for anything more.

# TABLE OF CONTENTS

Acknowledgements……ii

List of Tables and Figures……vii

List of Abbreviations……x

Abstract……xiv

Chapter 1

Introduction……1

Preface……3

Cancer……5

Breast Cancer……9

Detection……11

ERBB2……13

Phage Display……17

Peptides……21

Radiolabeling……23

Conclusion……25

Chapter 2

Affinity Maturation of an ERBB2-Targeted SPECT Imaging Peptide by *In Vivo* Phage Display……27

Introduction……..……...29

Materials and Methods…….…….…….33

Results…….…….……..39

Discussion…….…….……55

Conclusion…….……61

Acknowledgments…….…..……..63

Chapter 3

Identification of a Peptide from In Vivo Bacteriophage Display with Homology to EGFL6, A Candidate Tumor Vasculature Ligand in Breast Cancer…….……65

Introduction…….…...……67

Materials and Methods…….……..71

Results……...…….77

Discussion……..……89

Conclusion…….……95

Acknowledgments…….……...97

Chapter 4

Development of a Peptide by Phage Display for SPECT Imaging of Resistance-Susceptible Breast Cancer…….…….99

Introduction…….…….101

Methods and Materials…….…....107

Results…….….113

Discussion……....127

Conclusion……...133

Acknowledgments……..135

References……....137

Vita……...152

# LIST OF TABLES AND FIGURES

**Table**

2.1 $^{111}$In-DOTA-1-D03 Biodistribution…….……47

2.2 Radiolabeled Tumor:Organ Uptake Ratios…….…….48

2.3 Radiolabeled Peptide Kidney Retention……..52

**Figure**

2.1 Phage cell binding ratio of MDA-435/184A.1 cells……40

2.2 Phage ELISA for ERBB2 affinity…….……...42

2.3 Confocal microscopy of KCCYSL and 2$^{nd}$ generation peptides…….43

2.4 Radiolabeled cell binding of KCCYSL, 1-D03 and 3-G03…….45

2.5 $^{111}$In-DOTA-1-D03 and KCCYSL biodistribution comparison……..51

2.6 $^{111}$In-DOTA-1-D03 SPECT imaging……...53

3.1 EGFL6 and 3-G03 sequence comparison……....78

3.2 EGFL6 mRNA RT-PCR…….…80

3.3 EGFL6 protein immunoblot……..……...81

3.4 EGFL6 peptide confocal microscopy……...……...82

3.5 $^{111}$In-DOTA-EGFL6 cell binding……..……..84

3.6 $^{111}$In-DOTA-EGFL6 biodistribution……..……..85

3.7 $^{111}$In-DOTA-EGFL6 SPECT imaging…….……87

4.1 BT-474 i*n vivo* selection sequences and cell binding……114

4.2 Peptide 51 confocal microscopy and flow cytometry……116

4.3$^{111}$In-DOTA-51 cell binding competition assay……..…118

4.4 $^{111}$In-DOTA-51 biodistribution……..119

4.5 $^{111}$In-DOTA-51 SPECT imaging……...120

4.6 51 and V1 *in vitro* cell binding assays……...122

4.7 Truncated 51 Cell Binding Comparison……....125

# LIST OF ABBREVIATIONS

%ID/g: percent injected dose per gram

184A.1: normal breast epithelial cell line

ATP: adenosine triphosphate

BLAST: basic local alignment search tool

BSA: bovine serum albumin

BT-474: human breast cancer cell line

CB-TE2A: 4,11-bis(carboxymethyl)-1,4,8,11-

tetraazabicyclo[6.6.2]hexadecane

CHAPS: 3-[(3-cholamidopropyl)dimethylammonio]-1-propanesulfonate

cpIII: coat protein III

CPM: counts per minute

DMEM: Dulbelcco's modified eagle medium

DOTA: 1,4,7,10-tetraazacyclododecane-1,4,7,10-tetraacetic acid

DOTATOC: DOTA labeled octreotide

DTPA: diethylenetriaminepentaacetic acid

$EC_{50}$: half maximal effective concentration

EDTA: ethylenediaminetetraacetic acid

EGF: epidermal growth factor

EGFL6: epidermal growth factor-like ligand 6

EGFR: epidermal growth factor receptor

ELISA: enzyme-linked immunosorbent assay

FBS: fetal bovine serum

FDG: fluorodeoxyglucose

FI: fluorescent intensity

FMOC: fluorenylmethyloxycarbonyl

HEPES: 2-[4-(2-hydroxyethyl)piperazin-1-yl]ethanesulfonic acid

HER: human epidermal growth factor receptor

HYNIC: 6-hydrazinonicatonic acid

$IC_{50}$: half maximal inhibitory concentration

KeV: kiloelectron volt

LDS: lauryl doodecyl sulfate

MDA-MB-435: human breast cancer cell line

NOTA: 1,4,7-triazacyclononane-triacetic acid

Nrp1: Neuropilin-1

OV-CAR-3: human ovarian cancer cell line

PBS: phosphate buffered saline

PC-3: human prostate cancer cell line

PET: positron emission tomography

ReCCMSH: rhenium-cyclized melanocyte stimulating hormone peptide

RP HPLC: reverse phase-high pressure liquid chromatography

SAROTUP: scanner and relator of target unrelated peptides

SCID: severe combined immunodeficient

SDS PAGE: sodium dodecyl sulfate polyacrylaminde gel electrophoresis

SPECT: single photon emission computed tomography

TBS: Tris buffered saline

TBST: Tris buffered saline and tween-20

TETA: 1,4,8,11-tetraazacyclotetradecane-1,4,8,11-tetraacetic acid

TU/mL: tetracycline transducing units per milliliter

TU: tetracycline transducing units

# DEVELOPMENT OF NOVEL BREAST CANCER-TARGETED SPECT IMAGING PEPTIDES BY PHAGE DISPLAY

**By: Benjamin M. Larimer**

**Dr. Susan L. Deutscher. Dissertation Supervisor**

## ABSTRACT

Breast cancer is the second leading cause of cancer and cancer-related mortality among women. The survival rate of the malignancy declines considerably as the disease progresses, which necessitates rapid discovery and treatment [1]. Current methods of detection including mammograms and breast exams have been successful, however they have limitations [2]. Both technologies rely on the detection of a large mass of cells, which is not conducive to identifying aggressive cancer at an early stage. Additionally, these methodologies cannot provide biological information that may dictate the use of specific targeted therapies. As treatment for breast cancer continues to progress towards

therapies targeted at specific carcinogenic antigens, an ability to detect these antigens will improve patient care and prevent ineffective treatment regimens. Targeted imaging agents not only provide the ability to detect breast cancer, but also allow for simultaneous non-invasive characterization.

The choice of vector for a targeted imaging agent dictates its probability of success. Peptides provide several properties that make them a strong candidate for imaging agents. A peptide is easily synthesized, and can be conjugated in a site specific manner with a molecule allowing for *in vivo* detection. For breast cancer detection, the use of a bifunctional chelator allows for binding of a radiometal, which in turn permits clear signal detection at any depth of tissue [3, 4]. A radiolabeled peptide's small size provides it with rapid pharmacokinetics and enhanced tumor penetration, allowing for the peptide to quickly reach a tumor and bind, followed by clearance of unbound peptide [4]. This is especially important for radiolabeled imaging agents, as circulating radionuclide can deliver an unwanted dose of radiation to radiosensitive organs such as the bone [5]. A major drawback of a peptide is its moderate affinity, however the use of bacteriophage (phage) display technology allows for the selection of peptides with suitable affinity for *in vivo* imaging.

Phage display, pioneered by George P. Smith here at the University of Missouri, utilizes the tolerance of phage particles to the insertion of random peptides into its coat proteins in order to select a displayed peptide with a desired function [6]. A library of phage particles displaying random peptides can be created by altering the phage genome, allowing for production of up to $10^9$ unique peptide sequences. Phages can be incubated

with a t arget of i nterest, a nd onl y t hose bound recovered. R ecovered p hages a re t hen propagated in bacteria, creating an enriched subpopulation of phages displaying peptides with the desired function. Phage display can be used to select peptides with affinity for a purified a ntigen *in vitro* or a gainst w hole or gans or e ven t umors *in vivo* [7-9]. It is hypothesized in this dissertation that novel breast cancer targeted peptides can be selected by phage display for the purpose of imaging human breast tumors *in vivo*.

Development of a peptide for imaging purposes begins with the choice of a target. In b reast can cer, E RBB2 i s a h ighly i mportant t arget. E RBB2 i s a m ember o f t he epidermal growth factor re ceptor (E GFR/ERBB) fa mily of t ransmembrane r eceptors, consisting of E GFR, E RBB2, E RBB3 a nd E RBB4. E RBB2 i s ove r-expressed i n up t o 30% of breast cancers, and is expressed in almost 90% of all tumors [10]. Not only is the receptor h ighly p revalent, b ut its p resence co rrelates w ith i ncreased a ggressiveness an d decreased s urvival r ates [11]. S tability and pr omiscuity o f E RBB2 a ccount f or i ts unfavorable phenotype. The receptor does not have a ligand, and is instead constitutively receptive to dimerization and mitogenic signaling [12]. Additionally, a dimer containing ERBB2 is h ighly s table and tr ansmits s ignals lo nger th an o ther m embers o f its family. Fortunately, h ighly s table cel l s urface r eceptors ar e an i deal t arget f or i maging an d therapy. T wo cl inically approved therapeutic a ntibodies, t rastuzumab a nd pe rtuzumab, are u sed t o t reat b reast can cers w ith E RBB2 over-expression [13, 14] . W hile bot h therapies h ave i ncreased disease f ree survival r ates of pa tients w ith E RBB2 ove r-expressing b reast cancer by 5 m onths, r esistance to th e th erapy is common [15]. Currently, b reast can cers ar e s creened f or p otential t reatment w ith an ti-ERBB2 t herapy

by biopsy. Biopsies may not be ideal due to patient pain and use of *ex vivo* detection, which may not be physiologically relevant following removal from the patient [16]. A non-invasive imaging agent, such as a radiolabeled peptide, would provide real-time detection of ERBB2, and ensure that the antigen is biologically accessible to the therapeutic.

Previously, a 6 amino acid peptide (KCCYSL) was selected by *in vitro* phage display for ERBB2 extracellular domain binding, and was consequently demonstrated to image ERBB2 expressing tumors in mice [8, 17]. While tumor uptake was sufficient for SPECT imaging, non-target organ uptake posed potential problems for further studies. The biodistribution indicated the peptide would be better suited for clinical applications with a decreased non-target organ uptake. Here, it was hypothesized that a microlibrary displaying the KCCYSL peptide flanked by random amino acids at both the N- and C-termini could be used to select a peptide with improved *in vivo* tumor targeting and pharmacokinetics. This process, termed affinity maturation, is analogous to the development of high affinity antibodies by the immune system. The KCCYSL microlibrary was used for *in vivo* selections in mice bearing ERBB2-expressing MDA-MB-435 human breast xenografts. Selected phages and corresponding synthesized peptides were evaluated for ERBB2 and cancer cell binding affinity and specificity *in vitro*. Two target specific peptides were DOTA-conjugated and $^{111}$In-labeled for *in vivo* biodistribution and SPECT imaging analyses for comparison with previously published $^{111}$In-DOTA-KCCYSL.

Phage cell binding assays revealed 9 phages with higher breast carcinoma to breast epithelial cell binding ratios (>1.56) than KCCYSL phage. Two synthesized phage-displayed peptides, 1-D03 (MEGPSKCCYSLALSH) and 3-G03 (SGTKSKCCYSLRRSS), demonstrated affinities of 236 nM and 289 nM, respectively for recombinant ERBB2, compared to 351 nM for KCCYSL. The corresponding SPECT probes, $^{111}$In-DOTA-1-D03 and $^{111}$In-DOTA-3-G03 bound with higher affinity to target cancer cells than KCCYSL. $^{111}$In-DOTA-1-D03 also demonstrated higher specificity for MDA-MB-435 cells than $^{111}$In-DOTA-KCCYSL; however $^{111}$In-DOTA-3-G03 did not retain its specificity. Thus, $^{111}$In-DOTA-1-D03 was chosen for *in vivo* studies. Biodistribution analysis revealed tumor uptake of 0.661% ID/g at 1h post-injection for $^{111}$In-DOTA-1-D03, slightly less than $^{111}$In-DOTA-KCCYSL, which had a 0.78% ID/g uptake [17]. A slight diminishment of tumor uptake was accompanied by greater reduction in non-target accumulation, as $^{111}$In-DOTA-1-D03 displayed higher tumor to organ ratios for the heart (5.11 versus 3.54), lung (1.64 versus 0.95), muscle (13.62 versus 8.67), bone (7.6 versus 3.9) and brain (39 versus 26) than $^{111}$In-DOTA-KCCYSL. At 2 h post-injection, the rapid blood clearance of $^{111}$In-DOTA-1-D03 led to a higher tumor to blood ratio of 6.02:1 in comparison to 5.08:1 for $^{111}$In-DOTA-KCCYSL. Kidney retention of 1-D03 was 4.75% ID/g, a nearly 20 percent improvement over $^{111}$In-DOTA-KCCYSL (5.75% ID/g) [17]. SPECT imaging revealed tumor-specific uptake of $^{111}$In-DOTA-1-D03, which was confirmed by blocking with unlabeled 1-D03 peptide. These results demonstrate affinity maturation for enhanced pharmacokinetics of a targeted peptide can be accomplished by *in vivo* phage display. The combination of ERBB2-

specific binding, rapid clearance and tumor specificity may make 1-D03 a viable candidate for clinical imaging studies.

While it was successfully demonstrated that *in vivo* phage display can be used to improve the pharmacokinetics of a targeted peptide, selections can also be used to screen for peptides which mimic natural ligands. Phage display has been utilized to select peptides which mimic natural binding sequences, such as the integrin binding sequence RGD, and *in vivo* phage display has been verified to select tumor-avid phages, allowing for both techniques to be combined to screen for tumor-associated peptide mimetics [7, 18, 19]. Currently, *ex vivo* high throughput screening techniques are employed to identify genes, mRNA and proteins that are aberrantly expressed in tumor vasculature. One drawback of such techniques is the lack of functional *in vivo* data that they provide. While the primary focus of the *in vivo* KCCYSL microlibrary selection was affinity maturation, a secondary goal was to screen for peptides which mimic natural ligands associated with tumorigenesis. An *in vivo* selection for phage which targeted human breast cancer xenografts was hypothesized to identify peptides with homology to cancer-related proteins for *in vivo* imaging of breast cancer. For this, the recovered sequences of the KCCYSL microlibrary *in vivo* selection were screened for homology to known proteins, and one peptide, 3-G03, shared significant homology with a secreted protein termed EGFL6 [20]. *Egfl6* mRNA is upregulated in several transcriptomic analyses of human cancer biopsies, and the protein may play a role in tumor vascularization [21-23]. A crucial step in tumorigenesis is the recruitment of novel vasculature to the site of

neoplasia [24]. An imaging agent which could detect sites of neovascularization would greatly enhance discovery, understanding and treatment of tumorigenesis.

While EGFL6 has been identified in transcriptomic analyses, its protein expression in breast cancer had not been analyzed. In order to further characterize the role of the putative tumor vasculature protein EGFL6 in MDA-MB-435 human breast cancer, mRNA and protein expression was analyzed. *Egfl6* mRNA expression was demonstrated in MDA-MB-435 cells and EGFL6 was secreted from these cells, which was expected based on the predicted sequence and structure of the protein. Due to the homology of 3-G03 to EGFL6, an EGFL6 peptide was synthesized and shown to target MDA-MB-435 cells. EGFL6 peptide was conjugated to DOTA, radiolabeled with $^{111}$In and analyzed for biodistribution and tumor imaging capabilities. SPECT imaging revealed uptake of the peptide in a manner consistent with other tumor vasculature targeting agents [25, 26]. These results demonstrated that *in vivo* phage display provides a method for identifying potential peptide mimetics of tumor-associated proteins. Using *in vivo* phage display, a peptide with homology to EGFL6 was identified and successfully imaged tumor vasculature, indicating a role of EGFL6 in tumor vascularization. The EGFL6 peptide and full length protein should be investigated further for potential uses in detecting and preventing tumor vascularization.

The *in vivo* selection that identified both an improved ERBB2 targeting peptide and a novel EGFL6 peptide mimetic yielded important imaging peptides, however using these type of peptides for ERBB2 imaging and therapy can have limited utility. One of the major obstacles to successful treatment is the occurrence of resistance to targeted

therapies. Development of a peptide which can detect resistance-susceptible breast cancer prior to treatment would greatly aid in treatment of these malignancies. BT-474 human breast cancer cells overexpress ERBB2, in addition to another resistance susceptible target, the estrogen receptor. This cell line has been demonstrated to develop resistance to both trastuzumab, which targets ERBB2, and tamoxifen, which targets the estrogen receptor [27, 28]. A peptide which targets BT-474 human breast tumors may serve as a potential detection agent for therapy resistant breast cancer. Thus, it was proposed that an *in vivo* selection for tumor-avid phage in mice bearing BT-474 xenografts would identify targeted peptides for the resistance-susceptible breast cancer cell line.

A phage library displaying random 15 amino acids from the tip of coat protein III was used for four rounds of *in vivo* selection in BT-474 xenografted mice. Following selection, 14 phages were identified for cell binding assays due to the presence of multiple copies of the full length or partial sequence in the output of the selection, as this is often an indicator of a successfully selected phage. One phage, clone 51, had vastly superior BT-474 human breast cancer binding, and was synthesized for analysis as a peptide. The peptide, 51 (ATWLPVPVVFMASA), bound BT-474 cells specifically with an $EC_{50}$ = 2.33 μM, an affinity previously demonstrated to allow for tumor imaging *in vivo [29]*. Peptide 51 was therefore radiolabeled with $^{111}$In, its retained affinity confirmed *in vitro* and examined for biodistribution and SPECT imaging in BT-474 tumor-bearing mice. While tumor uptake was moderate at 0.11% ID/g, SPECT imaging revealed that the peptide was highly concentrated in the area surrounding the tumor, in a similar manner to vasculature targeted RGD peptides and anti-VEGF antibodies [25, 26]. Since vasculature

binding can be mediated by as few as three amino acids and phage display has been previously been established to target tumor vasculature, known vasculature targeting peptides reported in the literature were further examined for partial sequence identity to peptide 51.

It was discovered that the N-terminal 5 amino acids of 51 were identical to the N-terminal 5 amino acids of a peptide, V1 (ATWLPPR), shown to bind the tumor vasculature receptor Nrp1 [30]. Nrp1 is expressed in both tumor vasculature and BT-474 cells [31], therefore it was a possible target of peptide 51. Surprisingly, only full length 51 bound both BT-474 and HUVEC endothelial cells, while V1 only bound HUVEC cells. Additionally, comparison of the *in vivo* properties of peptide 51 and V1 revealed that the peptides exhibited different biodistributions and V1 was unable to differentiate tumor tissue by SPECT imaging [32]. The results suggested peptide 51 binding was not mediated by its shared sequence with V1. This was consistent with previous characterization of the V1 peptide, which determined that the critical binding sequence was the C-terminal LPPR [33]. Finally, it was determined that neither an N-terminal nor C-terminal truncated form of peptide 51 could bind to BT-474 cells with the same high affinity and specificity of the full length peptide. These results indicate that peptide 51 is a novel tumor imaging agent, capable of imaging resistance susceptible breast cancer xenografts in mice.

The work presented in this dissertation provides evidence of the utility of phage display for the discovery of novel breast cancer targeted peptides. Phage display can be used to select second generation peptides with improved pharmacokinetics, as

demonstrated with peptide 1-D03 [19]. Additionally, *in vivo* selection allows for a high-throughput screening of peptides which may mimic natural ligands. Discovery of a peptide homologous to EGFL6 and subsequent confirmation of EGFL6 expression and tumor vasculature targeting of the peptide has provided the foundation for future studies examining the role of EGFL6 in tumor vascularization and the ability of the EGFL6 peptide to detect neovascularization. Lastly, phage display can be used to address a disease phenotype, such as therapy resistant breast cancer. *In vivo* phage display selected a peptide which was able to bind BT-474 cells with good affinity *in* vitro and specifically target and image BT-474 human breast cancer xenografts *in vivo*. Development of three targeting peptides, while significant, is only a small fraction of what can be accomplished by phage display.

# CHAPTER 1

## INTRODUCTION

# Preface

From ancient Egyptian surgery scrolls, through Hippocrates, to Paul Ehrlich's "magic bullet", science has attempted to elucidate, describe, and eliminate cancer. With more than 1.5 million cases of cancer diagnosed each year, the prevalence of cancer is one of society's greatest burdens (1). One of the keys to eliminating the disease is through a thorough understanding of its induction and progression. As knowledge has progressed, cancers of various organs have been disseminated. Carcinomas of the breast, in particular, are one of the most common cancers among women, owing to the unique biology of the organ (2). Understanding the transformation from healthy to malignant tissue and the identifiable markers that accompany this transformation have allowed for more precise identification and treatment of cancer. Incremental steps have improved detection and subsequently treatment, enhancing outcome. Surgical removal, non-invasive imaging, radiation, chemotherapeutics and targeted therapy have each advanced quality of care (3). It is the combination of these established techniques, along with the incorporation of a new wave of imaging and therapeutic tools that will push the boundaries of cancer treatment.

# Cancer

Cancer occurs as a progression of a cell with a defined paradigm for replication and apoptosis to an unmitigated multiplying of a select group of cells, which lack the controlled growth, programmed death, or a combination of both, present in surrounding tissues. The external causes of cancer, which include but are not limited to chemicals, radiation, and viral infection, introduce a mutation in the cell's genetic code. Chemical and radiation induced genetic damage is random, and accumulates throughout the lifetime of an individual (4). Although single mutations may be phenotypically silent, a series of mutations may cause abnormal function of a gene or set of genes. The mutation of a gene that is critical to the regulation of cell division, growth or death can be the trigger point for carcinogenesis (5). Viral infection, on the other hand, can introduce a malignant gene to a normal cell, inducing cancer (6). Human papillomavirus, which has been detected in 99.7% of cervical cancers, produces two oncoproteins, E6 and E7 which stimulate cell growth and eliminate growth-related controls (7). Viral-mediated production of these proteins is enough to drive cancer initiation. Whether the infection or mutation leads to an over-expression of a factor causing cell growth, or the loss of a control point inhibiting it, the end result is a population of cells multiplying outside of the normal developmental controls. In order to detect and eliminate cancer, it is important to identify the inherited phenotypic changes that lead to cancer initiation and progression.

Maintenance of a population of cells is an ongoing balance of replication and cell death. Older cells are systematically destroyed, in a process known as apoptosis, while

new cells are created to replace them (8). In addition to maintenance, tissues must respond to biological changes such as puberty, pregnancy or injury. A complex network of receptors activated and repressed by local and systematic ligands acts as a careful coordinator of normal physiological processes. Tumorigenesis occurs when one or more of the processes no longer functions as it was intended. One of the methods of cancer formation is through the loss of apoptosis. Proteins such as p53, which regulates the production of proteins that are involved in a number of cellular viability checkpoints, may be altered or completely absent, resulting in an inability to produce controlled cell death (9). Growth factors, which typically function during development and wound repair, can be equally carcinogenic if uncontrolled. For example, over-expression of a ligand such as epidermal growth factor (EGF), or its receptor EGFR, often results in malignancy (10). Over-expression of growth factors leads to constitutive mitogenesis, however this is only the first step in the progression of cancer. In addition to mitogenic signaling, continuous uncontrolled growth can only be sustained after the tumor reaches 1-2 mm in diameter through angiogenesis (11). As a group of tumor cells proliferate, the existing vasculature is no longer sufficient to support new growth (12). In order to continue to proliferate, the cells must release factors which promote growth of new blood vessels, creating a new supply line of nutrients for further growth (13). However, rapid and disordered growth of a tumor affects the process of vascularization, with the end result being a disorganized and permeable set of blood vessels (14). Uncontrolled growth, improper vasculature and a poor lymphatic system ultimately contribute to a tumor environment that is hypoxic, acidic and partially necrotic. In this manner the tumor

progresses until it meets the basement membrane, where it encounters a new level of resistance.

As the tumor grows to approach the basement membrane, it must pass through the extracellular matrix and into the stroma, in a process known as invasion (15). After invasion, it is has been demonstrated that only select subpopulations of cells will have the ability to circumvent the host immune system, implant in a secondary tissue, invade and establish a new tumor microenvironment (16). In fact, for most cancer patients, it is the progression of metastatic lesions that will ultimately lead to death (17). Elucidation of metastatic properties of these subpopulations is, therefore, an intense focus of research. The "seed and soil" hypothesis, first postulated by Stephen Paget in 1889, states a tumor cell may implant in a tissue based on the characteristics of its tissue of origin (the seed) and its destination tissue (the soil) (18). Evidence to support the hypothesis has continued to collect, and it is generally regarded today that the tissue of origin is an important factor in assessing treatment options (19). Although there is certainly overlap in malignant development mechanisms, it is important to place emphasis on a specific tissue, due to shared characteristics of tissue-related cells among individual cancers. The scope of this dissertation focuses on breast cancer and proteins, such as ERBB2 and EGFL6, defined in the proceeding chapters, which contribute to the growth and metastasis of the disease.

# Breast Cancer

Breast cancer is the number one cause of cancer among women, and the second leading cause of cancer-related death. Although it is not known why breast tissue is most susceptible to malignant transformation, its extensive use of growth factors and hormones is thought to be a possible link to increased cancer risk (20). Approximately one in eight women will develop breast cancer in her lifetime, one in 25 before age 60, and one in 200 before they are 40. The relatively high probability of developing breast cancer before the age of 60 is compounded by the fact that breast cancer is the most deadly form of carcinoma in women of this age group (1). The high mortality could be due to the increased probability of aggressive, invasive tumors in young women (21). To understand the increased risks of cancer development and progression, it is important to examine the known biological functions of the breast and the conditions which facilitate malignant development.

Although breast tissue formation initially occurs during fetal development, the tissues undergo several postnatal changes. Remodeling of breast tissue during puberty and again following pregnancy are elicited by growth hormones, such as estrogen, and their corresponding receptors (2). Deregulated estrogen signaling has long been implicated in cancer progression, and clinically approved therapies that antagonize estrogen function, such as tamoxifen, can suppress estrogen driven cancers (22). However, the presence of estrogen receptors in the breast cannot solely account for the increased frequency of breast cancer development, as estrogen acts in a systematic

manner and plays a role in the development of several reproductive and non-reproductive tissues besides the breast. In addition to estrogen related transformation, the EGFR family of receptors (ERBB) has been shown to play a critical role in mammary maturation (23). The role of the ERBB proteins in development has been studied through tissue specific knockouts in developing mouse mammary glands. Loss of any of the ERBB family members results in incomplete mammary development, ranging from incomplete ductal growth to impaired lactation (24). Like the estrogen receptor, improper signaling of the ERBB family is also a driver of breast cancer. Although malignant transformation of breast tissue is a complex series of events undoubtedly involving many proteins, evidence has supported a major role of both the estrogen receptor and the epidermal growth factor receptors in breast cancer (2, 25). In fact, therapies targeting the estrogen receptor and ERBB family member, ERBB2, have both been successful as targeted breast cancer treatments (22, 26). It is clear that understanding the biological functions that drive breast tissue growth has proven valuable in later identifying the possible mechanisms of carcinogenesis. Additionally, detection of aberrant expression of receptors found solely or in higher amounts on the surface of cancer cells can be used to characterize and direct a course of treatment for individualized breast cancers.

## Breast Cancer Detection

Knowledge of the biological development of breast cancer can be used to advance detection capabilities. Early detection is paramount in breast cancer treatment, as survival drops precipitously following progression of the disease (27). Current detection methods are largely based on breast exams and mammography. Both methods of detection provide a means to non-invasively detect tumors based on abnormal masses of cells. Although both methods are valuable tools, they have at least two limitations. The first is both technologies are biased towards the detection of slower growing, less aggressive tumors. The bias originates from the need for a significant mass of tumor cells for diagnosis. The window of opportunity for detection is much longer for a slow growing mass, whereas aggressive tumors may be undetectable at the time of screening, but progress to an advanced stage before a subsequent test. Therefore mammograms and breast exams are excellent detection methods, but will do little to detect the most dangerous malignancies at an early stage. In addition to an inherent growth rate bias, the effectiveness of mammography and breast exams is diminished in younger or denser breast tissue (28). Unfortunately, the subpopulation of women who are most prone to aggressive tumor growth is also younger women or women with dense breast tissue (1). The second detriment of breast exams and mammograms is that they do not provide any information about the biochemical nature of the tumors. The expression pattern of specific proteins, or biomarkers, is crucial to determining susceptibility to different therapeutic approaches. Current methodologies simply identify the presence of a mass, which must be

characterized by other assays. While breast exams and mammograms are valuable tools in breast cancer diagnosis, identification and detection of cancer specific proteins can serve to simultaneously detect and characterize aggressive malignancies, at an earlier point than traditional methods.

In addition to detection by physical characteristics, biochemical diagnosis can also be achieved. A widespread non-invasive cancer imaging technique is the use of $^{18}$fluorine ($^{18}$F)-labeled deoxyglucose (FDG). It is thought that the enhanced growth and, by necessity, metabolism of cancer cells promotes enhanced uptake of the radiolabeled glucose analog used to diagnose many carcinomas (29). Unable to be broken down or released due to its altered chemical structure, the imaging agent collects in tissues of high glucose metabolism, e.g. tumor and brain. Concentration of FDG permits identification of small tumors and metastases through detection of a positron emitted during the decay of radioactive $^{18}$F. The success of high resolution imaging provided by FDG-guided positron emission tomography (PET) has led to many more attempts to identify cancer based on concentration of an imaging agent through delivery facilitated by differences between cancer cells and their surrounding normal tissues (30-32). However not all cancers have increased FDG uptake. An additional method of detecting cancer cells is through the differential expression of proteins and other molecules associated with the biological processes necessary for tumor development. These cancer-related molecules, termed biomarkers, provide a target for an imaging agent. Detection of biomarkers in cancer provides a twofold advantage. Not only are cancers detected at early stages and possibly before current methods of detection, but a key biological property is identified.

## ERBB2

In order to accomplish biomarker characterization, proteins must be identified that play a significant role in malignant transformation, while being absent or expressed at lower levels in surrounding tissue. In the breast, the ERBB family of tyrosine kinases is essential for normal development (23). Deregulation of the receptors, however, has been implicated in the development of breast cancer (33). The family consists of four members: EGFR (HER1), ERBB2 (HER2/neu), ERBB3 (HER3) and ERBB4 (HER4). The structure of each receptor includes an extracellular ligand binding domain, a single pass transmembrane domain, and an intracellular tyrosine kinase domain. Interactions in the extracellular domain drive signaling through homo- and heterodimerization with another EGFR family receptor (34). A typical EGFR receptor, in the absence of ligand, remains in a folded, closed state with a ligand binding portion of the extracellular domain exposed. Ligand binding by the receptor induces a conformational change in the external domain, exposing a dimerization arm that is buried in the non-liganded state. Two receptors in the active conformation can adjoin via interactions between dimerization arms, unlocking the potential for tyrosine kinase activity within the intracellular domain. Unlike the extracellular domain, intracellular domain dimerization is asymmetrical. After dimerization, the C-terminal tail of one receptor exposes an ATP binding pocket on its partner receptor. Bound ATP catalyzes transphosphorylation of specific tyrosine residues, with phosphorylation patterns dependant on activating ligands. Phosphorylated tyrosine residues serve as docking points for adaptor proteins used to initiate downstream

signaling. Through various combinations of ligand and receptor expression, cells are able to facilitate a vast array of responses using the ERBB signaling pathways.

Although canonical ERBB family signaling pathways require a ligand, ERBB2 is unique within the family because it has no known ligand. Crystallographic studies indicate that this is most likely due to the fact that it remains fixed in the open, active state with its dimerization domain (domain II) exposed (35). Due to its constitutive openness to dimerization, the receptor is the primary binding partner for all of the EGFR family (36). Additionally, dimers containing ERBB2 have several oncogenic characteristics. Each pair remains at the cell surface longer than non-ERBB2 containing dimers, allowing for increased signaling. Even after endocytosis of an ERBB2 heterodimer, the receptors are more likely to be recycled to the cell surface to continue signaling. In addition, the binding partner of ERBB2 retains its ligand longer than a dimer with no ERBB2. The enhanced formation, stability and signaling potency of ERBB2 dimers has made targeting the receptor an effective method of controlling breast cancers that overexpress ERBB2.

Two humanized, monoclonal antibodies, trastuzumab and pertuzumab, have been approved by the Food and Drug Administration for the treatment of ERBB2-positive breast cancers (26, 37). Trastuzumab binds to a portion of ERBB2 near the cell wall, and it is thought to act through a combination of steric hindrance and antibody-directed cellular cytotoxicity (35). Pertuzumab binds ERBB2 in its dimerization domain, effectively inhibiting dimerization with other family members (38). Both receptors have altered the prognosis of ERBB2-positive breast cancer, significantly increasing the disease free survival rates of women with these malignancies. Currently, detection of

ERBB2 in breast cancer is performed by immunohistochemistry and *in situ* hybridization, which require biopsies. Examining a tissue by biopsy is not ideal because the procedure can be painful for patients, and removing tissue from a person may alter the molecular expression patterns of cells (39). A non-invasive ERBB2 imaging agent would therefore alleviate the need for biopsies, while simultaneously detecting whether ERBB2 is accessible from the blood stream, the delivery route of both trastuzumab and pertuzumab. Owing to the need for novel imaging vectors, target-specific molecules have been developed by numerous methods, however one of the most widely used and successful strategies is the use of bacteriophage (phage) display.

# Phage Display

Phage display is a combinatorial technology pioneered by Dr. George P. Smith in 1985 at the University of Missouri (40). The technology was developed using filamentous phage, a long rod shaped particle approximately 1 µm in length and 30 nm in diameter. A phage particle consists of several coat proteins that encapsulate single-stranded DNA encoding for production of the viral proteins. A phage is able to infect a host bacterial cell, inject its genetic material, and generate many thousands of copies of itself. Phages are secreted out of the bacterial cell by assembly of coat proteins at the cell wall, insertion of the phage genome, and excretion. It was discovered that the outer coat proteins could tolerate insertion of foreign peptides, and thus libraries of phage displaying random molecules could be generated by manipulating the phage genome with altered coat protein genes.

The structure of a phage is dictated by its genome. The body of the phage consists mainly of coat protein VIII, which is present in ~2700 copies along the length of the phage. At each end of the phage are two pairs of proteins, at one tip coat proteins III and VI, and the other coat proteins VII and IX. The two most widely used coat proteins for phage display are coat protein VIII and III. Coat protein VIII is beneficial for displaying a targeted peptide because a phage can display ~100 copies of an altered coat protein VIII in combination with native coat protein VIII. Coat protein III is only displayed in 3-5 copies at the tip of the phage, however the protein is long (200 amino acids) and can tolerate insertion of molecules as large as an antibody heavy chain. Coat protein III has

been the primary site of foreign peptide display because of its flexibility, distance from the phage body, and low number of displayed foreign sequences allowing for selection of high affinity molecules. A phage library can be created by ligating DNA encoding for random peptides into the coat protein III gene, and transfecting host bacteria with the modified plasmids. The bacterial cells then produce thousands of each random sequence, creating a pool of phage displaying a highly diverse number of sequences.

A phage display selection utilizes the tolerance of phage to foreign peptide insertion, in addition to its self-replicating ability, to competitively isolate peptides for a desired function. A single phage library can contain up to $10^9$ unique peptide sequences present in approximately 1000 copies each. The entire phage library can then be incubated with a target, allowing specific phage to bind, and removing all unbound phage. The captured phage are then eluted and amplified by infection in bacteria, and the resulting purified phage pool is a subpopulation of phages with the capability of binding the desired target. This subpopulation of phage can then be subjected to another round of competitive selection, in which higher affinity peptides will outcompete lower affinity peptides, effectively further enriching the population with only the highest affinity phages. A single phage library can be subjected to a number of rounds of selection, with careful consideration given to the balance between selecting target-avid phages and phages with a growth advantage, due to the iterative infections that are necessary with each round of selection, which lead to bias toward phage with more efficient propagation (41). Peptides specific for a given function can then be determined using the genetic material of the phage for further refinement or characterization outside of the phage scaffolding.

Isolation of peptides from phage display selections can be accomplished using a number of targets both *in vitro* and *in vivo*. *In vitro*, phage display has been utilized to select peptides that bind transmembrane receptors, glycoproteins, integrins, carbohydrates, DNA, and even metals (42-46). The peptides are highly specific, and generally have moderate to high affinity for their target in the low µM to high nM range (42, 43). The targeted peptides have been used *in vivo*, most relevantly to detect and characterize human tumors in mice (47, 48). Recently, phage display technology has been translated to *in vivo* selections, in order to capitalize on the physiologically accurate nature of target display an *in vivo* system presents. Selections have been accomplished in both mice and humans, for targets including tumors, tumor vasculature, and specific tissues (49, 50). The success of these peptides demonstrates that the library size, robustness, and replication ability of phage display have positioned this combinatorial technique at the forefront of targeted peptide discovery.

## Peptides

Typically, the initial choice for a targeting agent is a monoclonal antibody. The exquisite specificity and affinity of antibodies has made them a highly attractive choice for molecular targeting. However, antibodies have had limited success for some applications *in vivo* for several reasons. First, antibodies are large foreign objects, and thus can elicit an immune response (51). Humanization of antibodies has lessened this response to some degree, however clinical trials with antibodies still report immune-related side effects (52). The large size of antibodies also poses an additional problem, in that their pharmacokinetics are often slow and result in high liver uptake. Additionally, the large molecular weight of antibodies limits tumor penetration, since the irregular vasculature of a tumor prevents active transport of blood-borne molecules. Instead, diffusion is the main source of transport, and the size of an antibody limits its diffusion rate. Peptides, on the other hand, can overcome many of the obstacles encountered by the use of antibodies. A typical peptide has a molecular weight under 3 kDa, approximately 50 times smaller than an antibody. The low molecular weight provides rapid pharmacokinetics and unbound peptide is cleared from the bloodstream in under 1 hour (30). Since diffusion is inversely proportional to molecular weight, a peptide also has superior tumor penetration. Peptides are not without drawbacks, and the trade-off for small size is typically a decreased affinity. The rapid pharmacokinetics also may result in the peptide being removed from the bloodstream too rapidly, decreasing overall tumor

uptake. Despite these limitations, peptides have been demonstrated to image human tumors *in vivo*, and thus are relevant for future targeting vectors.

Successful tumor imaging peptides can be derived from natural peptide ligands or combinatorial libraries. Peptides found in Nature that bind to receptors differentially expressed in cancer have had the most success clinically. These peptides include derivatives of somatostatin, gastrin releasing peptide, and α-melanocyte stimulating hormone (53-55). The peptides have been demonstrated to successfully image tumors expressing their receptors in both mice and humans. Targeted peptide discovery is not limited to naturally occurring peptides. Combinatorial libraries, including phage peptide display libraries, can be selected to home to tumor targets. The only peptide applied thus far to both mouse and human imaging is the arg-gly-asp peptide, termed RGD (56). Although RGD is a natural integrin binding sequence, phage display was used to elucidate that the peptide was more stable and had a higher affinity in a cysteine constrained form (57). In addition to RGD, phage display has been used to identify a number of peptides that successfully image tumors in mice. Peptides targeting ERBB2, galectin-3 and plectin, have been isolated by *in vitro* phage display, in addition to peptides targeting PC-3 prostate cancer, breast tumor vasculature, and a number of organs *in vivo* (47-50, 58). Ostensibly, any antigen can be targeted by phage-displayed peptides, providing a powerful tool for future applications in personalized medicine.

## Radiolabeling

Following the development of a targeted peptide, an imaging moiety must be conjugated to the peptide to allow for tracking of the peptide *in vivo*. Several considerations must be examined when choosing the type of radiolabeling system for a peptide, including conjugation, radioactive isotope, half-life and type of emission. Conjugation of a radioactive molecule can be accomplished either directly or through the addition of a radiometal chelator. Direct conjugation is often accomplished using $^{124/125}$I, $^{18}$F and $^{11}$C. While direct conjugation with radioactive fluorine or carbon produces a stable, radiolabeled peptide, the chemistry is often complex, and the half-life of $^{18}$F (110 min) and $^{11}$C (20 min) require large quantities of radioactivity to complete the synthesis. Iodine offers a simpler radiolabeling procedure, however the label can be more labile, resulting in dissociation from the targeted vector. The addition of a radiometal chelator allows for conjugation of unlabeled chelator followed by radiolabeling, allowing for a simpler and more rapid approach to radiolabeling.

The choice of chelator dictates the stability of the radiolabel and options for radiometal. Chelators may be acyclic, such as (DTPA) and 6-hydrazinonicatonic acid (HYNIC), or cyclic, including 1,4,7,10-tetraazacyclododecane-1,4,7,10-tetraacetic acid (DOTA), 1,4,7-triazacyclononane-triacetic acid (NOTA), 1,4,8,11-tetraazacyclotetradecane-1,4,8,11-tetraacetic acid (TETA) and (CB-TE2A) (48, 59-62). Although acyclic chelators offer rapid and labile labeling conditions, their stability is often not suitable for *in vivo* use (63). Cyclic chelators are ideal for peptides because they

provide stable chelation, are able to bind a wide variety of radiometals, and their harsher labeling chemistry usually does not alter the properties of the peptide.

Often chelators may bind several radiometals, requiring one specific label to be chosen. The choice of a radiometal is based on the type of emission and half-life desired. Single photon emission computed tomography (SPECT) is a widely used imaging platform, relying on the detection of gamma emission from specific radioisotopes (64). Radiometals used for SPECT imaging include $^{99m}$Tc, $^{111}$In and $^{203}$Pb (55, 65). These are often employed because their gamma energies are low (140 keV-270 keV) and their half-lives (6-52 h) are suited for biological imaging applications. Positron emission tomography (PET) has received much attention of late because its sensitivity is 1-2 orders of magnitude greater than SPECT and it allows for quantification (66). Several radiometals, including $^{64}$Cu, $^{68}$Ga and $^{89}$Zr are commonly utilized for PET imaging. PET imaging operates by detecting the coincident gamma particles emitted following an annihilation of a positron emitted by the radionuclide and a surrounding electron (67). The half-lives range from 68 min for $^{68}$Ga to 78 h for $^{89}$Zr, allowing for a wide range of time scales. The choice of PET or SPECT imaging can be made based on availability of imaging equipment, cost and half-life however both moieties offer sensitive detection *in vivo*. Together, SPECT and PET imaging provide several options for *in vivo* imaging applications, allowing for a host of imaging vectors for improved detection and characterization of cancer.

# Conclusion

A need exists for novel and improved imaging agents for detection and characterization of breast cancer. It was hypothesized in this dissertation that phage display could be used to select peptides with optimal pharmacokinetics that target and image human breast cancers based on a specific target or phenotype. Herein, the work presented describes the development of these targeted peptides for molecular imaging of breast cancer. The targets include the receptor ERBB2, tumor vasculature, and resistance-susceptible human breast cancer xenografts. Each peptide was selected using *in vivo* phage display, and completely characterized *in vitro* prior to biodistribution and imaging analysis. In order to accomplish *in vivo* characterization, peptides were conjugated with DOTA and radiolabeled with $^{111}$In. An $^{111}$In-DOTA chelation strategy was chosen because it is highly stable and well characterized. The data presented will demonstrate that *in vivo* phage display is capable of selecting peptides that are capable of imaging a wide variety of targets, and thus is a powerful tool for future imaging agent discovery.

# CHAPTER 2

## AFFINITY MATURATION OF AN ERBB2-TARGETED SPECT IMAGING PEPTIDE BY *IN VIVO* PHAGE DISPLAY

# Introduction

It is estimated that 1 in 8 women will develop breast cancer in their lifetime (1). Early detection and characterization of breast carcinomas will allow for an improved understanding of individual malignancy and proper course of treatment. Thus, new methods to visualize tumor associated antigens are being sought. The epidermal growth factor tyrosine kinase receptors including: epidermal growth factor receptor (EGFR)/HER1, ERBB2/HER2/neu, ERBB3/HER3 and ERBB4/HER4 have received particular attention because of their roles in proliferation, migration and survival signaling (10). ERBB2 acts preferentially as a dimerization partner, and breast tumors over-expressing the receptor are associated with increased malignancy and poor prognosis (36). In breast cancer, ERBB2 is over-expressed in 20-30% of cases, and 80-90% of breast cancers express the protein to some extent (25, 33).

The ability to differentiate tumors based on a molecular marker, such as ERBB2, would allow for detection and categorization of individual breast carcinomas based on the molecular composition of the tumor. Although monoclonal antibodies and antibody fragments have high specificity and affinity for their targets, slow clearance and poor tumor penetration can hinder their effectiveness as imaging agents (68, 69). Peptides, in contrast, demonstrate rapid clearance and tumor penetration, but are limited by low target affinity (70). However, development of high affinity, target-specific peptides has been accomplished through bacteriophage (phage) display (71). Enrichment of rare, high affinity peptides is achieved through successive rounds of selection and amplification of

phages displaying target-avid peptides (44, 72). Previously, a six amino acid peptide, KCCYSL, was discovered by phage display after *in vitro* selection with a recombinant ERBB2 extracellular domain (43). The affinity of KCCYSL for its target was approximately 300 nM, and it was able to clearly delineate ERBB2-expressing tumors in mice bearing MDA-MB-435 human breast carcinoma xenografts (48). The radiolabeled peptide was used to image ERBB2-expressing ovarian and prostate carcinomas as well (48, 73). Biodistribution studies revealed modest tumor uptake in breast carcinoma xenografts at 0.66% injected dose (ID)/g 2 h post-injection. However, non-target organ uptake, including kidney retention at 5.75% ID/g 2 h post-injection, was likely too high for clinical applications. Thus, a means to improve the pharmacokinetic properties of the KCCYSL peptide was needed.

One method to improve the desired qualities of a peptide is through combinatorial evolution. Combinatorial evolution is a technique based on the principle of affinity maturation in antibodies. In affinity maturation, primary antibodies produced with low intrinsic target affinity are subsequently mutated in their hypervariable regions, ultimately leading to higher affinity antibodies (74). Addition of random amino acids to a core binding sequence can be used to mimic the mutation of hypervariable regions of antibodies in the pursuit of higher affinity. Unlike affinity maturation, combinatorial evolution is not limited to selection for increased affinity. Previously, a peptide with high target affinity for a disaccharide with low solubility was selectively evolved *in vitro* from a phage display library with greater solubility while maintaining target affinity (75). It follows that combinatorial evolution could be used to select for a novel property, such as *in vivo* target recognition, without impeding the original function of the core peptide. In

order to improve the *in vivo* pharmacokinetics and imaging ability of the ERBB2-targeting peptide, a novel phage microlibrary, termed "KCCYSL microlibrary", was engineered. The phages in the microlibrary display the targeted peptide flanked by five and four random amino acids on the N- and C-termini, respectively. It was hypothesized that second generation peptides could be selected *in vivo* from the KCCYSL microlibrary with enhanced pharmacological properties including specific tumor accumulation, reduced non-target organ uptake, and rapid clearance.

# Materials and Methods

## Materials

Cell culture materials were purchased from Invitrogen (Carlsbad, CA). All other materials were purchased from Sigma Chemical Co. (St. Louis, MO) unless otherwise specified.

## Mouse Strains and Handling

Four- to 6-week-old severe combined immunodeficient (SCID) outbred mice (Taconic, Germantown, NY) were maintained in approved pathogen-free institutional housing. Animal studies were conducted as outlined in the NIH Guidelines for the Care and Use of Laboratory Animals and the Policy and Procedures for Animal Research of the Harry S. Truman Veterans Memorial Hospital. To establish solid tumors, MDA-MB-435 human breast cancer cells ($5 \times 10^6$) were subcutaneously injected into the flank of SCID mice. Visible tumors (~1-3$mm^3$) formed after approximately 5 weeks.

## Phage Selection and Characterization

A library of double-stranded oligonucleotide cassettes was commercially synthesized (Sigma-Genosys, Inc., Woodlands, TX). Each cassette retained the core ERBB2-binding amino acid sequence KCCYSL, while displaying additional 5 and 4 random amino acids adjacent to the parent peptide on the N- and C-termini, respectively. Cassettes ligated into the fUSE5 vector, for display on the pIII coat protein. Following

ligation, the phage library was transfected into *E. coli* and propagated as described previously (76).

### *In Vivo* Affinity Selection

Phages with a propensity to bind normal tissues and proteins that are not tumor specific were cleared from the library in a normal mouse, per previous methods (50). Briefly, $1x10^{12}$ TU of the KCCYSL microlibrary were injected into normal CF-1 mice, incubated 15 min, sacrificed, blood collected and injected phages recovered and amplified. The pre-cleared phage pool then served as the starting library for subsequent selection processes. A 100 µL solution of $1x\ 10^{12}$ TU KCCYSL microlibrary was intravenously injected into MDA-MB-435 xenografted SCID mice. After 1h, mice were perfused to clear the tumor vasculature of unbound phage particles. Tumors were excised and homogenized before extraction of phages with a 2.5% (w:v) 3-[(3-cholamidopropyl)dimethylammonio]-1-propanesulfonate (CHAPS) solution at 4°C for 2 h. The extracted phages were amplified and purified as previously described (50). *In vivo* selection was repeated for a total of four rounds of selection. A portion of the recovered phage clones from the final selection were sequenced to ascertain the foreign peptide sequences. Peptide sequences were analyzed by the basic local alignment search tool (BLAST) and sequence composition comparison and scanner and reporter of target unrelated proteins (SAROTUP) to obtain clones of interest for further characterization (77, 78). Selected phage binding to MDA-MB-435 and 184A.1 cells was performed as described previously (50).

**Peptide Synthesis**

All peptides were synthesized using an Advanced Chem Tech 396 multiple peptide synthesizer by solid phase FMOC chemistry. Biotin and 1,4,7,10-tetraazacyclododecane-1,4,7,10-tetraacetic acid (DOTA) (Macrocyclic, Inc. Dallas, TX) were covalently linked to peptides through the N-terminus of a Gly-Ser-Gly (GSG) spacer.

**ERBB2 Peptide Binding Assay**

Recombinant human ERBB2 extracellular domain was produced and purified as previously described (43). In order to analyze peptide binding, 20 ng of ERBB2 diluted in $Na_2CO3$ buffer (pH 9.6) was immobilized on Immulon™ 2HB 96-well microtiter EIA plates (ImmunoChemistry Technologies Bloomington, MN) overnight at 4°C. After removing the protein solution, the plates were blocked with BioFx synthetic block (BioFx Laboratories, Owing Mills, MD). The block was aspirated and wells were incubated with peptide serially diluted in Tris buffered saline and 0.1% Tween-20 (0.1% TBST). Following vigorous washing with 0.1% TBST, wells were incubated with streptavidin-conjugated horse radish peroxidase diluted 1:1000 in 0.1% TBST. Wells were once again vigorously washed and bound peptide was visualized by the addition of 2,2'-azino-bis(3-ethylbenzothiazoline-6-sulfonic acid) and absorbance read on a plate reader at 405 nm.

**Fluorescent Microscopy**

MDA-MB-435 and 184A.1 cells dried onto microscope slides were blocked with 6% (w:v) BSA in TBS. Biotinylated peptides were diluted to 10 μM with 0.1% TBST.

Individual peptides were incubated with the cells for 1 h, followed by washing with 0.1% TBST and incubation with Neutravidin Texas Red (Life Technologies, Rockville, MD) for 1h at room temperature. Following washing with 0.1% TBST, cells were visualized by an epifluorescent Nikon T1-SM inverted microscope (Nikon, Melville, NY).

**Radiolabeling and Peptide Cell Binding Assays**

DOTA-conjugated peptides were labeled with $^{111}$In and purified by RP-HPLC as previously described (48). MDA-MB-435 and 184A.1 cells were diluted to $1x10^6$ cells in 200 µL of DMEM with 0.1mg/mL BSA. Cells (200 µL) were incubated with $1x10^6$ CPM of peptide (100 µL) at 37°C for the appropriate time, washed three times with ice-cold PBS with 1% BSA and counted via gamma counter.

**Radiolabeled Peptide Biodistribution**

$^{111}$In-DOTA-GSG-1-D03 peptide was diluted to 1.85 MBq/mL in sterile PBS. Three mice bearing MDA-MB-435 tumors were intravenously injected and sacrificed at 30 min, 1, 2 and 4 h. Relevant organs and tissues were removed for weighing and counting by gamma counter. Uptake was reported as percentage of injected dose per gram of tissue (%ID/g). For blocking experiments, mice were injected with 100 µg of unlabeled DOTA-GSG-1-D03 15 min prior to injection of radiolabeled peptide.

**MicroSPECT/CT Imaging**

An 11.1 MBq dose of $^{111}$In-DOTA-GSG-1-D03 was intravenously injected into a MDA-MB-435 tumor-bearing mouse. After 2 h, the mouse was euthanized with carbon

dioxide and imaged at the Biomolecular Imaging Center at the Harry S. Truman Veterans Memorial Hospital. Images were collected overnight (7 h) using a Siemens Inveon Micro-SPECT/CT (Siemens, Knoxville, TN) equipped with mouse whole body 1.0 mm collimators. Image data were processed using Inveon Research Workplace processing software and fan beam (Feldkamp) filtered back projection algorithms were used to reconstruct the CT tomographic image.

**Statistical Analysis**

Quantitative data were expressed as mean ± standard error. Means were compared using 1-way ANOVA and the Student *t* test. *P* values of less than 0.05 were considered statistically significant.

# Results

## KCCYSL Microlibrary *In Vivo* Selection and Phage Characterization

Following four rounds of selection, individual displayed sequences were analyzed by the BLAST and SAROTUP programs to determine homology to human proteins as well as peptides from previously published phage display selections. No significant homology to known cancer-related proteins was discovered by BLAST search, and analysis by SAROTUP indicated that the peptides had not been previously published (77, 78). Previous work has demonstrated that analyzing phage affinity and specificity by comparing target to non-target binding ratios is a successful predictor of *in vivo* tumor homing ability (50). Thus, 33 phage clones were arbitrarily selected and analyzed for the ability to selectively bind MDA-MB-435 human breast cancer cells and not 184A.1 normal human breast epithelial cells. The cancer to epithelial cell binding ratio of each clone was compared to that of phages bearing the parent sequence, KCCYSL. Nine phage clones bound with a ratio greater than 1.56, which was higher than KCCYSL (Figure 2.1). Corresponding peptides from the 9 clones with higher binding ratios than KCCYSL from the cell binding assay were then synthesized.

## *In Vitro* Peptide Binding

Although the primary goal of the *in vivo* selection was to improve the pharmacokinetics of KCCYSL, it was also essential to ensure that the second generation peptides maintained binding to ERBB2. An ERBB2-peptide binding assay was

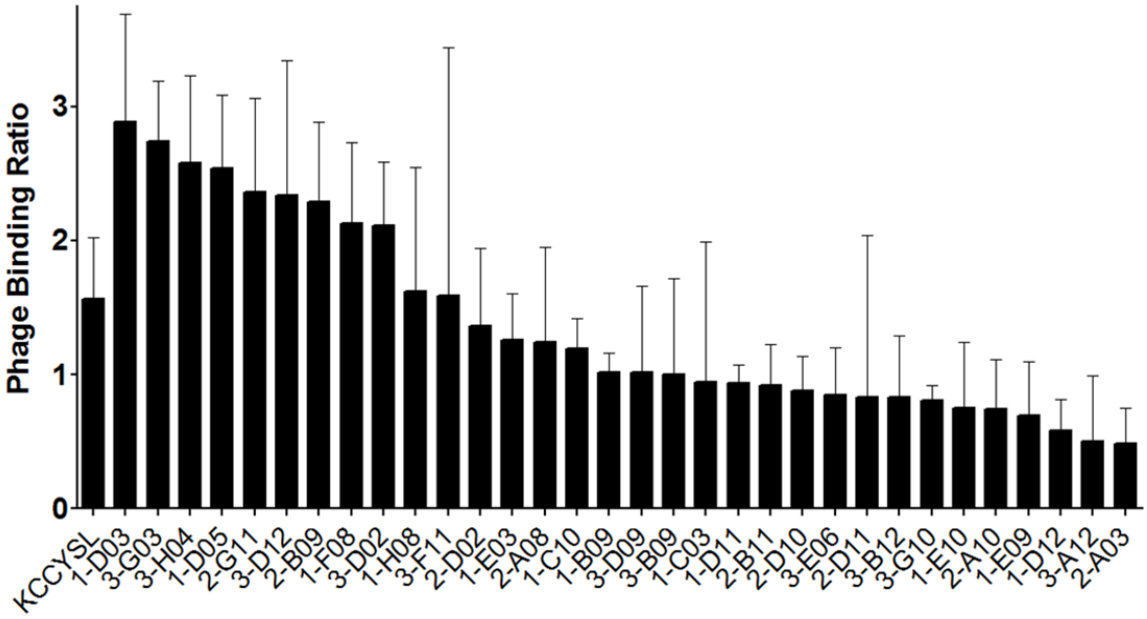


**Figure 1.1** Individual phage populations were incubated with either MDA-MB-435 human breast cancer or 184A.1 breast epithelial cells. Recovered phages were quantified by infection in *E. coli*. Binding was plotted as a ratio of cancer:normal cell binding. Error bars represent the standard deviation of 3 replicates.

performed in order to assess the affinity of each peptide for its target. The results indicated that two peptides, 1-D03 (MEGPSKCCYSLALSH) and 3-G03 (GTKSKCCYSLRRSS) bound ERBB2 with apparent affinities of 236±83 nM and 289±13 nM, respectively (Figure 2.2). Both peptides had a significantly higher apparent affinity for ERBB2 ($P$<0.05) than the parent peptide KCCYSL (351±32 nM) (48).

After confirming retained ERBB2 binding, the specificity of each peptide for the target cell line, MDA-MB-435, and normal breast epithelial cells was investigated. 1-D03, 3-G03 and KCCYSL all successfully discriminated the target cell line from normal breast epithelial cells (Figure 2.3a). To further assess specificity, peptides were screened for binding with a panel of cultured cells, including breast, prostate and pancreatic cancers. Figure 2.3b demonstrates 1-D03 bound only MDA-MB-435 cells, while 3-G03 appeared to bind all of the carcinoma cell lines tested, but with a lower affinity than for MDA-MB-435 cells.

**DOTA-Peptide Radiolabeling and *In Vitro* Cell Binding**

DOTA-(GSG)MEGPSKCCYSLALSH (DOTA-1-D03) and DOTA-(GSG)TKSKCCYSLRRSS (DOTA-3-G03) peptides were chemically synthesized for radiolabeling with $^{111}$In. Analysis of the RP-HPLC trace revealed >95% radiochemical purity of labeled peptides. Recovery of the radiolabeled peptide following HPLC purification was routinely 40-50% and stability in buffer of both peptides was greater than 24

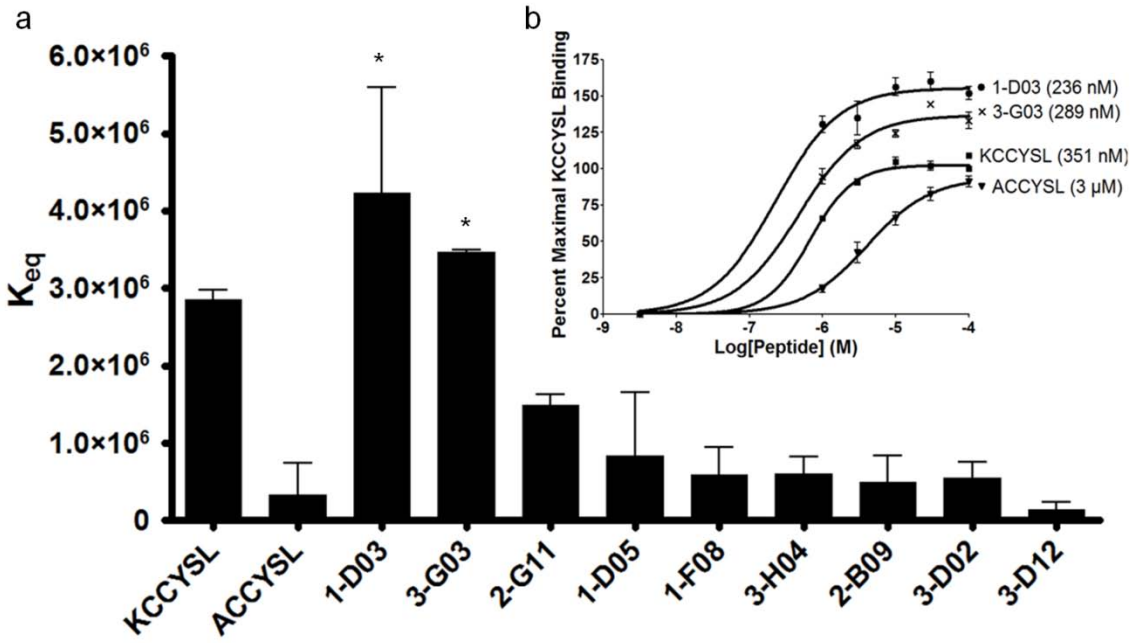


**Figure 2.2** Serial dilutions of biotinylated peptide were incubated with immobilized human ERBB2 extracellular domain. Binding was detected by incubation with HRP-conjugated streptavidin followed by colorimetric substrate. (a) Binding affinities of peptides for ERBB2 plotted as the $K_{eq}$ or inverse $K_D$. (b) Individual binding data of the two highest affinity peptides (1-D03 and 3-G03), parent peptide (KCCYSL) and control peptide (ACCYSL). * - $P<0.05$

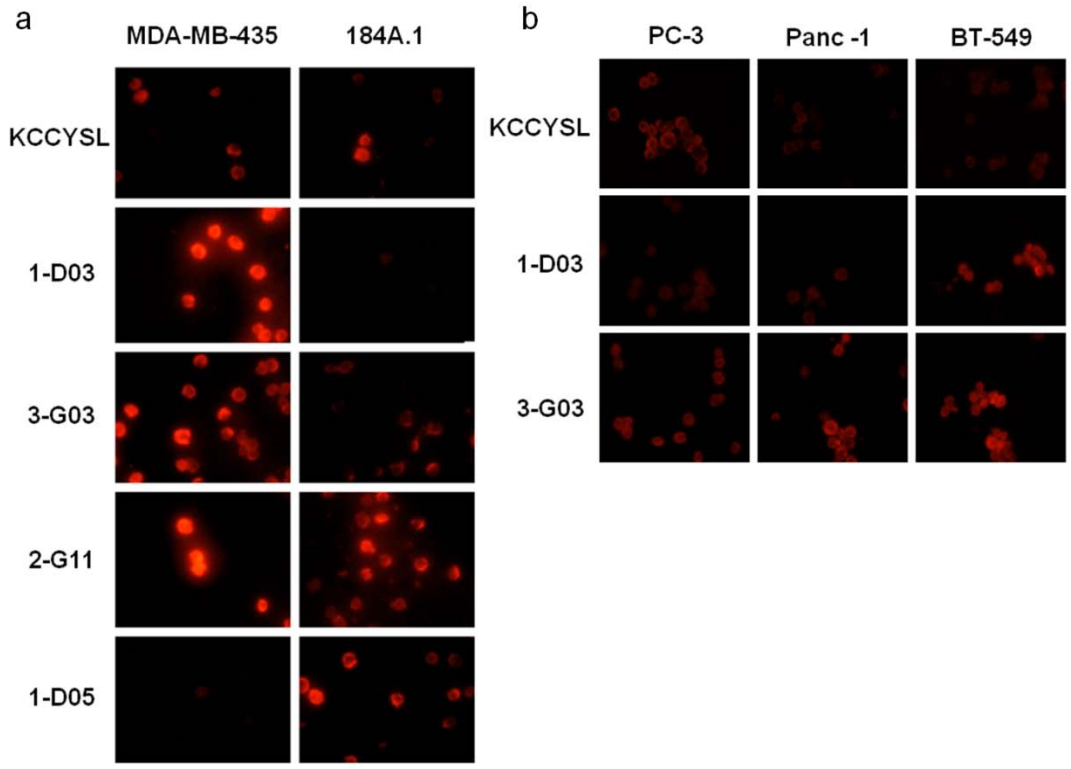


**Figure 2.3** (a) Fluorescent imaging of anti-ERBB2 biotinylated peptides against MDA-MB-435 human breast carcinoma and 184A.1 normal breast endothelial cells. (b) Additional cancer cell binding panel for top two clones (1-D03 and 3-G03) and parent peptide (KCCYSL). Cell lines include human prostate (PC-3), pancreatic (Panc-1) and breast (BT-549) cancers.

h. The half-life of the peptide incubated in mouse serum was determined to be greater than 24 h (not shown).

In order to confirm retained specificity and affinity of the DOTA-conjugated peptides, *in vitro* cell binding was performed. Total bound peptide was used as a measure of apparent affinity, while the ratio of MDA-MB-435 to 184A.1 binding was used as a measure of specificity. The results in Figure 2.4a display the cell binding of the $^{111}$In-labeled peptides to both cancer and epithelial cells. $^{111}$In-DOTA-KCCYSL bound to target cells (1038±106 CPM) with a specificity ratio of 3.49. $^{111}$In-DOTA-1-D03 demonstrated higher binding (1681± 119 CPM) to MDA-MB-435 and specificity (7.44) than KCCYSL ($P$<0.001). Similar binding of $^{111}$In-DOTA-1-D03 was achieved by $^{111}$In-DOTA-3-G03 (1494±141 CPM) to MDA-MB-435 cells, but its specificity ratio (1.4) was less than KCCYSL. Additionally, serial dilutions of $^{111}$In-1-D03 incubated with MDA-MB-435 cells demonstrated saturable binding (Figure 2.4b) Thus, only $^{111}$In-DOTA-GSG-1-D03 was chosen for *in vivo* radiolabeled peptide analysis.

### *In Vivo* Biodistribution

The biodistribution of $^{111}$In-DOTA-1-D03 peptide was investigated in mice bearing MDA-MB-435 human breast tumor xenografts (Table 2.1). Tumor to blood ratios of the peptide reached 1.95±0.17 at 1 h and 6.02±0.13 at 2 h post-injection (Table 2.2). In order to compare pharmacokinetics between first and second generation peptides, tumor and organ uptake for KCCYSL and 1-D03 were compared at 1 and 2 h post-injection

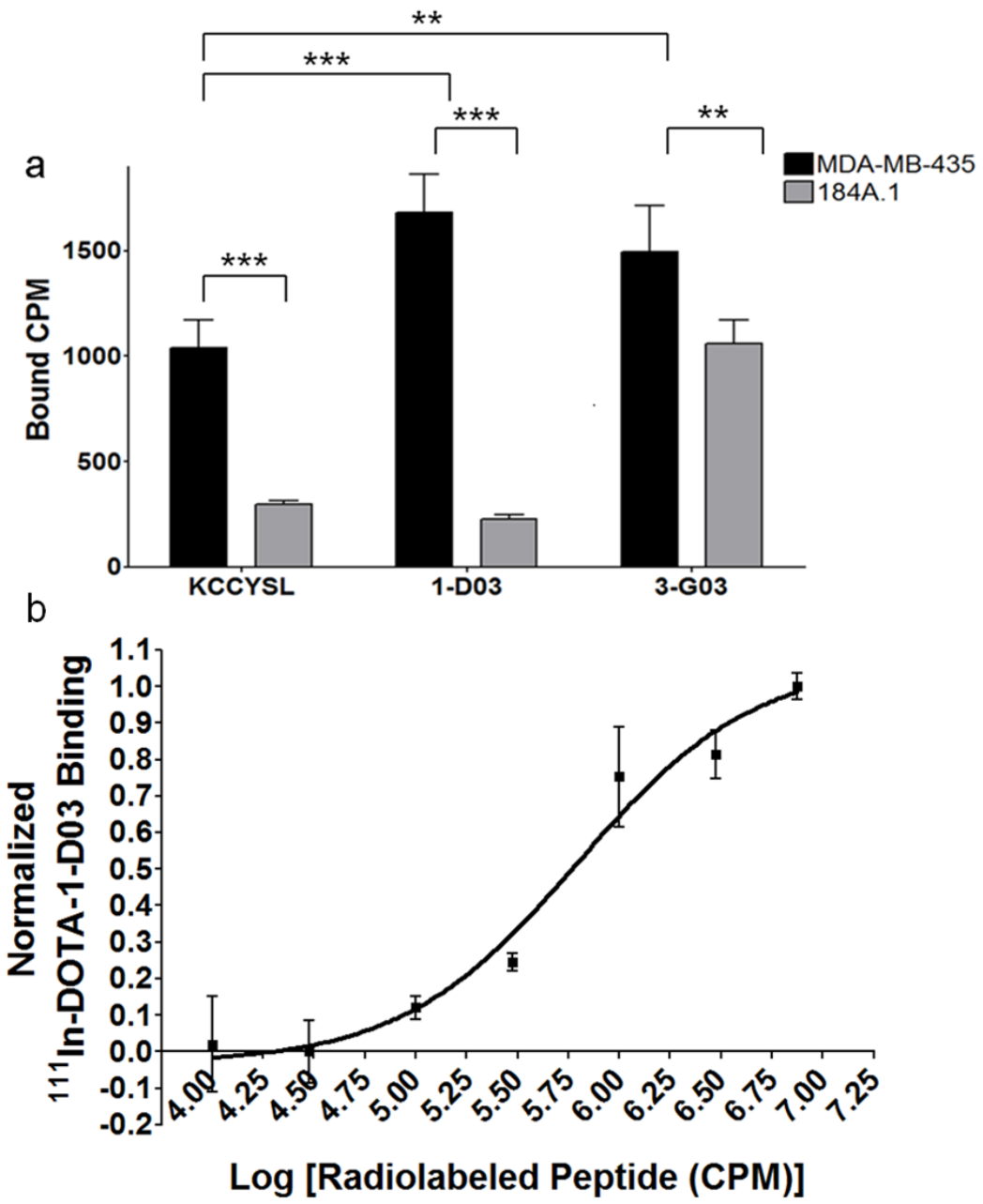


**Figure 2.4** a) HPLC-purified $^{111}$In-DOTA-KCCYSL, 1-D03 and 3-G03 peptides were incubated with MDA-MB-435 human breast carcinoma and 184A.1 breast epithelial cells. Following washing, bound peptide was detected by gamma counter. Bars represent the mean of 3 replicates with standard deviation. (b) HPLC-purified $^{111}$In-DOTA-1-D03

was s erial di luted a nd i ncubated w ith M DA-MB-435 c ells. F ollowing w ashing c ell binding was detected by gamma counter. Binding values were normalized for minimum and ma ximum b inding values a nd pl otted a s a fraction o f m aximum bi nding. CPM - counts per min. ** - $P<0.01$; *** $P<0.001$.

**Table 2.1** – $^{111}$In-DOTA-1-D03 Biodistribution

| Organ | 30 Min %ID/g | 1 h %ID/g | 2 h %ID/g | 4 h %ID/g |
|---|---|---|---|---|
| Tumor | 0.973 ± 0.26 | 0.664 ± 0.09 | 0.336 ± 0.03 | 0.144 ± 0.04 |
| Blood | 1.542 ± 0.42 | 0.342 ± 0.06 | 0.056 ± 0.01 | 0.049 ± 0.01 |
| Heart | 0.489 ± 0.15 | 0.130 ± 0.03 | 0.043 ± 0.01 | 0.036 ± 0.01 |
| Lung | 1.195 ± 0.32 | 0.403 ± 0.04 | 0.213 ± 0.05 | 0.123 ± 0.04 |
| Liver | 0.496 ± 0.11 | 0.174 ± 0.02 | 0.141 ± 0.03 | 0.144 ± 0.02 |
| Spleen | 0.419 ± 0.08 | 0.132 ± 0.02 | 0.084 ± 0.01 | 0.083 ± 0.02 |
| Stomach | 0.479 ± 0.35 | 0.338 ± 0.50 | 0.184 ± 0.13 | 0.079 ± 0.04 |
| Large intestine | 0.265 ± 0.08 | 0.072 ± 0.01 | 0.297 ± 0.09 | 0.654 ± 0.26 |
| Small intestine | 0.523 ± 0.18 | 0.220 ± 0.07 | 0.263 ± 0.17 | 0.128 ± 0.50 |
| Intestines | 0.424 ± 0.14 | 0.159 ± 0.05 | 0.275 ± 0.11 | 0.352 ± 0.13 |
| Kidneys | 7.557 ± 1.82 | 4.729 ± 0.65 | 4.746 ± 0.31 | 5.310 ± 0.99 |
| Brain | 0.043 ± 0.01 | 0.017 ± 0.01 | 0.007 ± 0.00 | 0.005 ± 0.00 |
| Muscle | 0.230 ± 0.05 | 0.049 ± 0.01 | 0.019 ± 0.00 | 0.019 ± 0.00 |
| Pancreas | 0.475 ± 0.01 | 0.109 ± 0.02 | 0.031 ± 0.01 | 0.043 ± 0.01 |
| Bone | 0.177 ± 0.04 | 0.087 ± 0.04 | 0.027 ± 0.00 | 0.028 ± 0.01 |
| Skin | 0.851 ± 0.23 | 0.184 ± 0.05 | 0.071 ± 0.02 | 0.047 ± 0.01 |
|  | 30 Min %ID | 1 H %ID | 2 H %ID | 4 H %ID |
| Urine | 84.59 ± 3.76 | 93.07 ± 2.84 | 95.46 ± 0.07 | 96.03 ± 0.37 |

Mice bearing MDA-MB-435 were injected with $^{111}$In-DOTA-1-D03 and sacrificed at designated time points. Organs were removed and counted by gamma counter. Peptide uptake is reported as %ID/g. %ID/g – Percent injected dose/gram

**Table 2.2** – Radiolabeled Tumor:Organ Uptake Ratios

| | **Tumor:Organ 1 h P.I.** | | **Tumor:Organ 2 h P.I.** | |
|---|---|---|---|---|
| | KCCYSL | 1-D03 | KCCYSL | 1-D03 |
| Blood | 1.95 ± 0.32 | 1.94 ± 0.65 | 5.08 ± 1.11 | 6.01 ± 0.81 |
| Heart | 3.54 ± 0.53 | 5.11 ± 1.84 | 6.60 ± 2.75 | 7.89 ± 1.16 |
| Lung | 0.95 ± 0.13 | 1.65 ± 0.49 | 1.16 ± 0.31 | 1.57 ± 0.36 |
| Liver | 3.12 ± 0.54 | 3.81 ± 1.12 | 3.00 ± 0.52 | 2.38 ± 0.48 |
| Brain | 26.0 ± 5.89 | 39.0 ± 15.8 | 33.0 ± 13.8 | 49.7 ± 11.7 |
| Muscle | 8.67 ± 1.43 | 13.6 ± 4.78 | 22.0 ± 13.4 | 17.9 ± 3.44 |
| Bone | 3.90 ± 0.54 | 7.61 ± 3.80 | 7.33 ± 4.48 | 12.7 ± 1.77 |

Mice bearing MDA-MB-435 were injected with $^{111}$In-DOTA-1-D03 and sacrificed at designated time points. Organs were removed and counted by gamma counter. Uptake is represented by the tumor % ID/g divided by the specific organ % ID/g. P.I. – Post injection

(Figure 2.5) (48). A reduction in non-specific organ binding was evident in just 1 h. 1-D03, in comparison to KCCYSL had significantly lower heart (0.13±0.03 versus 0.22±0.04 $P<0.05$), lung (0.40±0.04 versus 0.82±0.14 $P<0.01$), muscle (0.04±.01 versus 0.09±.02 $P<0.05$) and bone (0.09±0.04 versus 0.20±0.03 $P<0.01$) organ uptake. At 2 h, the specificity was maintained, as 1-D03 had lower residual peptide in the blood (0.06±0.01 versus 0.13±0.03 $P<0.01$). Organ uptake, including lung (0.21±0.05 versus 0.57±0.18 $P<0.01$) and liver (0.144±0.03 versus 0.22±0.02 $P<0.05$), continued to be lower than KCCYSL. Additionally, total kidney retention for the 1-D03 was 4.73±0.31 %ID/g at 1 h and 4.75±0.91%ID/g at 2 h (Table 2.3), which was significantly less ($P<0.05$) than KCCYSL kidney uptake at 2 h (5.75±0.69%ID/g).

**SPECT/CT Tumor Imaging**

The imaging capabilities of $^{111}$In-DOTA-1-D03 were investigated in mice bearing MDA-MB-435 xenografts. Whole body SPECT/CT was performed 2 h following injection of 1.85 MBq of $^{111}$In-DOTA-1-D03 peptide. Images (Figure 2.6a) demonstrate clear tumor uptake of the radiotracer. In order to confirm specificity of the peptide for the tumor xenograft, 100 µg unlabeled 1-D03 was injected 15 min prior to radiolabeled 1-D03. Pre-injection of cold peptide eliminated detectable radiolabeled peptide uptake in the SPECT/CT (Figure 2.6b), suggesting tumor specific uptake of 1-D03. Kidney retention of radiolabeled peptide was consistent with biodistribution data. The inability to

reduce ki dney upt ake by p reinjection with unl abeled pe ptide s uggests s equence independent renal retention of radiolabeled peptides.

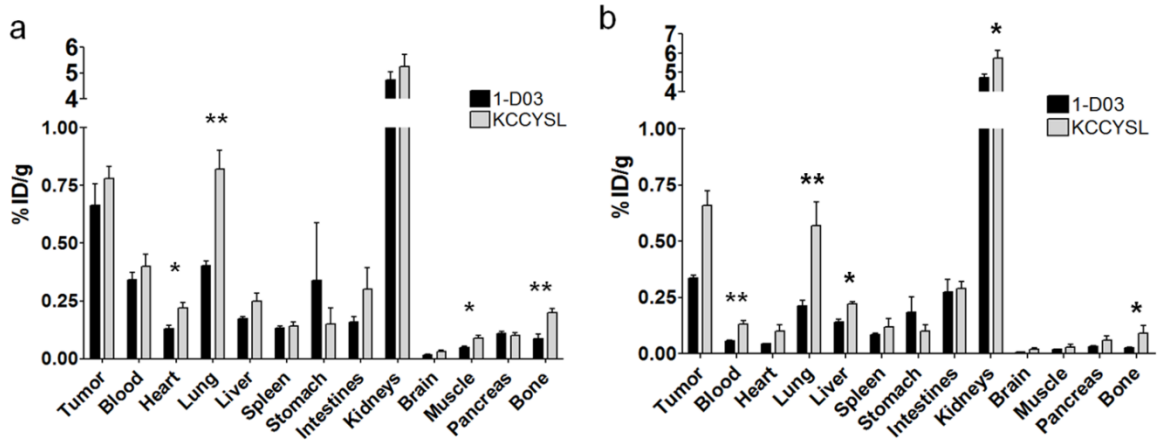


**Figure 2.5** HPLC-purified $^{111}$In-DOTA-1-D03 was injected into MDA-MB-435 tumor bearing SCID mice. At the specified time, mice were sacrificed, organs removed and peptide uptake analyzed by gamma counter. Bars represent the tumor:organ ratio at a) 1 h and b) 2 h post-injection with standard error of 4 replicates. * - $P<0.05$; ** - $P<0.01$.

**TABLE 2.3 –** Radiolabeled Peptide Kidney Retention

| Time P.I. | 1-D03 Kidney %ID/g | KCCYSL Kidney %ID/g |
|---|---|---|
| 1 h | 4.729 ± 0.654 | 5.26 ± 0.78 |
| 2 h | 4.746 ± 0.309* | 5.75 ± 0.69 |
| 4 h | 5.309 ± 0.994 | 6.45 ± 0.69 |

Mice bearing MDA-MB-435 were injected with $^{111}$In-DOTA-1-D03 and sacrificed at designated time points. Organs were removed and counted by gamma counter. Kidney uptake at specific time points is compared. %ID/g – Percent injected dose/gram; P.I. – Post injection; * - $P<0.05$.

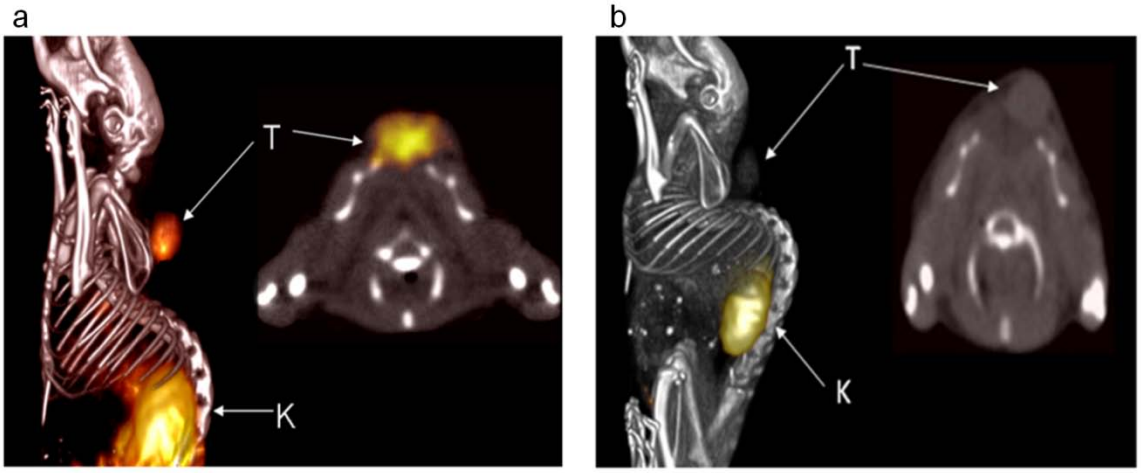


**Figure 2.6** (a) A SCID mouse bearing MDA-MB-435 human breast cancer xenografts was injected with HPLC-purified $^{111}$In-DOTA-1-D03 and SPECT images were collected 2 h following injection. (b) An MDA-MB-435 tumor bearing SCID mouse was preinjected with 100 μg of unlabeled DOTA-1-D03 peptide followed by $^{111}$In-DOTA-1-D03 15 min after unlabeled peptide injection. SPECT/CT imaging was performed 2 h post injection. Arrows from (T) indicate tumors and (K) indicate kidneys.

# Discussion

ERBB2 is a mediator of carcinogenesis and is the target of two clinically approved therapeutic antibodies, pertuzumab and trastuzumab, which bind to domains II and IV of the receptor, respectively (25, 35, 38). Where pertuzumab acts by inhibiting dimerization of the receptor, trastuzumab acts through a number of proposed mechanisms, including inhibiting ERBB2 shedding and antibody dependent cytotoxicity (79). Although the antibodies are successful therapeutics, the large size of monoclonal antibodies renders them less effective as radioimaging or radiotherapeutic agents, due to long circulation times and clearance organ accumulation (51). In comparison, a radiolabeled ERBB2 binding peptide, such as KCCYSL, could simultaneously detect and characterize a carcinoma; because its rapid pharmacokinetic profile is more suitable for imaging than an antibody. Additionally, an ERBB2 targeting peptide could be used to probe antigen status during therapeutic intervention, which would allow for real time assessment of target status. For example, KCCYSL has been demonstrated to bind cells expressing moderate ERBB2 levels, however it does not bind cancer cells devoid of the receptor (80). In order for SPECT or PET imaging peptides to gain relevance clinically, it is important that their pharmacokinetic properties be optimized to provide the highest tumor dose with minimal non-target uptake. Current radiolabeled peptide modification strategies include amino acid substitution, cyclization, and spacer or chelate modification (54, 81, 82). For example, substitution of tyrosine for phenylalanine in the somatostatin-

mimicking peptide (D)-Phe[1]-Thy[3]-octreotide (DOTATOC) increased tumor uptake greater than 9 fold (83). However, amino acid variation is not always well tolerated by a peptide, as changing glutamic acid residues in minigastrin analogues reduced tumor uptake 50% (84). Another strategy to enhance affinity and stability of a peptide is through cyclization. The alpha-melanocyte stimulating hormone (ReCCMSH) peptide had a greater than 4 fold increase in tumor to blood and over a 100 fold increase in tumor to muscle ratios when it was cyclized by coordination with rhenium oxide (85). Interestingly, cysteine-based disulfide cyclization did not enhance, and, in fact, reduced total tumor uptake and tumor to blood ratios of the peptide. In cases where rational modification strategies are unsuccessful, a combinatorial approach, such as *in vivo* phage display may offer a solution to an otherwise difficult problem.

In this study, as well as others, *in vivo* selection did not result in a consensus sequence or motif for tumor targeting (50, 86). Although emergence of a predominant sequence is traditionally a measure of a successful phage display selection, the large diversity of selected phages may have resulted from the complex target environment (87). In addition, the core binding sequence, KCCYSL, may have been sufficient if not optimal to target each phage to the tumor. This is supported by the ERBB2 peptide binding data, in which the highest affinity second generation peptides bound with similar affinity as the parent peptide. The inability to select higher affinity peptides could be the result of KCCYSL being the optimal ERBB2 targeting peptide or evidence that the receptor exists in close proximity to a number of other molecules or binding partners, creating a heterogeneous target. Although individual second generation peptide affinity for ERBB2 was not higher than KCCYSL, 9 phage clones exhibited higher ERBB2-expressing

tumor to normal breast cell binding ratios compared to the parent peptide. Higher affinity for cultured breast carcinoma cells, in combination with similar affinity as KCCYSL to purified target suggests that the improved cancer targeting ability of the second generation phages and corresponding peptides may result from improved detection of ERBB2 in the complex cellular environment, as opposed to enhanced affinity. This notion is bolstered by fluorescent microscopy data, which revealed higher apparent binding of both 1-D03 and 3-G03 peptides to the target MDA-MB-435 breast carcinoma cells than KCCYSL. 1-D03 peptide also exhibited exceptional specificity, in that it displayed low to no binding to normal breast epithelial cells or to other cancer cell lines tested. Together, these results are evidence that *in vivo* phage display affinity maturation may offer the unique advantage of presenting a target in its physiological configuration, allowing for selection of peptides otherwise unattainable by *in vitro* selection protocols.

The purpose of our studies was to create an improved ERBB2-targeted radioimaging peptide based on a KCCYSL core sequence. The two peptides with the highest affinity for ERBB2, 1-D03 and 3-G03, were synthesized conjugated to the macrocyclic chelator DOTA for radiolabeling with $^{111}$In. The use of DOTA radiolabeled with $^{111}$In served two purposes. Chelation of $^{111}$In by DOTA is highly stable and has been used clinically for peptides, and the stable chelation allowed for focus on peptide pharmacokinetics, without non-target uptake artifacts due to free radiometal (55). It was necessary to reanalyze peptide binding following chelator conjugation and radiolabeling, as both have sometimes been observed to alter peptide properties (65). Similar to results with biotinylated peptides, radiolabeled 1-D03 bound with higher affinity and specificity than radiolabeled KCCYSL to MDA-MB-435 cells. Although 3-G03 bound with high

affinity to target cells, it was less specific than KCCYSL and was eliminated from *in vivo* characterization. The decreased specificity of 3-G03 may be the result of the additional amino acid sequence of the second generation peptide interfering with binding to ERBB2 on the cell surface. Radiolabeled 1-D03 demonstrated MDA-MB-435 saturable binding, which indicated specificity for its target. The combination of specific and high affinity binding of the $^{111}$In-DOTA-conjugated 1-D03 peptide to MDA-MB-435 cells provided the necessary evidence to continue into animal studies.

Nude mice bearing MDA-MB-435 human breast tumor xenografts were used for biodistribution studies with $^{111}$In-DOTA-1-D03. Although MDA-MB-435 human breast cancer cells express low to moderate levels of ERBB2, KCCYSL has been demonstrated to image a range of tumors that express moderate to high levels of ERBB2, including MDA-MB-435, human ovarian OV-CAR 3, and human prostate PC-3 human prostate cancers (48, 73), which express lower levels of ERBB2 than human breast cancer cell lines such as BT-474 and SK-BR-3 (88). Since most human cancers express moderate levels of ERBB2, the MDA-MB-435 animal model was used as a sensitive means to gauge the new imaging peptides (33). In contrast to *in vitro* data, 1-D03 had slightly lower tumor uptake than KCCYSL at both 1 and 2 h post-injection. One reason for the slightly diminished tumor uptake may have been the rapid overall clearance of 1-D03. In fact, despite reduced overall tumor uptake, 1-D03 had an equal tumor to blood ratio at 1 h and a significantly higher tumor to blood ratio at 2 h post-injection compared to KCCYSL. The tumor to blood ratio of 1-D03 at 2 h was 6:1, which compares well with the 7.6:1 tumor to blood ratio of clinically approved octreoscan, and is higher than radiolabeled analogs of minigastrin, bombesin and vasoactive intestinal peptide, all of

which have been examined in human studies (89-92). In addition to rapid blood clearance, non-target organ uptake was significantly reduced in a number of organs at both 1 and 2 h post-injection for 1-D03 in comparison to KCCYSL. When examining non-target uptake, successful imaging peptides share two properties: they minimize exposure of radiosensitive organs and they have limited accumulation in areas surrounding the tissue of interest in order to provide the highest tumor to background ratios possible. 1-D03 exhibited both of these properties. For the radiosensitive organs such as the bone, the tumor to bone ratio was increased from 7:1 to 12:1 for 1-D03 compared to KCCYSL, at 2 h post-injection. The organs surrounding the breast, including the heart and lungs, also displayed significant increases in tumor to organ contrast of 20% and 40%, respectively. Total kidney retention, which can limit the effectiveness of radiolabeled peptides due to toxicity, was also reduced by ~20% in the second generation peptide. These results demonstrate that the *in vivo* phage display affinity maturation did indeed improve KCCYSL pharmacokinetics, in that tumor specificity was enhanced and non-target retention was reduced, which was the goal of the phage display selection.

The most critical component of a targeted peptide is the ability to clearly visualize tumors *in vivo*. In order to analyze its imaging properties, $^{111}$In-labeled 1-D03 was used in SPECT/CT and clearly displayed tumor uptake. Subsequent blocking studies with unlabeled peptide confirmed specificity. Although 1-D03 reduced kidney retention, uptake was still very prominent in the SPECT image. Ultimately, reduction or elimination of kidney uptake by peptide modification would enhance the peptide as both a radioimaging and therapeutic agent. A synergistic effort combining phage display with

successful strategies such as coinjection with cationic amino acids, succinylated gelatin, or bovine serum albumin fragments in addition to spacer or chelate modification could be utilized in future studies (54, 81, 93, 94).

The results presented here demonstrate *in vivo* phage display affinity maturation of a cancer-targeting peptide. Although *in vivo* selection clearly improved the pharmacokinetics of 1-D03, it may be worthwhile to consider the merits of combining both *in vivo* and *in vitro* affinity maturation when modifying a targeted peptide. By combining both techniques in a selection, one may capture the benefits of both the target affinity increase of *in vitro* selections, in addition to the pharmacokinetic enhancements afforded by *in vivo* selection. Such a strategy may in the future produce improvements seen in DOTATOC and ReCCMSH (83, 85).

# Conclusion

To the best of our knowledge, we have demonstrated the first use of i*n vivo* phage display a ffinity m aturation t o i mprove t he pha rmacokinetic pr operties of a n E RBB2-targeted SPECT imaging peptide. Phages and corresponding peptides were evaluated for both E RBB2 a nd hum an br east carcinoma bi nding *in vitro*. O ne p eptide, 1 -D03, wa s radiolabeled w ith $^{111}$In a nd us ed i n bi odistribution a nd S PECT i maging s tudies. 1 -D03 demonstrated improved t umor t o non -target u ptake i n blood, bone , he art a nd l ung i n comparison to the first generation KCCYSL peptide. In fact, tumor to blood ratios were comparable t o t hose f or c linically t ested and a pproved pe ptides. These results i ndicate that *in vivo* phage display can be utilized to optimize the pharmacokinetics of peptides for radioimaging applications. A ccordingly, 1 -D03 may s erve a s a us eful c linical pr obe for ERBB2-expressing malignancies.

## Acknowledgments

The authors would like to acknowledge the contributions of Jessica Newton-Northup, Marie T. Dickerson and the VA Biomolecular Imaging Core. This material is based upon work supported (or supported in part) by the Department of Veterans Affairs, Veterans Health Administration, Office of Research and Development, Biomedical Laboratory Research and Development, Clinical Sciences Research and Development including the Cooperative Studies Program, Rehabilitation Research and Development Service, and Health Services Research and Development through a VA Merit Award (I01BX000964). Additional support provided by an NIBIB Training Grant NIBIB 5 T32 EB004822.

# CHAPTER 3

## Identification of a Peptide from In Vivo Bacteriophage Display with Homology to EGFL6, A Candidate Tumor Vasculature Ligand in Breast Cancer

# Introduction

Much effort has been placed on identifying the process of human tumor vascularization (95). As tumor size increases, new vasculature is required to provide blood flow and nutrients to the growing malignancy, a process termed angiogenesis (96). The network of blood vessels in each organ, including tumors, is differentiated by tissue specific expression of ligands and receptors (97). These proteins serve as a molecular address, and in the case of tumorigenesis, may prove effective for delivery of imaging agents or cytotoxic drugs (98). Although tumor vasculature proteins such as vascular endothelial growth factor, $\alpha_v\beta_3$ integrin, and platelet derived growth factor are well known, resistance to therapies targeting these proteins reveals that tumor vasculature is a complex system that remains incompletely characterized (99). The ability to identify and help validate novel ligands and their corresponding receptors responsible for tumor angiogenesis would prove advantageous. Not only could the ligands serve as potential targeting vectors for imaging applications, but blockade of receptors could prevent increased blood supply for a tumor and limit its growth.

In order to determine novel cancer biomarkers, techniques must be used that illuminate cancer-specific ligands and receptors. Deciphering the differential protein expression between malignant and non-malignant cells is often attempted using high throughput screening methods, due to the complex nature of the tumor microenvironment. One process for identifying novel cancer-specific ligands and

receptors is mRNA profiling, which has been used to identify genes with significantly higher transcription levels in tumors (100-102). Human cancer transcriptional profiles have served to create a reservoir of hypothetical tumor interacting transcripts, encoding for tumor vasculature proteins such as adlican, collagen type-XI alpha-1, glycoprotein M6B and epidermal growth factor-like domain multiple 6 (*egfl6)* (103). The *egfl6* transcript, in particular, was first reported in several fetal tissues and human glioma tumor biopsy samples using a high throughput screening by hybridization technique (104). Recently, several human tumor biopsy transcription analyses have indicated *egfl6* mRNA is expressed at high levels in meningioma, glioma and ovarian and breast carcinomas, while levels in normal tissues were virtually undetectable (20, 100, 102, 105, 106). The reports of tumor specific *egfl6* expression suggest a need for investigation into its possible role in tumorigenesis.

The *egfl6* gene encodes for an approximately 60 kD a secreted protein with epidermal growth factor (EGF) structural homology (107). Although EGFL6 has been detected at the mRNA level in numerous cancers, the protein has not been detected in carcinoma cells and little is understood regarding its *in vivo* function. *In vitro*, full-length recombinant EGFL6 has been demonstrated to induce migration and angiogenesis in endothelial cells through activation of the extracellular signal-related kinase pathway (107). These data suggest that EGFL6 may contribute to vascularization of new and perhaps malignant tissue. However, its roles in both development and tumorigenesis remain unclear.

One method of exploring the vast array of protein interactions and associations in a system such as the tumor vasculature is through bacteriophage (phage) display (40). A

single phage library can contain up to $10^9$ unique peptide sequences, offering a sizeable potential for selection of a peptide fragment of a natural ligand, such as EGFL6, which is thought to be specific to tumor vasculature (72). Previous selections have demonstrated the feasibility of phage-based ligand identification, most notably isolating the peptide RGD (57). The RGD motif was identified in 28 of 32 phage-displayed peptides selected for binding to $\alpha_5\beta_1$ integrin, and consequently demonstrated to have high affinity for a number of integrins, including $\alpha_v\beta_3$ (45, 57). Use of peptide phage display to identify binding epitopes, such as RGD, *in vitro* has spawned investigation into the ability of phage display to isolate tissue and tumor specific peptides *in vivo* (108). *In vivo* phage display has previously identified tumor vasculature-homing peptides, and specific tripeptide sequences have been mapped to the vasculature of numerous human organs (49). Additionally, our laboratory has developed a strategy for isolating not only tumor vasculature but also solid tumor-specific peptides (50). These works indicate that phage can localize specifically to tumors, and recovered phage can be used to identify receptor-binding peptide epitopes.

It was hypothesized that *in vivo* phage display could be used to select peptides which mimic tumor-associated ligands. The peptides would serve not only as tumor imaging vectors but may also be used to help validate novel tumor biomarkers. Phage displayed peptides with homology to a known protein could help validate potential ligands identified by genomic or transcriptomic studies, or elucidate possible proteins underrepresented or absent from traditional proteomic analyses. To test this idea, a phage library was subjected to four rounds of *in vivo* selection in mice bearing human MDA-

MB-435 breast cancer xenografts. Displayed peptides of phages recovered from the tumors were analyzed by the basic local alignment search tool (BLAST). Although a number of peptides matched potential tumor related proteins, one peptide, with 9 of 14 amino acids identical (GTKSKCCYSLRRSS versus GTKLACCYGWRRNS) to EGFL6, was chosen for further study due to its significant homology and the growing evidence that EGFL6 is a potential tumor vasculature ligand. The tumor cell line used for selection, as well as several other cancer and non-cancer cell lines, was probed for mRNA and protein expression of EGFL6. Additionally, the tumor targeting and SPECT imaging properties of the EGFL6 peptide were investigated *in vivo*.

# Materials and Methods

## Materials

Materials for cell culture were purchased from Invitrogen (Carlsbad, CA). Unless otherwise specified, all reagents and materials were obtained from Sigma Chemical Co. (St. Louis, MO).

## Mouse Strains and Handling

Four- to 6-week-old severe combined immunodeficient (SCID) outbred mice (Taconic, Germantown, NY) were maintained in approved pathogen-free institutional housing. Animal studies were conducted as outlined in the NIH Guidelines for the Care and Use of Laboratory Animals and the Policy and Procedures for Animal Research of the Harry S. Truman Veterans Memorial Hospital. MDA-MB-435 human breast cancer xenografts ($5 \times 10^6$) were established by subcutaneous injection into the flank of SCID mice. Mice were utilized when visual tumors (~1-3$mm^3$) formed after approximately 5 weeks.

## Phage Display Selection and Analysis

*In vivo* phage display was performed as described previously (50). Briefly, a phage library containing approximately $1x\ 10^{12}$ tetracycline transducing units of phage was injected into SCID mice bearing MDA-MB-435 human breast cancer xenografts. Phages were allowed to circulate for 1 h and following perfusion with phosphate buffered

saline (PBS), tumors were excised and frozen in liquid nitrogen. Tumors were manually homogenized and bound phages eluted by incubation with 2.5 % (w:v) 3-[(3-cholamidopropyl)dimethylammonio]-1-propanesulfonate (CHAPS) solution. Recovered phages were used to infect log phase K91BK *E. coli* cells, amplified for 16 h in a 37°C incubator with shaking and purified by polyethylene glycol/sodium chloride precipitation (76). Purified phages were quantified and used for subsequent rounds of selection, for a total of four selection rounds. Following the final round of selection, individual phages were isolated and their relevant DNA was sequenced in order to ascertain the displayed foreign peptide of each phage. Peptide sequences were then queried using the BLAST search program for sequence homology to proteins with known or putative cancer correlations (77).

**EGFL6 RT-PCR**

In order to assay *egfl6* mRNA expression, three human breast cancer cell lines, MDA-MB-435, MDA-MB-468, SK-BR-3, and a normal cell line HEK-293, were grown to 80% confluency in T75 flasks and their RNA was isolated using Trizol (Ambion, Life Technologies, Grand Island, NY). Total RNA was quantified by spectrophotometry and 500 ng was reverse transcribed to cDNA using SuperScript III Reverse Transcriptase (200 units/μL) and oligodT primers (2.5 μM) (Life Technologies, Grand Island, NY). The subsequent cDNA was utilized for PCR reactions with *egfl6* specific primers previously demonstrated to amplify the gene of interest (104). The primers [(5'-CGGGATCCCTGTGCTACGTCGCCCTGGAC- 3') and (5'-CGGAATTCACTGGCGCAGGCGGTGATCTCCTT-3')] were diluted to 10 μM and

added to 2 µL of cDNA for the reaction. The cycling conditions were 98°C for 30 s for one cycle, followed by 30 cycles of 98°C for 10 s, 60°C for 30 s and 72°C for 30 s. Primers for beta-actin were used as a loading control. PCR products were run on 1% agarose gels and visualized by ethidium bromide staining.

**Immunoassay**

Each cell line was analyzed by immunoassay for EGFL6 protein expression in the cell lysate and supernatant using a polyclonal anti-EGFL6 antibody (Prestige Antibodies, Sigma, St. Louis, MO). Cells were grown to 80% confluency, supernatant harvested and both cells and supernatant were incubated with Laemmli buffer (2% w:v sodium dodecyl sulfate, 10% glycerol, 60 mM Tris, 0.01% bromophenol blue). Protein concentrations were determined by Bio-Rad protein assay (Bio-Rad, Hercules, CA) and 500 µg of total protein was incubated with NuPAGE LDS sample buffer (Life Technologies, Grand Island, NY) at 80°C for 10 min and loaded onto NuPAGE Novex 4-12% Bis-Tris gels. Samples were electrophoresed for 90 min at 120 mV and transferred to 0.2 µm nitrocellulose membrane (Bio-Rad, Hercules, CA). Following transfer, membranes were blocked with 5% non-fat dry milk. Blocked membranes were incubated with anti-EGFL6 antibody diluted 1:50 in Tris buffered saline and 0.1% Tween-20 (0.1% TBST) for 10 min and vacuum aspirated by SNAP i.d. (Merck Millipore, Billerica, MA). Membranes were washed three times with 0.1% TBST and polyclonal anti-rabbit horseradish peroxidase-conjugated antibody diluted 1:1000 in 0.1% TBST was incubated with the membrane for 10 min. Vacuum aspiration and washing were completed as with the primary antibody. Membranes were developed using SuperSignal West Pico

chemiluminescent substrate (ThermoFisher Scientific, Rockford, IL) and visualized using a VersaDoc Molecular Imager (Bio-Rad, Hercules, CA).

**Peptide Synthesis**

Synthesis of all peptides was accomplished with an Advanced Chem Tech 396 multiple peptide synthesizer using solid phase FMOC chemistry. Peptides were designed with an N-terminal GSG peptide spacer covalently linked at its N-terminus with biotin or 1,4,7,10-tetraazacyclododecane-1,4,7,10-tetraacetic acid (DOTA) (Macrocyclic, Inc. Dallas, TX).

**Biotinylated Peptide Fluorescent Microscopy**

All cell lines were grown to 80% confluency and fixed with 4% paraformaldehyde. Cells were dried onto microscope slides overnight followed by rehydration with PBS. Slides were blocked with 5% BSA in PBS for 2 h at room temperature. Biotinylated EGFL6 peptide was diluted to 10 µM in PBS and 100 µL was added to each cell sample for incubation at room temperature for 1 h. Slides were washed 3 times with 0.1% TBST and cells were incubated with Neutravidin Texas Red (Life Technologies, Rockville, MD) diluted to 5 µg/mL in 0.1 % TBST for 1 h at room temperature. Washing was performed in the same manner and cells were visualized by an epifluorescent Nikon T1-SM inverted microscope (Nikon, Melville, NY).

## DOTA-EGFL6 Radiolabeling and Purification

DOTA-EGFL6 was diluted to 1 mg/mL in water and incubated with 0.1 M ammonium acetate (pH 5) and 18.5 MBq of $^{111}$In at 80°C for 1 h. Reactions were quenched by addition of 10 µM EDTA. Radiolabeled peptide was purified by reverse phase HPLC using a linear gradient of acetonitrile plus 0.1% trifluoroacetic acid from 5-95% over 35 min. Acetonitrile was evaporated by nitrogen gas flow, and peptide was diluted to appropriate concentration using sterile PBS.

## $^{111}$In-DOTA-EGFL6 Cell Binding

MDA-MB-435, MDA-MB-468, SK-BR-3 and HEK-293 cells were diluted to $2x10^6$ cells/mL in Dulbelco's modified eagle medium (DMEM) with 0.1 mg/mL BSA. $^{111}$In-DOTA-EGFL6 was diluted to $1x10^7$ CPM/mL in DMEM plus 0.1% BSA and 100 µL of peptide was added to 200 µL of cells and incubated at 37°C for 1 h. Cells were washed three times with ice-cold PBS with 1% BSA and counted via gamma counter.

## $^{111}$In-DOTA-EGFL6 Biodistribution and MicroSPECT/CT Imaging

DOTA-EGFL6 peptide was radiolabeled with $^{111}$In and purified peptide was prepared at 1.85 MBq/mL in sterile PBS. Three mice bearing MDA-MB-435 tumors were intravenously injected with $^{111}$In-DOTA-EGFL6 and sacrificed at 2 h. Organs and tissues pertinent to tumor uptake and clearance were excised, weighed, and counted by gamma counter. Percentage of injected dose per gram (%ID/g) of tissue was reported to normalize uptake by tissue mass.

Radiolabeled, purified $^{111}$In-DOTA-GSG-EGFL6 was diluted to 11.1 MBq in 100 µL of sterile PBS. The peptide was injected intravenously in a mouse bearing an MDA-MB-435 human breast cancer xenograft. Following injection, radiolabeled peptide was permitted to circulate for 2 h, followed by euthanization by carbon dioxide. The treated mouse was imaged at the Harry S. Truman Veterans Memorial Hospital Biomolecular Imaging Center. Overnight (7 h) image acquisition was performed with a Siemens Inveon Micro-SPECT/CT (Siemens, Knoxville, TN) equipped with mouse whole body 1.0 mm collimators. Data were processed with Inveon Research Workplace processing software and fan beam (Feldkamp) filtered back projection algorithms were used for reconstruction of the CT tomographic image.

# Results

## Phage Display Selection and Analysis

Completion of four rounds of *in vivo* phage display selection resulted in a sub-population of presumed human breast tumor-avid phage clones. DNA sequence corresponding to the foreign displayed peptide of 269 tumor avid phages was obtained and analyzed by the BLAST algorithm for homology to human cancer-related proteins (77). For each peptide sequence, the top 10 matching proteins were evaluated for percent homology and previous identification as a cancer-related or putative cancer-related protein. One displayed peptide, from the phage clone 3-G03, revealed 64% identical homology to a protein termed EGFL6 (Figure 3.1). The match returned a score of 24.0 bits consisting of 9/14 positive identities and 0 gaps. The match returned an expected value of 4.9, indicating that random assignment of amino acids would only return approximately 5 random matches in the entire protein database. No other sequence returned a cancer-related protein and had sequence similarity greater than 50%.

## EGFL6 RT-PCR and Immunoassay

Due to the significant homology of the phage displayed peptide to EGFL6, it was inferred that the MDA-MB-435 cell line used for xenograft establishment for the *in vivo* phage display selection expressed EGFL6. In order to confirm *egfl6* transcription, RT-PCR was performed. Additionally, two more breast cancer cell lines, MDA-MB-468 and SK-BR-3, and a non-cancer cell line, HEK-293, were also assessed. PCR products from

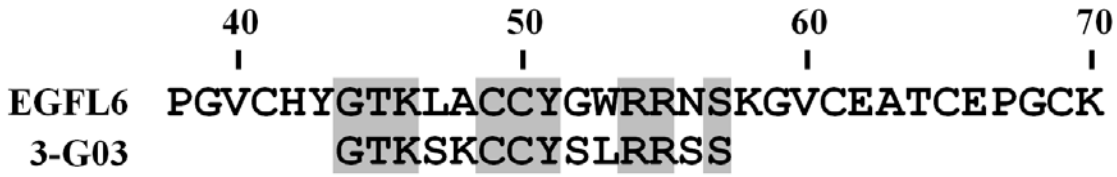


**Figure 3.1** The *in vivo* selected peptide 3-G03 was aligned with EGFL6 for sequence comparison. A portion of the full length EGFL6 protein corresponding to the homologous selected peptide is displayed, with the hashed numbers representing the amino acid position from the N-terminus. Identical matches are highlighted.

EGFL6 specific primers first used to identify the mRNA were visualized by ethidium bromide stain in agarose gel (104). The results demonstrated a band corresponding to the expected fragment size of 801 nucleotides in the lane corresponding to MDA-MB-435 cDNA and a fainter band in the lane containing cDNA from MDA-MB-468 cells (Figure 3.2). No band was identified in the SK-BR-3 and HEK-293 lanes. Loading controls were accomplished using beta actin-specific primers producing a 315 nucleotide band, which was found in similar intensity in all cell lines analyzed.

Identification of *egfl6* at the mRNA level provided impetus to analyze protein expression of each cell line. Since EGFL6 is a secreted protein, both the cells and the cultured supernatant were used for immunoblotting (Figure 3.3). A band was identified in the supernatant of MDA-MB-435 cells that corresponded to the expected molecular weight of EGFL6, ~66 kDa. No band was detected in the supernatant of all other cell lines, nor the cell pellet of any cells examined, including MDA-MB-435.

**Biotinylated EGFL6 Peptide Fluorescent Microscopy**

In order to confirm EGFL6 peptide affinity for MDA-MB-435 cells, the peptide sequence of EGFL6 (GTKWACCYGWRNSS) directly corresponding to the identified phage displayed peptide was synthesized and conjugated at the N-terminus with biotin for detection by a fluorophore labeled streptavidin. Peptide binding was analyzed in the same four cell lines, MDA-MB-435, MDA-MB-468, SK-BR-3 and HEK-293, used for RT-PCR and immunoassay experiments. The results demonstrated the peptide bound strongly to MDA-MB-435 and MDA-MB-468 cells, while showing less binding to SK-BR-3 cells and no binding to HEK-293 cells (Figure 3.4).

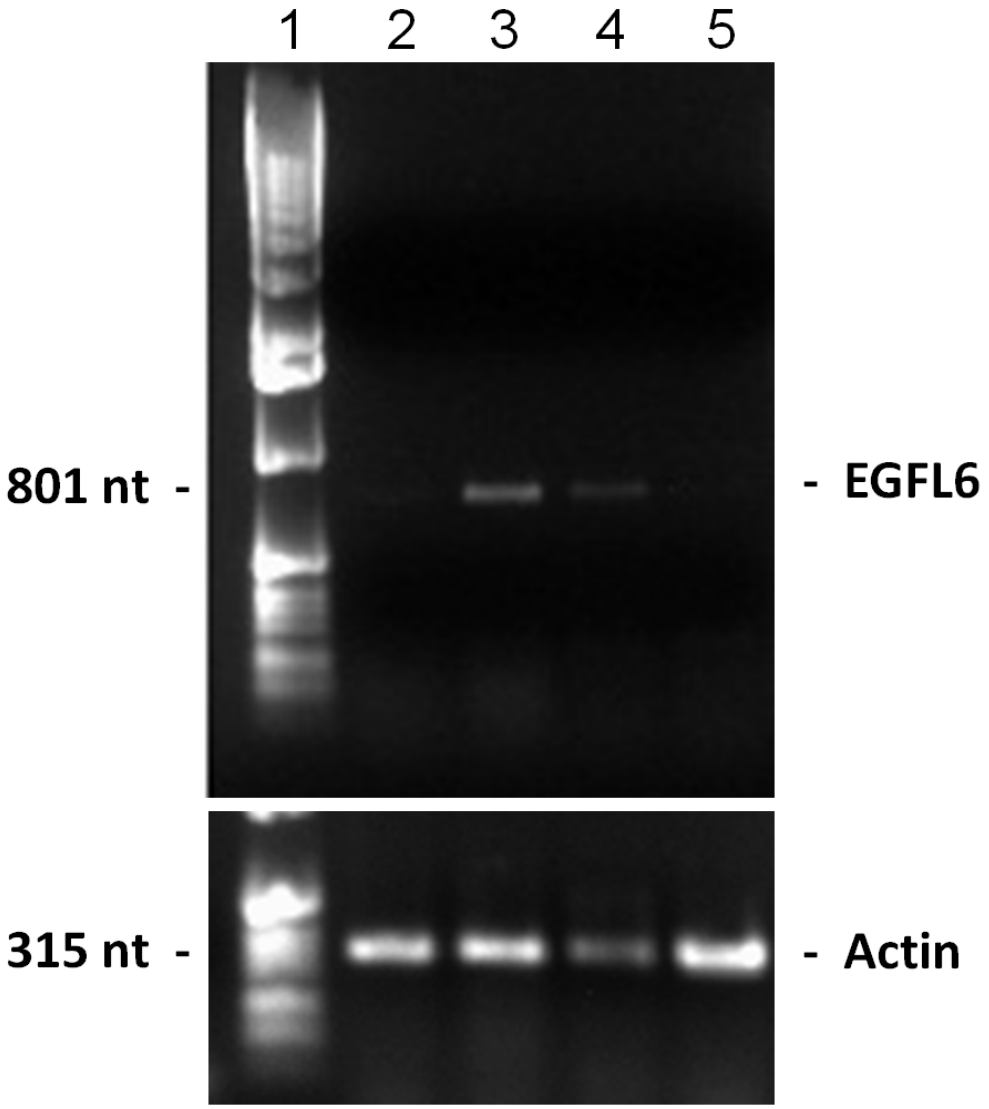


**Figure 3.2**

Isolated RNA from 3 human breast cancer cell lines and one human kidney cell line was reverse transcribed and amplified using EGFL6-specific primers. Bands of the expected nucleotide length were detected in MDA-MB-435 and MDA-MB-468 samples. Additionally, a primer for β-Actin was used as a loading control. Numbered lanes represent the following: 1) Ladder, 2) SK-BR-3, 3) MDA-MB-435, 4) MDA-MB-468, 5) HEK-293.

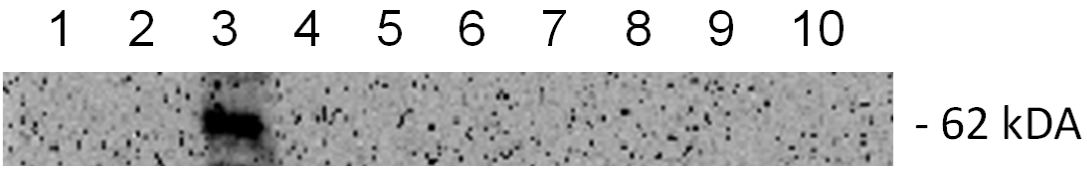


**Figure 3.3** Total protein from cell lysates and cultured medium from corresponding cells were run on SDS-PAGE gels, transferred to nitrocellulose, and EGFL6 detected by immunoblot. One band was detected at the expected molecular weight for EGFL6 in the cultured supernatant of MDA-MB-435 cells. Numbered lanes represent the following: 1) Ladder, 2) MDA-MB-435 cell lysate, 3) MDA-MB-435 supernatant, 4) MDA-MB-468 cell lysate, 5) MDA-MB-468 supernatant, SK-BR-3 cell lysate, 6) SK-BR-3 supernatant, 7) HEK-293 cell lysate, 8) HEK-293 supernatant, 9) ladder, 10) loading buffer.

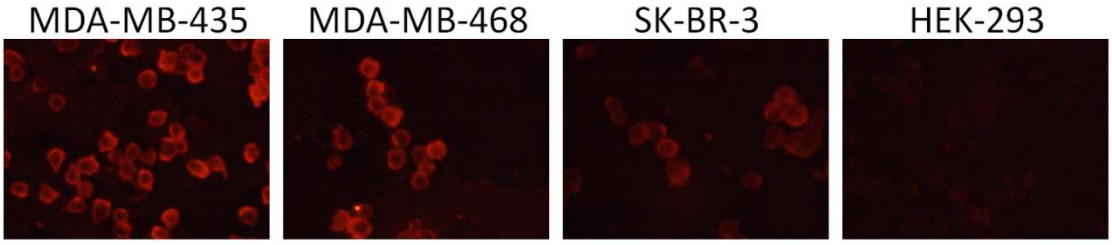


**Figure 3.4** Human breast cancer and kidney cells were incubated with biotinylated peptides and visualized by fluorescent Neutravidin. Fluorescent signal was detected in MDA-MB-435 and MDA-MB-468 cells, but not in SK-BR-3 or HEK-293 cells.

## $^{111}$In-DOTA-EGFL6 Cell Binding

After confirmation of cell binding with biotinylated peptide, the peptide was conjugated to the macrocyclic chelator DOTA for radiolabeled peptide binding assays. Radiolabeled peptide was examined for its ability to bind MDA-MB-435, MDA-MB-468, SK-BR-3 and HEK-293 cells. Peptide binding was determined to be 12.3±1.0% (12284 CPM) of total peptide added for MDA-MB-435, 10.5%±2.7% (10508 CPM) for MDA-MB-468, 4.7±0.2% (4731 CPM) for SK-BR-3 and 5.4±0.5% (5411 CPM) for HEK-293 cells (Figure 3.5). The binding of $^{111}$In-DOTA-EGFL6 was significantly higher to MDA-MB-435 than SK-BR-3 ($P < 0.001$) and HEK-293 ($P < 0.001$) cells. Peptide binding was similar between MDA-MB-435 and MDA-468 cells and binding to MDA-MB-468 cells was also significantly higher ($P < 0.05$) than binding to SK-BR-3 or HEK-293 cells.

## $^{111}$In-DOTA-EGFL6 Biodistribution

$^{111}$In-DOTA-EGFL6 binding to MDA-MB-435 cells *in vitro* warranted *in vivo* analysis of the tumor targeting and non-target organ accumulation of EGFL6. In order to ascertain a preliminary understanding of the biodistribution, the pharmacokinetics of the peptide were analyzed at 2 h post-injection (Figure 3.6). Tumor uptake of the radiolabeled peptide was 0.36± 0.08 % ID/g, while blood retention of the peptide was 1.30±0.51 % ID/g. Non-target organ accumulation was below 1.0 % ID/g for all organs measured, except for the kidneys. Kidney retention of the peptide was 28.61±4.24 %ID/g. The tumor to blood ratio of the peptide was 0.27, while the tumor to muscle ratio was 2.7.

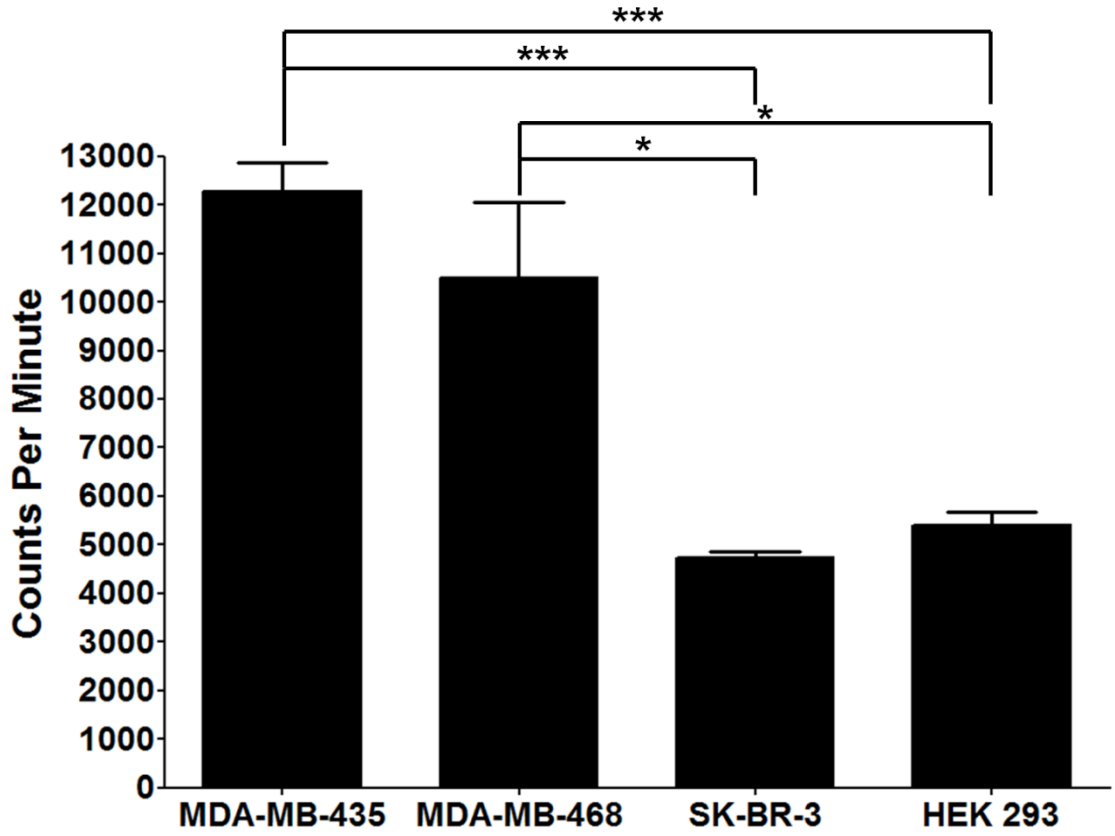


**Figure 3.5** $^{111}$In-DOTA-EGFL6 peptide was incubated with cell lines and binding was quantified. The peptide bound to MDA-MB-435 and MDA-MB-468 cells significantly higher than SK-BR-3 and HEK-293 cells. Error bars represent the standard deviation of 4 samples. *- $P < 0.05$ *** - $P < 0.001$

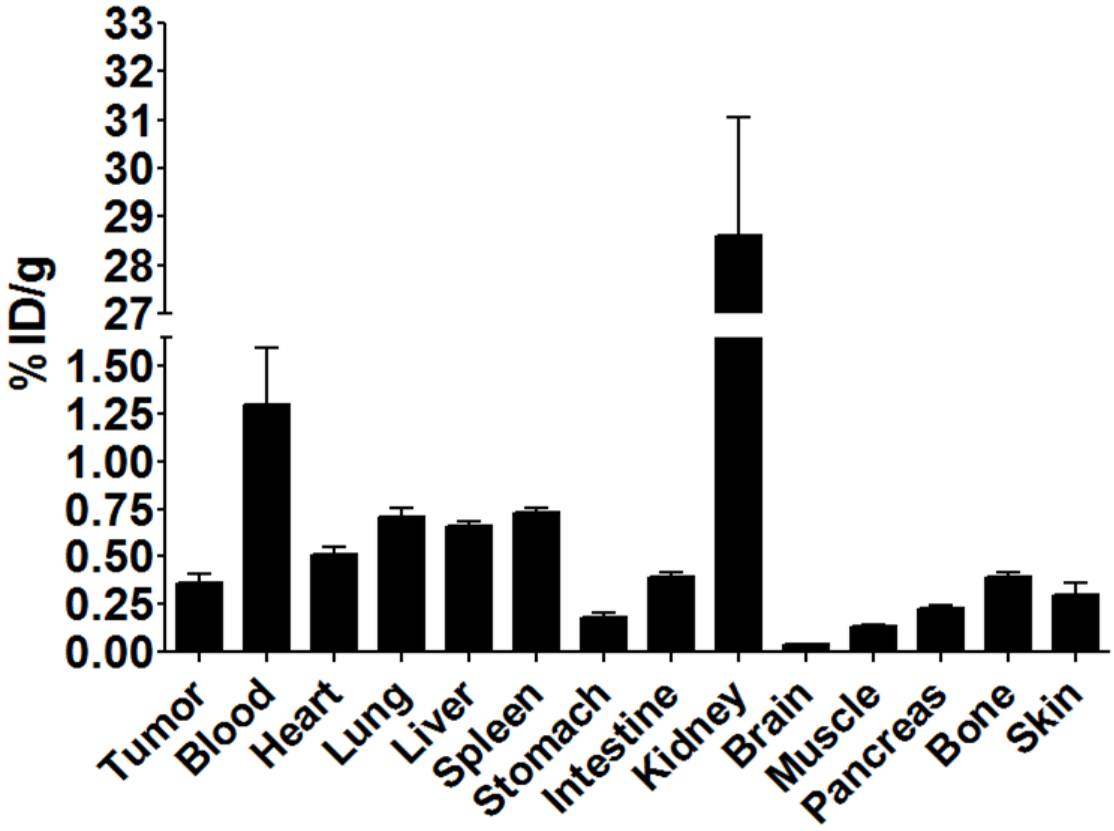


**Figure 3.6** $^{111}$In-DOTA-EGFL6 was injected into mice bearing MDA-MB-435 human breast cancer xenografts. Tissue biodistribution was analyzed 2 h post injection. Bars represent the mean of n=4 and error bars signify the standard deviation. %ID/g – percent injected dose/gram.

## $^{111}$In-DOTA-GSG-EGFL6 SPECT/CT Imaging

In addition to biodistribution, tumor imaging capabilities of $^{111}$In-DOTA-GSG-EGFL6 were explored. SPECT/CT images were collected at 2 h post-injection in order to correspond with the biodistribution data (Figure 3.7). Imaging revealed low tumor uptake, however, the interface between the xenograft and the muscle of the mouse had a strikingly high concentration of radiolabel. Kidney retention was also visible in the mouse, in addition to apparent cranio-facial, esophageal, and stomach intake, consistent with incidental ingestion of the radiolabeled peptide following oral cleaning of the injection site.

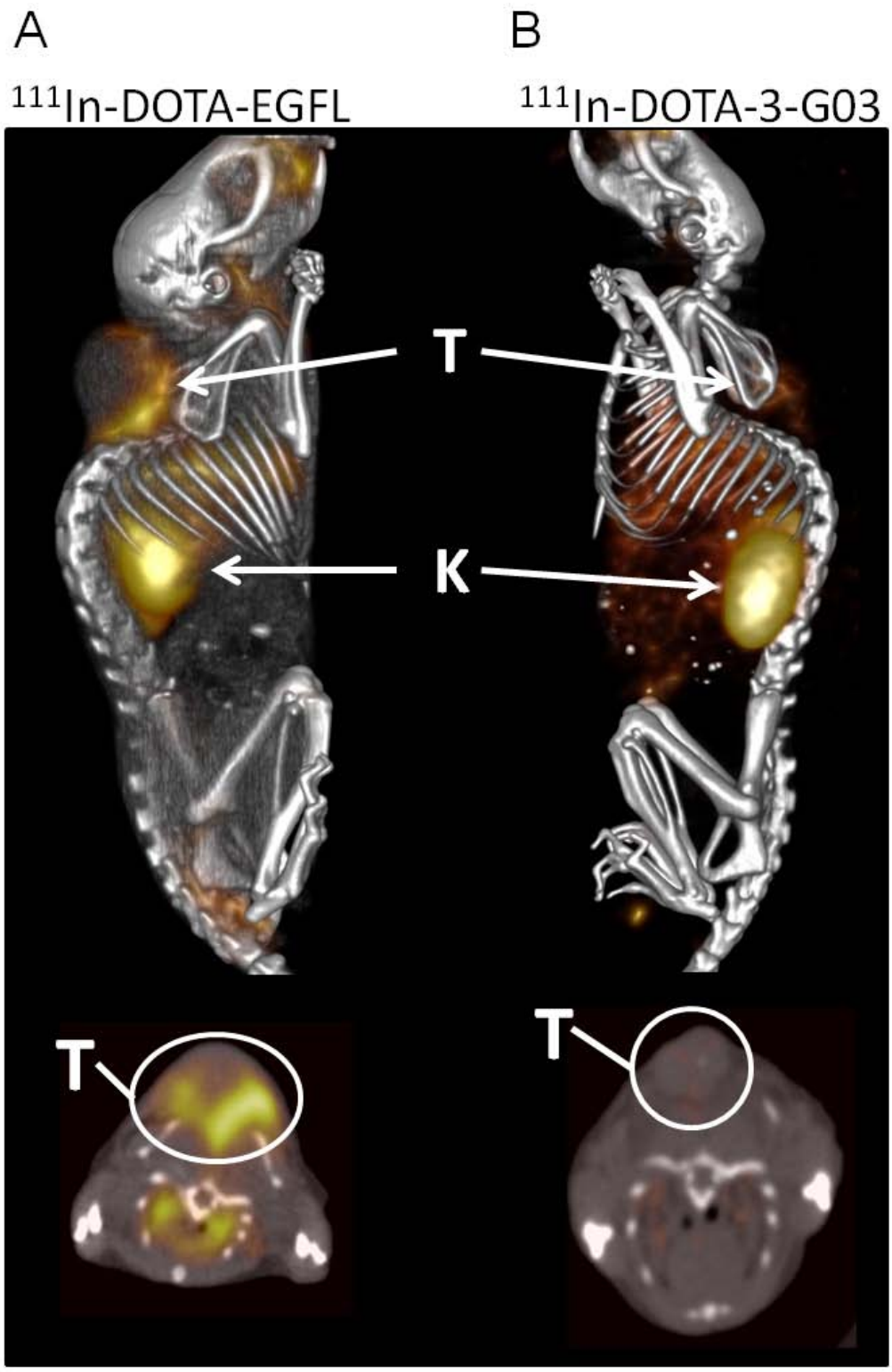
A
B
$^{111}$In-DOTA-EGFL
$^{111}$In-DOTA-3-G03
T
K
T
T

**Figure 3.7** $^{111}$In-DOTA-EGFL6 and $^{111}$In-DOTA-3-G03 were injected into MDA-MB-435 human breast carcinoma tumor bearing mice. SPECT/CT imaging was acquired 2 h post-injection. Uptake of $^{111}$In-DOTA-EGFL6 is consistent with tumor vasculature accumulation. Sequence specificity of the EGFL6 peptide was confirmed by using the 3-G03 peptide, which differs by only 5 amino acids. 3-G03 did not have a tumor uptake pattern similar to EGFL6, but did show similar kidney uptake, which is typical of radiolabeled peptides.

# Discussion

Angiogenesis in cancer is a key component of tumor progression and, as such, has received much attention in both basic and translational research. Clinically-approved drugs including bevacizumab (Avastin®; Genentech) and sunitinib (Sutent®; Sugen) in addition to counterparts in clinical trials, including VEGF-Trap$_{R1R2}$ (Aflibercept; Regeneron Inc.) and vendatanib (Caprelsa; AstraZeneca), illustrate the major emphasis placed on preventing tumor angiogenesis (109-112). Unfortunately, response to current anti-angiogenic therapy is generally transient, and relapse is common (113). One hypothesis for the eventual ineffectiveness of anti-angiogenic therapy is circumvention of therapeutic blockade by upregulation of complementary growth factors and receptors, such as EGFR and fibroblast Bv8 (114, 115). Identification of the potential ligands that promote tumor angiogenesis is necessary to help overcome resistance to current therapies. Although the list of tumor-associated ligands is extensive, it is unlikely to be complete (95).

Proteins involved in tumorigenesis can be identified at three levels: the genome, transcriptome and proteome. While high throughput DNA, RNA and protein expression interrogation techniques provide unique advantages including large sample size, quantification and breadth of results, each by itself is incomplete. Genetic differences may not be transcribed, transcriptional differences may not be translated, and proteomic differences may be too small to be distinguished. Additionally, *ex vivo* analysis cannot directly investigate physiological location or function. In order to supplement these

techniques, a method, such as *in vivo* phage display, can be used to explore protein interactions in a physiological environment. *In vivo* phage display has been utilized previously to map vascular signatures and identify novel tumor-associated proteins, such as proteome activator complex 28 and plectin-1 (49, 58, 116). *In vivo* phage display provides two key supplementary features to current high throughput screening techniques: the ability to identify proteins that are expressed at low levels and not likely to be recognized by proteomic procedures, and the potential to identify targets that are biologically accessible for targeted imaging and therapy. Therefore, it was hypothesized that an *in vivo* phage display selection could identify tumor associated ligands by isolation of peptides with a similar sequence and function.

The *in vivo* selection enabled identification of peptides with tumor imaging capabilities in addition to providing an opportunity to explore whether peptides were similar to sequences of known or putative cancer proteins. Peptides corresponding to 267 phage clones recovered from human breast cancer xenografts were analyzed by the BLAST algorithm for homology to known cancer-related proteins. Since the sequences being analyzed were relatively short (15 amino acids), it was necessary to arbitrarily limit the scope of what was considered a match to greater than 50% homology. This greatly reduced the number of artificial hits that would be generated by random chance. Of the 267 peptides analyzed, only one, 3-G03, fit the criteria specified. 3-G03 (GTKSKCCYSLRRSS) matched a secreted protein, EGFL6 (GTKLACCYGWRRNS), with 64% homology and returned a score of 24 bits, primarily due to the number of identical matches (9) and the absence of gaps needed to make the identical pairs. It was interesting to note that the 9 identical pairs consisted of 2 tripeptide sequences, and an

additional 4 peptide sequence with one mismatch. This is consistent with previous selections that have identified three amino acid sequences capable of mediating interaction between a ligand and a receptor, as is the case of RGD and several integrins (57). Furthermore, tripeptide motifs have been demonstrated to target phage to specific organs *in vivo*, including the tumor vasculature (49). The high homology between 3-G03 and EGFL6, in addition to the potential tumor vasculature promoting properties of the protein, led to further investigation into EGFL6 expression and peptide characterization.

Because a peptide with homology to EGFL6 was identified by the *in vivo* selection, it was assumed that the xenografted breast cancer cell line expressed EGFL6. For confirmation, RT-PCR was used to analyze *egfl6* transcription in three breast cancer cell lines and a control cell line. The results confirmed that *egfl6* was expressed in MDA-MB-435 cells, in addition to MDA-MB-468 cells, although at apparently lower levels. This result was consistent with identification of *egfl6* expression in biopsy samples from ovarian and breast cancer, as well as meningioma (100, 102, 106).

While *eglf6* mRNA has been identified, EGFL6 protein has not been confirmed in cultured carcinomas. In order to verify the *egfl6* transcript was translated, an immunoassay probing EGFL6 expression was performed. EGFL6 is a secreted protein; therefore immunoassay was performed on both the cultured supernatant and cell pellet of all cell lines previously analyzed. Interestingly, EGFL6 protein was only identified in the supernatant of MDA-MB-435 cells and not in MDA-MB-468 cells. Lack of detectable protein in MDA-MB-468 cells could have resulted from the protein concentration being undetectable by immunoassay, which is feasible due to the apparent diminished amount of mRNA detected by RT-PCR. Also EGFL6 translation in MDA-MB-468 cells may

have been disrupted, as protein production in cancer cells has been demonstrated to be aberrant (117, 118). Additionally, the protein may be degraded rapidly under *in vitro* conditions by the cells. Detection of EGFL6 protein expression in cultured MDA-MB-435 cells confirmed the assumption that EGFL6 was expressed by the cell line used in the *in vivo* selection and provided motivation to further investigate the properties of the EGFL6 peptide.

Although EGFL6 protein expression was demonstrated by immunoblot, the affinity and specificity of the corresponding EGFL6 peptide for human breast carcinomas needed to be assessed. The exact peptide sequence for EGFL6 corresponding to the phage displayed homologue was selected for analysis. This approach was chosen to maximize the possibility that the properties of the peptide were mediated by the natural EGFL6 sequence, and not selected by phage display. EGFL6 peptide was chemically synthesized with a covalently linked biotin to determine *in vitro* peptide specificity for the cell lines previously analyzed. Fluorescence microscopy revealed strong binding to MDA-MB-435 and MDA-MB-468 human breast cancer cells. Binding was undetectable to SK-BR-3, a third human breast cancer cell line, and HEK-293 human kidney cells. Peptide affinity for the carcinomas corresponded with cell lines that expressed *egfl6* mRNA, even though the protein expression would suggest binding in only MDA-MB-435 cells. The receptor for EGFL6 is not known; therefore it is impossible to predict how the peptide or protein may bind to cells. A correlation between peptide binding and *egfl6* mRNA expression suggests that peptide uptake may predict cellular expression of the *egfl6* transcript. Obviously a short peptide sequence cannot fully mimic a full-length protein, which may

contain several domains, post-translational modification sites and tertiary structure (104, 107).

Identification of a peptide that bound to human breast carcinoma cells expressing EGFL6 offered the potential that the EGFL6 peptide could be used *in vivo* to detect tumorigenesis in xenografts expressing the potential tumor vasculature ligand. To evaluate the biodistribution and imaging properties of the EGFL6 peptide, it was necessary to conjugate the peptide to a radiometal chelator. Bifunctional macrocyclic DOTA was chosen due to its stable chelation with a number of radiometals, including indium-111, and well understood *in vivo* properties (47, 53, 73). Prior to *in vivo* studies, retained specificity and affinity of the radiolabeled peptide was monitored by *in vitro* cell binding. $^{111}$In-DOTA-EGFL6 bound to MDA-MB-435 and MDA-MB-468 cells significantly higher than SK-BR-3 or HEK-293 cells, confirming retention of the breast cancer targeting properties of the peptide.

Radiolabeled, purified $^{111}$In-DOTA-EGFL6 was injected into mice bearing MDA-MB-435 human breast cancer xenografts for biodistribution studies. Surprisingly, tumor uptake was low at 0.36± 0.08 %ID/g. The tumor to blood ratio was also suboptimal at 0.27, but a tumor to muscle ratio of 2.7 indicated specificity for the tumor. A corresponding SPECT/CT image was acquired for further insight into the low tumor uptake. Image analysis correlated with the results of the biodistribution. Although the solid tumor lacked significant uptake of $^{111}$In-DOTA-EGFL6, there appeared to be a high concentration at the interface of the tumor and the site of xenograft formation, presumably a sight of high neovascularization (119). The SPECT/CT image was consistent with other vasculature-targeted imaging agents, such as radiolabeled RGD

peptide (120). Absence of solid tumor-retention could be the result of peptide binding to its target at the novel vasculature and not permitting further diffusion into the tumor (56). Another reason for low tumor uptake might be differential expression of the receptor for EGFL6 *in vitro* and *in vivo*. *In vivo* expression of the receptor may be limited to cells near the site of neovascularization, thus limiting uptake to the interface of tumor and normal endothelial cells (56). Previous work had demonstrated the phage selected peptide, 3-G03, bound to MDA-MB-435 cells *in vitro*, and its sequence similarity to EGFL6 made $^{111}$In-DOTA-3-G03 a unique control to determine whether the precise EGFL6 sequence was necessary for its *in vivo* imaging properties. While a very slight tumor uptake was observed for $^{111}$In-DOTA-3-G03, the distinct vasculature-like binding observed with $^{111}$In-DOTA-EGFL6 was not present in the $^{111}$In-DOTA-3-G03 images. Kidney uptake, which is not sequence specific and instead a result of filtration of low molecular weight peptides, was present for both peptides. SPECT/CT imaging revealed that EGFL6 was targeted to the tumor-epithelial interface of human breast carcinoma xenografts, and the binding was specific to the EGFL6 peptide sequence.

# Conclusion

An *in vivo* phage display selection resulted in the identification of a potential tumor vasculature ligand, EGFL6. Additionally, a peptide with homology to EGFL6 was radiolabeled with $^{111}$In and used to image tumor vasculature by SPECT/CT. This data presents evidence that EGFL6 should be further investigated for its roles in tumorigenesis and as a possible imaging agent.

## Acknowledgments

The authors would like to acknowledge the contributions of Jessica Newton-Northup, Marie T. Dickerson and the VA Biomolecular Imaging Core. This material is based upon work supported (or supported in part) by the Department of Veterans Affairs, Veterans Health Administration, Office of Research and Development, Biomedical Laboratory Research and Development, Clinical Sciences Research and Development including the Cooperative Studies Program, Rehabilitation Research and Development Service, and Health Services Research and Development through a VA Merit Award (I01BX000964). The work is also supported by an NIH R21 grant (1R21CA179069-01). Additional support provided by an NIBIB Training Grant NIBIB 5 T32 EB004822.

# CHAPTER 4

## Development of a Peptide by Phage Display for SPECT Imaging of Resistance-Susceptible Breast Cancer

# Introduction

The ability to detect malignant tissue non-invasively remains an important factor in diagnosing and treating carcinomas, including breast cancer. Traditionally, methods of diagnosis, such as mammography and $^{18}$F-fluorodeoxyglucose positron emission tomography, are used to identify areas of malignancy. Other targeted imaging agents, including radiolabeled peptides for single photon emission computed tomography (SPECT/CT), have been incorporated in diagnostic procedures to not only precisely pinpoint tumors, but also provide biologically relevant information about the malignancy non-invasively (32). Additionally, molecular characterization of the tumor often dictates the course of treatment. For example, breast cancers that express the estrogen receptor and the receptor tyrosine kinase ERBB2 are often treated with the estrogen receptor antagonist tamoxifen and anti-ERBB2 antibody trastuzumab in combination with a chemotherapeutic agent (121, 122). Despite the success accomplished using these treatment strategies, a major obstacle is the occurrence of resistance to the targeted therapies, with 30% developing tamoxifen resistance, and greater than 50% developing trastuzumab resistance (123, 124). A targeting agent with the ability to distinguish cancers prone to develop resistance would greatly aid in the direction of treatment strategies.

Currently, there is no predictive diagnostic agent to assess resistance to targeted therapies. In order to develop an imaging agent capable of detecting carcinomas susceptible to therapeutics such as tamoxifen and trastuzumab, a proper animal model of breast cancer expressing the estrogen receptor and ERBB2 that can be investigated *in vivo* and accurately mimicked *in vitro* is needed. A breast cancer cell line that forms reliable tumors in a mouse, expresses both the estrogen receptor and ERBB2 at physiologically relevant levels, and has been shown to develop resistance to therapies such as tamoxifen and trastuzumab could potentially serve as a template for resistance-susceptible breast cancer. When choosing an applicable cell line for targeted therapy resistance, the most often used human breast cancer cell lines that form tumors in mice can be surveyed for estrogen receptor and ERBB2 status. It is well established that T47D and MCF7 cell lines, which are estrogen receptor positive, do not express ERBB2 (125, 126). Likewise, SK-BR-3 and MDA-MB-453 cells over-express ERBB2 but lack detectable estrogen receptor (126). However, BT-474 human breast cancer cells are estrogen-dependant, over-express ERBB2 and form tumors in mice (127, 128). Although estrogen dependant, BT-474 tumors are naturally resistant to tamoxifen, a widely used anti-estrogen therapy (129). Tamoxifen resistance is thought to be mediated by the over-expression of ERBB2, a major driver of breast cancer (123). Trastuzumab, a humanized monoclonal antibody, has been successfully used for treating approximately 50% of cancers that over-express ERBB2 (121). Interestingly, BT-474 cells have been demonstrated to develop resistance to trastuzumab (124). The BT-474 cell line, therefore, offers a unique opportunity as a target for developing an imaging agent capable of detecting breast carcinomas susceptible to resistance to multiple targeted therapies,

namely tamoxifen and trastruzumab. A targeted agent specific for BT-474 breast cancer may offer a novel method of identifying resistance susceptible cancers prior to treatment.

Bacteriophage ( phage) display has been used to successfully select imaging agents, such as peptides, with the affinity and specificity to image human cancer *in vivo* (86). Following the discovery that phages tolerate insertion of foreign peptide sequences while retaining the functions of infection and replication, phage display has been used to identify peptides from a library of random sequences based on a desired target (40). The power of phage display is derived from the ability to test up to $10^9$ unique phage displayed sequences simultaneously for the optimal peptide based on a desired function. Phages are incubated with a target, allowing a portion to bind, while the unbound phages are removed. Although only a small portion may bind to the target, the recovered phages are exponentially increased by propagation in a host bacterial cell. The enriched subpopulation is then subjected to a subsequent round of selection, providing an enhanced level of competition due to the increased number of target-avid clones represented in the total phage population. Following a number of rounds of selection, the output of phage generally represents the fittest clones for the desired function. This process can be used to identify peptides which bind specifically to an antigen which is expressed or over-expressed in cancer, in addition to identifying peptides specific for breast cancer cell lines (130). Phage display has been used *in vitro* to identify peptides which bind to a host of antigens and image tumor cells *in vivo*, including integrins, receptor tyrosine kinases, and carbohydrate antigens (43-45).

*In vivo* phage display provides the combinatorial power of a traditional selection, while offering unique advantages. By probing a tumor in the context of a living system,

antigens are more likely to be presented in the manner in which they would be found in a patient. The selection is favorably biased towards antigens that are accessible to the tumor vasculature, which may differ from those identified *ex vivo* or *in vitro* (49). An additional benefit is that peptides must successfully avoid binding to antigens displayed in non-target organs in order to be captured, decreasing the likelihood of non-target organ uptake. *In vivo* phage display has been demonstrated to select peptides that bind human tumors and specifically target the vasculature of most organs, including tumor vasculature (50, 108).

*In vivo* phage display is especially useful when a specific protein target is not known. For example, BT-474 cells are known to express ERBB2 and estrogen receptor, however, neither marker by itself is predictive of susceptibility to resistance (124, 128, 129). It is extremely likely, however, that many potential targets on BT-474 cells may serve not only as novel breast cancer antigens, but also as predictors of therapeutic resistance. *In vivo* phage display can serve as an initial screen for peptides which specifically target BT-474 cells, providing the basis for development an imaging agent for further refinement and characterization. It was hypothesized that a novel BT-474 targeted peptide could be selected by *in vivo* phage display, which would possess the capability of detecting human breast tumors in xenografted mice. To test this, 4 rounds of *in vivo* selection were performed, and individual phages were characterized for their ability to bind BT-474 cells *in vitro*. A peptide corresponding to a phage with high specificity and affinity for the target cells was synthesized as a biotinylated conjugate and tested for cell binding using fluorescent confocal microscopy, flow cytometry and colorimetric binding assays. Retained affinity and specificity of the biotinylated peptide

*in vitro* warranted analysis of the peptide as an $^{111}$In-radiolabeled SPECT imaging agent. Following confirmation of specificity and high affinity of the radiolabeled peptide, *in vivo* biodistribution was assessed. Finally, the peptide was tested as for the ability to detect BT-474 human breast tumors by SPECT/CT.

# Materials and Methods

## Materials

Materials for cell culture were obtained from Invitrogen (Carlsbad, CA). Unless otherwise specified, all other materials were purchased from Sigma Chemical Co. (St. Louis, MO).

## Cell Lines

BT-474 cells were grown in RPMI-1640 with 10% heat-inactivated FBS, 4.5g/L D-glucose, 2.83 g/L HEPES buffer, L-glutamine, 1.5 g/L sodium bicarbonate, 110 mg/L sodium pyruvate, and 48 µg/ml gentamicin at 37°C in 5% $CO_2$. 184A.1 cells were grown in RPMI 1640 with 10% FBS and 48 µ g/ml gentamicin. Cell lines were examined for viability and presence of pathogens prior to injection into mice.

## Mouse Strains and Handling

Four- to 6 -week-old athymic nude mice were purchased from Harlan (Indianapolis, IN) and maintained in approved pathogen-free institutional housing. Animal studies were conducted as outlined in the NIH Guidelines for the Care and Use of Laboratory Animals and the Policy and Procedures for Animal Research of the Harry S. Truman Veterans Memorial Hospital. To establish solid tumors, BT-474 human breast cancer cells ($5 \times 10^6$) were subcutaneously injected into the rear flank of athymic nude

mice. Time-release 17β-estradiol pellets (Innovative Research, Sarasota, FL) were implanted subcutaneously to supplement tumor growth. Visible tumors formed after approximately 5 weeks. Mice injected with either phage or radiolabeled peptide were euthanized prior to excision of tumors and organs of interest.

### *In Vivo* Phage Display Selection

A library of phage displaying 15 random amino acids from the N-terminal tip of cpIII, in the fUSE5 vector, was a generous gift from Dr. George P. Smith. In order to remove phages with a propensity to bind normal tissues and vasculature, $1x\ 10^{12}$ transducing units (TU) of library was injected into non-tumor bearing mice and unbound phages were recovered from the blood 15 min after initial injection, amplified and purified, as previously described (131). The pre-cleared library was used for the ensuing rounds of selection in BT-474 tumor bearing mice. Briefly, $1x\ 10^{12}$ TU of pre-cleared phage was injected into BT-474 xenografted mice and allowed to circulate for 4 h. Mice were anesthetized and tumors excised and frozen in liquid nitrogen. The tumors were manually homogenized and washed 10x with Tris buffered saline with 0.1% Tween-20 (0.1% TBST) in order to remove non-specifically bound phages. The tumor homogenate was then incubated with 2.5% (w:v) 3-[(3-Cholamidopropyl)dimethylammonio]-1-propanesulfonate (CHAPS) for 1 h to elute bound phages and disrupt cells for recovery of any phage that had been internalized by cells. Eluted phages were used to infect log phase K91BK *Escherichia coli* (*E. coli*) for amplification, followed by purification by polyethylene glycol as described previously (76). The tumor-avid, amplified library was used for the subsequent round of selection, which proceeded exactly as the first round. A

total of four rounds of selection were performed in BT-474 human breast tumor bearing mice.

**Analysis of Selected Phages**

Following the fourth round of selection, 96 individual phages were sequenced in order to ascertain their displayed peptides. The sequences were analyzed for multiple occurrences, partial sequence multiple occurrences, amino acid frequency and by algorithms including basic local alignment search tool (BLAST) and the scanner and reporter of target-unrelated peptides algorithm (SAROTUP) (77, 78). Phage displayed peptides found in previous unrelated selections were removed from consideration and 14 phages were chosen for cell binding assays. Each purified phage clone was diluted to $1x10^8$ TU/mL in RPMI and 100 µL was incubated with either $1x 10^5$ BT-474 human breast cancer or 184A.1 normal breast epithelial cells for 1 h at 37°C. Cells were washed three times with 0.1% TBST and bound phage were eluted by incubation with 2.5% CHAPS at 4°C for 1 h. Eluted phage were quantified by titration and infection of *E. coli*.

**Peptide Synthesis**

The amino acid sequence corresponding to the displayed peptide of clone 51, in addition to the N-terminal 7 amino acid sequence (51N) and C-terminal 8 amino acid sequence (51C) and a VEGF inhibiting peptide (V1) were chemically synthesized. Synthesis occurred using an Advanced Chem Tech 396 multiple peptide synthesizer (Advanced Chem Tech, Louisville, KY) by solid phase FMOC chemistry. Biotin was covalently coupled to each peptide at the n-terminus with a tripeptide GSG tripeptide

spacer. The full length 51 peptide was also conjugated to 1,4,7,10-tetraazacyclododecane-1,4,7,10-tetraacetic acid (DOTA) (Macrocyclic, Inc. Dallas, TX) by a GSG spacer.

**Fluorescent Microscopy**

BT-474, 184A.1 and HUVEC human endothelial cells were fixed in 4% paraformaldehyde and dried onto microscope slides. Following rehydration with TBS, cells were blocked with 6% (w:v) bovine serum albumin (BSA) for 1 h at room temperature. Peptides 51, 51N and V1 were diluted to 10 µM in 0.1% TBST. After blocking, 100 µL of the appropriate peptide solution was added to cells and allowed to bind for 1 h at room temperature. Slides were washed three times with 0.1% TBST and 100 µL of α-Biotin-Alexafluor 488 conjugated monoclonal antibody diluted 1:1000 in 0.1% TBST was added to cells and incubated at room temperature for 1 h. Slides were washed 3x with 0.1% TBST and analyzed by an epifluorescent-equipped Nikon T1-SM inverted microscope (Nikon, Melville, NY).

**Flow Cytometry Analysis of Peptide Binding**

In the same manner as fluorescent microscopy, BT-474, 184A.1 and HUVEC cells were fixed and diluted to $1x10^6$ cells/mL in RPMI and preincubated with a 1:1000 dilution of α-Biotin-Alexafluor 488 antibody. Peptides (51, 51N, V1) were diluted to 10 µM and incubated with cells for 1 h at 37°C. Cells were washed three times with 0.1% TBST, counted and fluorescence quantified per cell by a BD FACScan flow cytometer (BD Biosciences, San Jose, CA).

**96 Well Colorimetric Cell Binding Assay**

BT-474 and 184A.1 cells were grown to 80% confluency in TPP 96 well flat bottom tissue culture plates and fixed with 4% paraformaldehyde. Biotinylated 51, 51N and 51C were diluted to appropriate concentrations in RPMI and incubated with cells for 1 h at room temperature. Cells were washed three times with 0.1% TBST and 100 µL horseradish peroxidase-conjugated streptavidin (1 µg/mL) was added to cells and allowed to bind for 1 h at room temperature. Again, washing occurred in the same manner and 100 µL of 2,2′-azino-bis(3-ethylbenzothiazoline-6-sulfonic acid) was incubated with cells for 15 min at room temperature. Color development was terminated by the addition of 1% (w:v) sodium dodecyl sulfate and absorbance at 405 nm was quantified.

**Radiolabeling and Peptide Cell Binding Assays**

DOTA-conjugated 51 peptide was diluted to 1 mg/mL in water and 20 µL was added to 200 µL of 0.1 M ammonium acetate and 18.5 MBq of $^{111}InCl_3$. The reaction was incubated at 85°C for 1 h and terminated by the addition of 10 µL of 0.1 M ethylenediaminetetraacetic acid. Reversed phase HPLC using a linear gradient from 5-95% acetonitrile and 0.1% (v:v) trifluoroacetic acid was used to purify the radiolabeled peptide. For cell binding analysis, BT-474 cells were diluted to $1x10^7$ cells/mL in RPMI with 1% (w:v) BSA. Purified, radiolabeled $^{111}$In-DOTA-51 peptide was diluted to $1x10^6$ CPM/mL in RPMI plus 1% BSA and 100 µL were added to 200 µL cells. Unlabeled DOTA-51 was serial diluted and added to radiolabeled peptide and cells at concentrations from 10 pM to 1 µM and incubated at 37°C for 1 h. Cells were washed with ice cold

PBS with 0.1% BSA three times and counted by gamma counter (Perkin Elmer, Santa Clara, CA).

**Radiolabeled Peptide Biodistribution**

$^{111}$In-DOTA-51 peptide was radiolabeled and purified as described in *in vitro* cell binding. Radiolabeled peptide was then diluted with sterile PBS to 1.85 MBq/mL. Four mice bearing BT-474 tumors were intravenously injected with 100 µL of $^{111}$In-DOTA-51 and sacrificed at 2 h post-injection. Following sacrifice, pertinent organs and tissues were excised, weighed and counted via gamma counter. Uptake was normalized by weight as percentage of injected dose per gram of tissue (%ID/g).

**MicroSPECT/CT Imaging**

$^{111}$In-DOTA-51 was radiolabeled, purified and diluted to 11.1 MBq in 100 µL of sterile PBS. The radiolabeled peptide was injected intravenously into a mouse bearing a BT-474 human breast tumor xenograft. After allowing the peptide to circulate for 2 h post-injection, the mouse was sacrificed and imaged at the Biomolecular Imaging Center at the Harry S. Truman Veterans Memorial Hospital. Acquisition of the image proceeded for 7 h using a Siemens Inveon Micro-SPECT/CT (Siemens, Knoxville, TN) outfitted with mouse whole body 1.0 mm collimators. Processing of the image data was accomplished using Inveon Research Workplace processing software. Fan beam (Feldkamp) filtered back projection algorithms were employed to reconstruct the CT tomographic image.

# Results

## *In Vivo* Selected Phage Characterization

Following the completion of four rounds of *in vivo* selection, 96 individual phages were isolated and their relevant DNA sequenced to obtain the displayed peptide amino acid sequence. Selection of phages for cell binding characterization was first accomplished by analyzing peptides for the presence of target unrelated peptides. Sequences were compared to those from previous published selections with unrelated targets using the scanner and reporter of target unrelated peptides algorithm (78). Of the 96 total sequences, 28 were reported in previous selections. Phages that bound targets unrelated to breast cancer, including the blood-brain barrier, hemagglutinin A, polyclonal rabbit antibody, and normal tissue were excluded from consideration (41, 132-134). Instead, 14 phages unique to the selection, and listed in Figure 4.1A, were chosen because they were found multiple times, or a portion of the sequence was present in multiple phages. Phages were purified and analyzed for BT-474 specificity and apparent affinity.

Individual phages were tested for their ability to selectively bind BT-474 human breast cancer cells while not binding 184A.1 cells, a normal breast epithelial cell line. Recovered phages were normalized to the binding of insertless wild-type phage as an internal control between experiments. The relative binding ratio of each phage in comparison to the wild-type phage was used to assess the relative specificity and affinity

A.

| Phage | Sequence |
|---|---|
| Clone 51 | ATWLPVPVVGYFMASA |
| Clone 93 | ASWVAPPLWLGPFALP |
| Clone 34 | ANFVGWPVGLWTGFDV |
| Clone 19 | AGLGVLGSAVVVSRAS |
| Clone 8 | ARGLFPFFYLLGPAGG |
| Clone 32 | AFPGFLSLGPFSFYPE |
| Clone 81 | AGLLPGSFVGQAYWLP |
| Clone 1 | ADGPHFFSPAVLFPYS |
| Clone 22 | ACARGEYFACSAFRVF |
| Clone 62 | AGTIVLTSARAPLGLL |
| Clone 24 | AFDRASFCSVFAGPDC |
| Clone 60 | AVPWAGSSLYAILVPT |
| Clone 44 | AIVEDLVAFRPWVWIG |
| Clone 42 | APRIFAYRGSSDRLHL |

B.

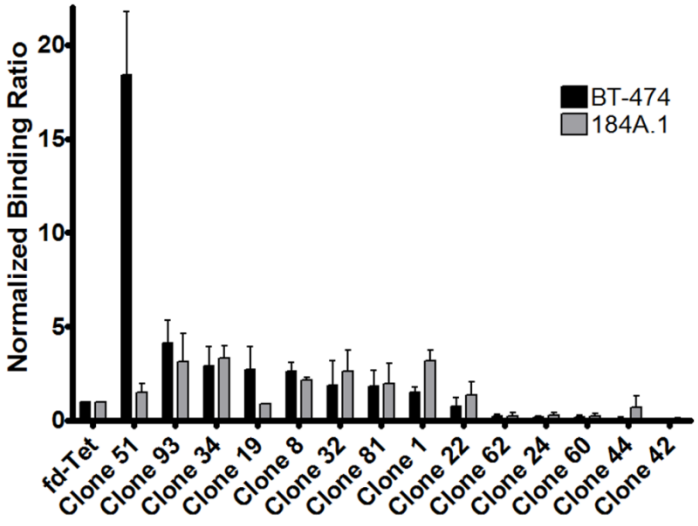


**Figure 4.1** Round 4 of the *in vivo* phage display selection was sequenced and 14 individual phages were chosen for cell binding analysis. A) Individual phage and the corresponding amino acid sequence are depicted. B) Individual phages were incubated with either target BT-474 cells or normal 184A.1 breast epithelial cells. Total bound phages were quantified and normalized to wild-type phage. Shaded bars represent a mean of three replicate experiments, error bars denote standard deviation.

of each displayed peptide (Figure 4.1B). Of the 14 phages analyzed, 5 bound 2-fold greater or higher than wild-type to the target BT-474 cell line. However, when accounting for specificity by assessing the binding to 184A.1 breast epithelial cells, only 2 clones appeared to be specific for BT-474 cells. Clones 51 and 19 bound 18.4 and 2.7 times higher to BT-474 cells than the wild-type phage, respectively. Additionally, the phages preferentially bound breast cancer cells, with binding ratios to BT-474/184A.1 cells of 1.48 for Clone 51 and 0.78 for Clone 19. Clone 51, which bound nearly 7 times more to BT-474 cells than any other phage and did not bind normal breast epithelial binding, was chosen for investigation of its displayed peptide outside of the phage scaffolding.

**Peptide 51 *In Vitro* Cell Binding**

Peptide 51 (ATWLPVPVVGYFMASA) was covalently linked to biotin for detection in cell binding assays. The peptide was first analyzed by fluorescent microscopy as a qualitative assessment of binding. Fluorescent images demonstrated that the peptide bound to BT-474 human breast cancer cells and had no detectable binding to normal breast epithelial cells (Figure 4.2A). A control peptide chosen from a target unrelated phage was used as a control and demonstrated no binding to either cell line. For confirmation of the results of fluorescent microscopy and to attempt to quantify peptide 51 binding, flow cytometry was performed. Peptide 51 bound with moderate affinity for BT-474 cells, with a calculated $EC_{50}$ = 2.33±0.66 μM (Figure 4.2B). Binding to BT-474 cells was also significantly higher than 184A.1 cells at all peptide concentrations

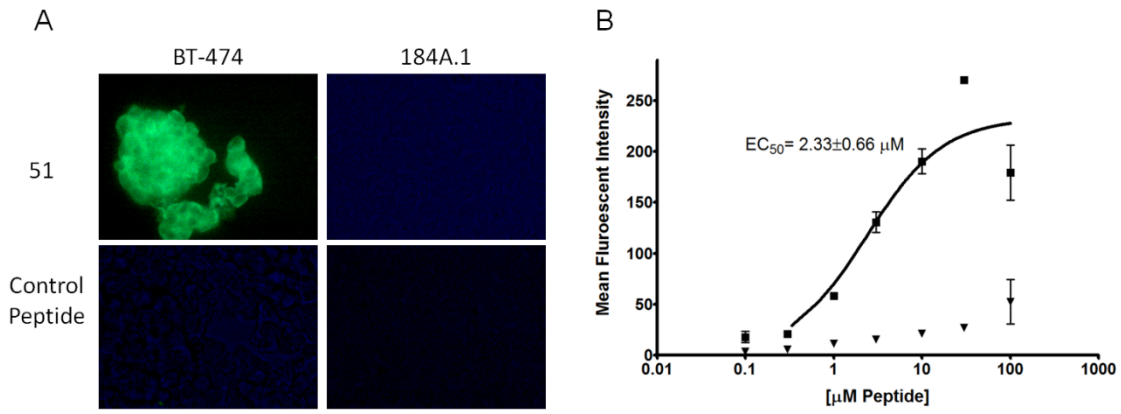


**Figure 4.2** A) Biotinylated peptide 51 and a control peptide were incubated with BT-474 human breast cancer and 184A.1 normal breast epithelial cells fixed onto microscope slides. Following washing, bound peptides were detected by addition of an anti-biotin Alexafluor 488-conjugated antibody. Strong binding is observed for 51 with the target BT-474 cells, but not normal breast epithelial cells. The control peptide does not exhibit binding to either cell line. B) Peptide 51 was analyzed for BT-474 and 184A.1 specificity and affinity by flow cytometry. Following incubation of peptide with cells, bound peptide was detected by anti-biotin Alexafluor 488. Squares represent the mean of 3 BT-474 replicates at the indicated peptide concentration, triangles represent the mean of 3 184A.1 replicates. Error bars represent the standard deviation.

analyzed, and peptide 51 binding to 184A.1 cells did not display a sigmoid dose response, indicating a lack of specificity for the cells. A satisfactory affinity for BT-474 cells, in addition to minimal normal breast tissue binding, indicated that the peptide would be a suitable candidate for development as a radiolabeled imaging agent.

### *In Vitro* and *In Vivo* $^{111}$In-DOTA-51 Analysis

For radiolabeled peptide assessment, peptide 51 was conjugated to DOTA through an N-terminal GSG spacer and radiolabeled with $^{111}$In. $^{111}$In-DOTA-51 was first tested for a retained affinity for BT-474 cells *in vitro* using unlabeled peptide in a competition assay. The relative $IC_{50}$ was calculated at 16±7 nM, an affinity comparable to previous peptides used for *in vivo* analysis (Figure 4.3) (43, 48). $^{111}$In-DOTA-51 was injected into mice bearing BT-474 human breast cancer xenografts for pharmacokinetic analysis. The biodistribution of $^{111}$In-DOTA-51 revealed tumor uptake of 0.12± 0.02 %ID/g (Figure 4.4). The tumor to blood ratio was determined to be 2.3 and the tumor to muscle ratio was 7.1, indicating specificity of the peptide for BT-474 human breast tumors. Tumor uptake in all other organs was low, further confirming tumor specificity. In particular, organs that could produce background signal for breast cancer imaging, including the heart (0.04±0.01 %ID/g), and lung (0.13±0.03 %ID/g) were low (Figure 4.4). Radiosensitive organ uptake, such as bone (0.03±0.02 %ID/g) was also minimal (Figure 4.4), which is important in the development of a safe and effective radiolabeled imaging agent. SPECT/CT image analysis revealed high peptide uptake surrounding the tumor, in addition to kidney uptake, which coincided with the measured kidney retention of 30.4 %ID/g. (Figure 4.5). The pattern of tumor uptake

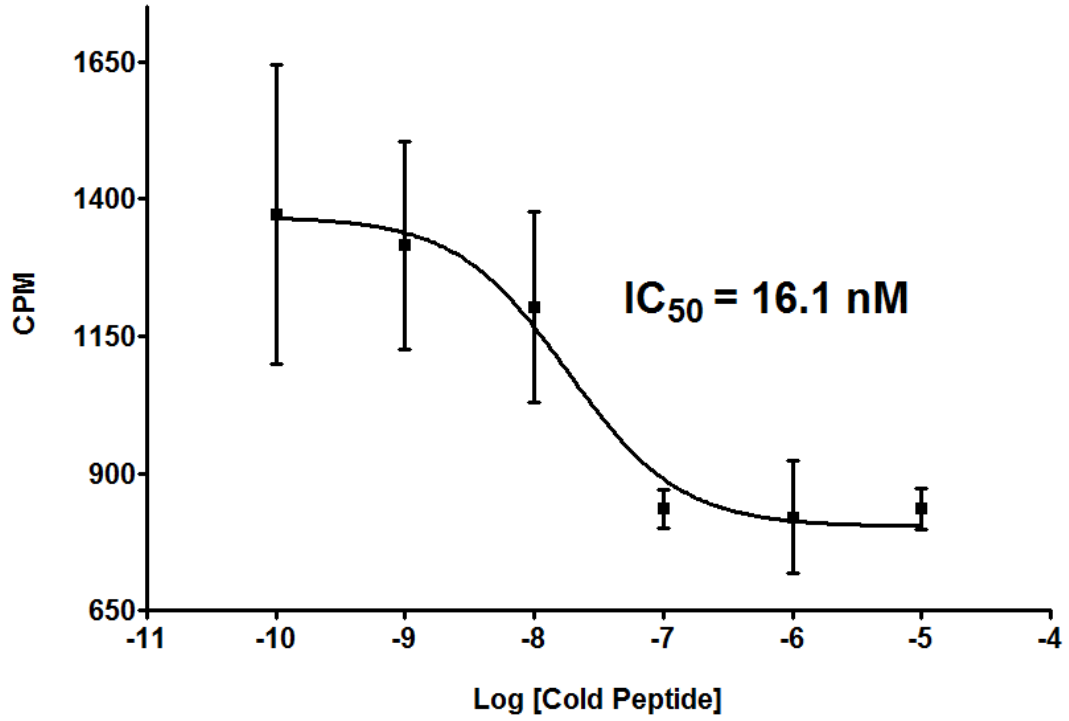


**Figure 4.3** $^{111}$In-DOTA-51 was diluted to 1x10$^{6}$ CPM/mL in RPMI and 1% BSA and 100 µL was added to 1 million BT-474 cells suspended in 100 µL of the same buffer. Unlabeled DOTA-51 was serially diluted and added to labeled peptide and cells. Following 1 h incubation at 37°C, cells were washed and bound radioactivity quantified. Square boxes represent the mean of 3 replicates and error bars represent standard deviation. CPM – Counts per min.

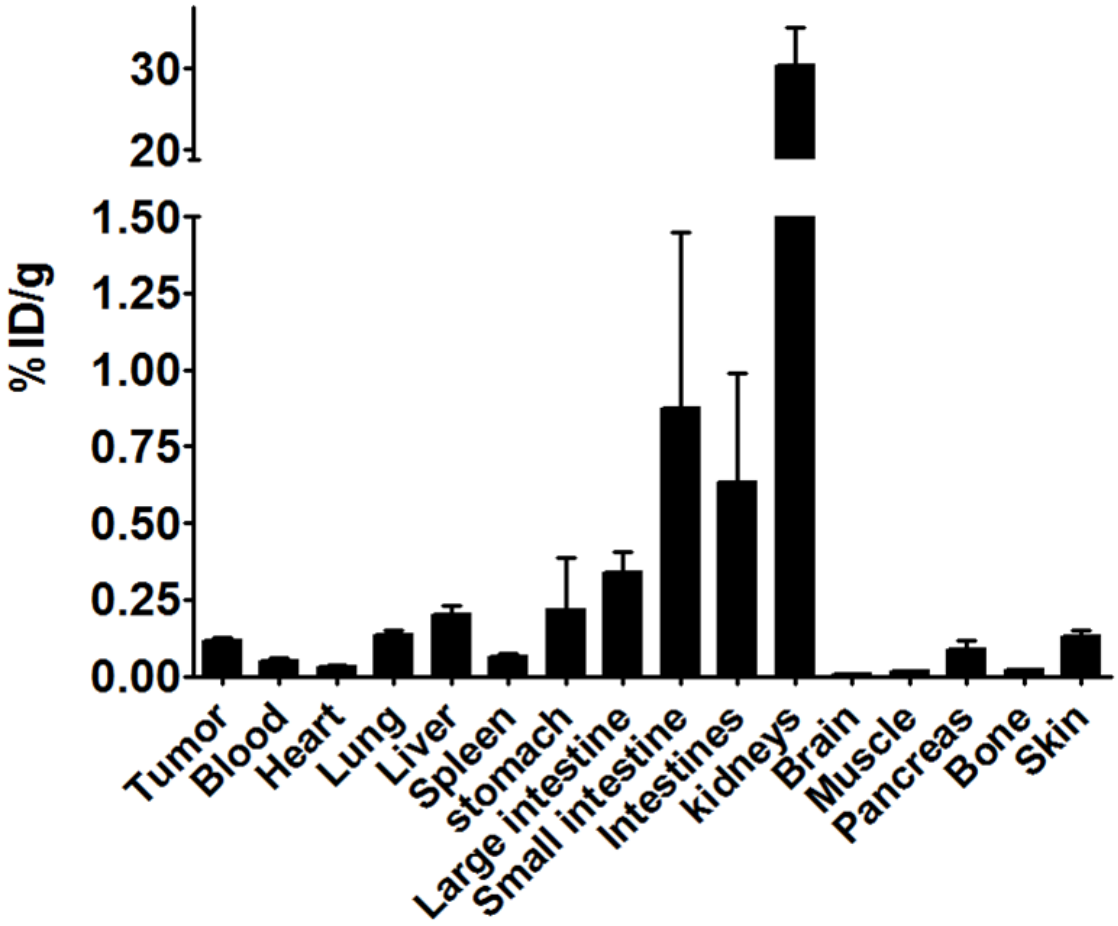


**Figure 4.4** $^{111}$In-DOTA-51 was prepared at 1.85 MBq/mL in sterile PBS and injected into BT-474 xenograft bearing mice. At 2 h post-injection, animals were sacrificed, organs removed, and total radioactivity counted by gamma counter. Each bar represents the average of 4 mice, and error bars denote standard deviation.

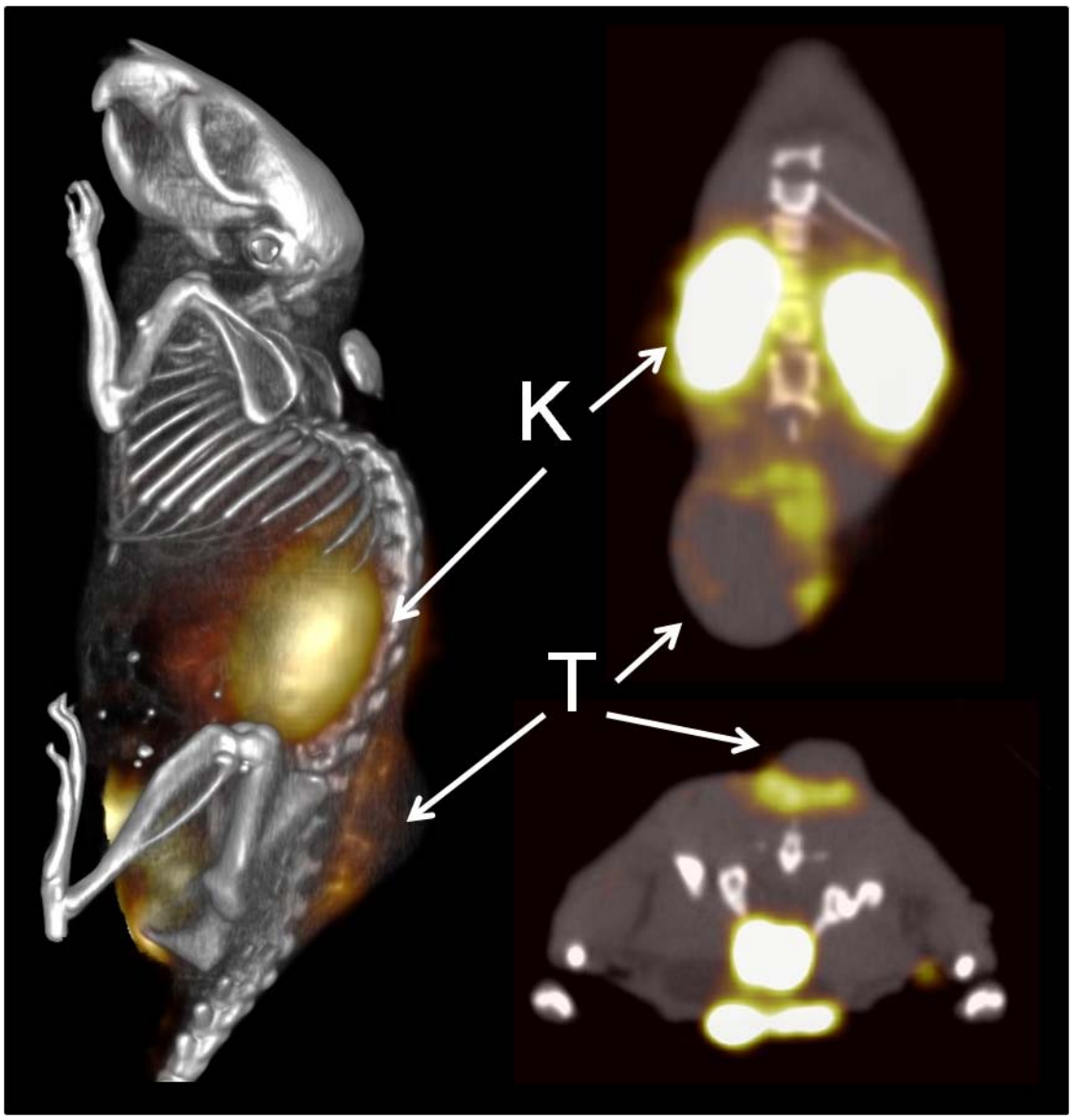


**Figure 4.5** A BT-474 tumor bearing mouse was injected with 11.1MBq of $^{111}$In-DOTA-51 and peptide was allowed to circulate for 2 h prior to imaging. SPECT/CT images were acquired overnight. All images are from the same mouse. T – Tumor, K – Kidney.

was similar to known vasculature targeting agents such as radiolabeled anti-vascular endothelial growth factor (VEGF) antibody and RGD (56, 92). Although the sequences did not contain any well known vasculature targeting motifs, such as RGD, peptide 51 sequence was rigorously compared to known vasculature targeting peptides in order to determine if they shared any other partial homology.

Upon extensive literature review, it was noticed that peptide 51 shared a 5 amino acid homology with a peptide that had been previously selected by phage display and demonstrated to bind neuropilin-1 (Nrp1) and inhibit vascular endothelial growth factor (VEGF)-mediated angiogenesis (135). The peptide, V1 (ATWLPPR), was remarkably similar to the N-terminal residues in Clone 51, whose full length sequence was ATWLPVPVVGYFMASA. Since V1 did not share exact identity to peptide 51 and the peptides were of differing sequence lengths, preliminary searches for target unrelated peptides did not identify the similarity between V1 and 51.

**Examining the Role of a Homologous V1 Sequence in Peptide 51**

Since peptide 51 shared homology with a vasculature antigen-targeting peptide, it was necessary to determine whether the properties of peptide 51 were mediated by the shared ATWLP sequence. Binding of the full length peptide (51), the N-terminal 7 residues (51N - ATWLPVP) and the V1 peptide (ATWLPPR) was analyzed using fluorescence microscopy for target BT-474 breast cancer cells, 184A.1 breast epithelial cells, and an endothelial cell line demonstrated previously as a target of V1 (136). Full length 51 bound strongly to BT-474 cells, while neither 51N nor V1 displayed detectable

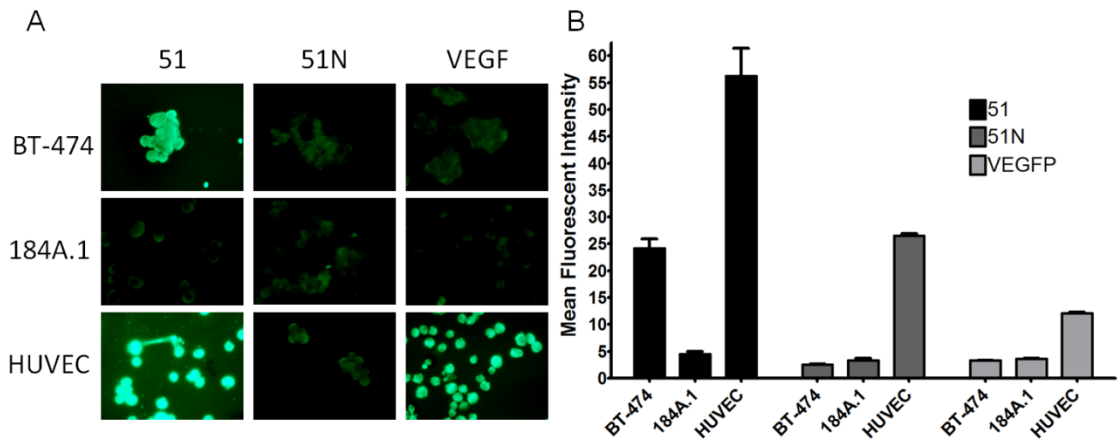


**Figure 4.6** A) Biotinylated peptides were examined for BT-474, 184A.1 and HUVEC binding by fluorescent confocal microscopy. Ten µM peptide was incubated with 4% paraformaldehyde fixed cells dried onto microscope slides and peptide binding visualized by anti-biotin Alexafluor-488 conjugated antibody. B) Flow cytometry was performed to quantify peptide binding to cells. Binding is plotted as the mean fluorescent intensity of the total cell population. Bars illustrate a mean of three replicate experiments and error bars correspond to the standard deviation.

fluorescence to the same cell line, indicating only 51 visibly bound BT-474 cells (Figure 4.6A). All three peptides did not bind normal breast epithelial cells. Interestingly, both full length 51 and V1 bound strongly to HUVEC endothelial cells, while 51N binding was visibly weaker in fluorescent intensity than 51 or V1.

Confirmation and quantification of fluorescent peptide binding to each of the cell lines was investigated using flow cytometry. The mean fluorescence intensity (mean FI) was quantified for each cell line incubated with 10 μM of peptide (Figure 4.6B). Peptide 51 had a significantly higher ($P$<0.01) BT-474 cell binding (mean FI = 24.2±2.98), 9.5 and 7.4 times higher than 51N (mean FI = 2.53±0.11) and V1 (mean FI = 3.27±0.11), respectively. The mean FI of 51 for 184A.1 cells was 4.47±0.90 in comparison to 3.27±0.73 for 51N and 3.63±0.06 for V1, indicating no binding of any peptide to the breast epithelial cell line. Finally, binding to HUVEC cells was significantly higher ($P$<0.05) for 51 (mean FI = 56.2±9.05) and V1 (mean FI = 26.5±0.46) than for 51N, which was consistent with fluorescent microscopy results.

Since the BT-474 targeting capability of 51 was not mediated by the N-terminal 7 residues, a peptide corresponding to the C-terminal 9 residues (51C - VVGYFMASA) was synthesized to determine if this sequence alone contributed to the cell binding properties. A 96-well, colorimetric cell binding assay was chosen to monitor binding over a number of concentrations for determination of the specificity and affinity of 51, 51N and 51C. Peptide 51 demonstrated saturable binding and an $EC_{50}$ = 4.71±0.3 μM. 51N did not reach binding saturation, and 51C bound with a calculated $EC_{50}$ of approximately 2 mM, 1000 fold worse than full length 51 (Figure 4.7). These results indicated that the

BT-474 targeting properties of 51 were not mediated by the N- or C-terminal sequences by themselves.

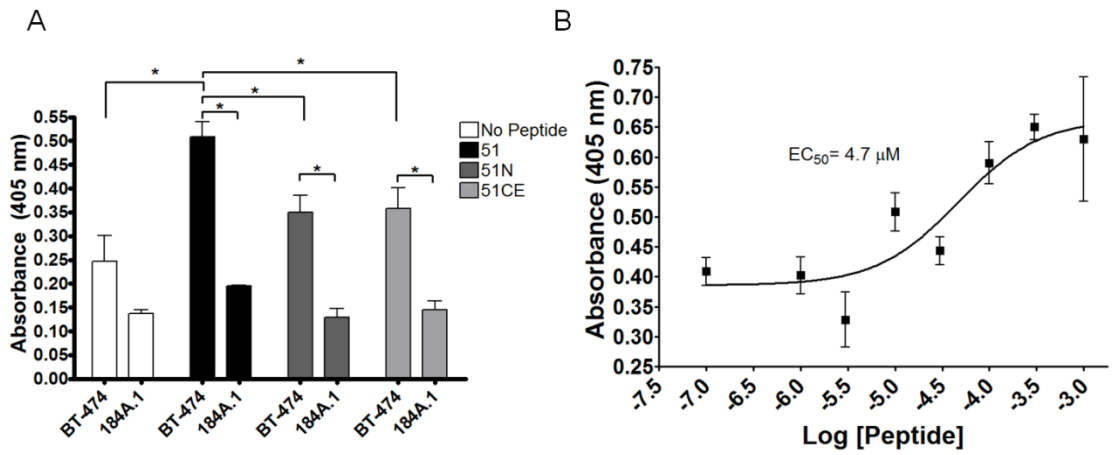


**Figure 4.7** Full length (51), N-terminal (51N) and C-terminal (51C) truncated peptides were assessed for BT-474 and 184A.1 cell binding using a colorimetric 96 well cell binding assay. A) 1 µM biotinylated peptide was incubated with cells and binding was detected by the addition of streptavidin-conjugated horseradish peroxidase followed by addition of 2,2'-azino-bis(3-ethylbenzothiazoline-6-sulfonic acid). Total bound peptide was measured by absorbance at 405 nm. Bars represent a mean of 3 replicate experiments and error bars denote standard deviation. B) Peptide 51 binding from 10 nM to 100 µM to BT-474 cells is plotted for calculation of $EC_{50}$.

# Discussion

Detection and characterization of breast carcinomas is essential to effectively treating molecularly distinct malignancies. Therapeutic management of breast cancer has benefitted from the introduction of targeted therapies including tamoxifen and trastuzumab (121, 122). Unfortunately, resistance has been demonstrated to occur for both therapies, negating the beneficial effects of targeted therapy in certain patients (124, 129). Development of a targeted imaging agent, such as a radiolabeled peptide, that could detect human breast carcinomas and simultaneously reveal whether the tumor would be susceptible to developing therapeutic resistance would, therefore, be highly beneficial. BT-474 human breast cancer cells express the targets of both tamoxifen and trastuzumab, and have innate resistance to tamoxifen and can develop resistance to trastuzumab (127, 137). Therefore, this cell line may serve as an ideal model for developing targeted peptides for imaging therapy-resistant breast cancer.

In order to develop a peptide with BT-474 imaging capabilities, *in vivo* phage display was performed with mice bearing BT-474 human breast cancer xenografts. Phages for further characterization were obtained by eliminating target unrelated phages, leaving 68 potential candidates. From these, 14 phages that were identified multiple times in the selection were chosen for cell binding analysis. Binding of the phages was assessed with BT-474 breast cancer target cells and 184A.1 normal breast epithelial cells as a negative control. Clone 51 was chosen for analysis as a synthesized peptide because in addition to minimal non-target binding, the phage bound over 18 times higher than wild-

type phage to BT-474 cells. Due to its apparent superior targeting properties, the displayed sequence of clone 51 was synthesized and analyzed for cell binding. Fluorescent microscopy confirmed BT-474 specific binding of the peptide, and flow cytometry was used to quantify a relative $EC_{50}$ = 2.33 μM of peptide 51 for the target cells. The peptide once again did not bind to 184A.1 cells at any concentration tested. A calculated $EC_{50}$ that had been previously demonstrated to be sufficient for *in vivo* imaging, in addition to its specificity for BT-474 cells, lead to synthesis and analysis of the peptide as a radiotracer (43, 131).

Radiolabeling of the peptide for *in vivo* studies was accomplished by conjugating the peptide to the macrocyclic chelator DOTA and incubating with $^{111}$In. The radiolabeled peptide was subjected to a peptide binding inhibition assay to confirm specificity and affinity. $^{111}$In-DOTA-51 binding inhibition was measured at a relative $IC_{50}$ = 16.7 nM, confirming retained affinity of the radiolabeled peptide. The difference between the $EC_{50}$ and $IC_{50}$ could be the result of enhanced affinity of the radiolabeled peptide, radiolabeling providing a more sensitive means of quantification, or a difference between the concentration of peptide necessary to reach half maximal saturation ($EC_{50}$) and the concentration necessary to inhibit 50% of submaximal peptide binding ($IC_{50}$). Further characterization may resolve the difference; however, *in vitro* cell binding revealed that the peptide affinity had not been diminished by addition of a radiolabeled chelator, which was the goal of the assay. Therefore, $^{111}$In-DOTA-51 was subsequently analyzed in BT-474 tumor bearing mice for biodistribution and SPECT imaging capability. Tumor uptake of the peptide was under 1% ID/g, but highly specific. Two measures of specificity, tumor to blood (2.3) and muscle (7.1) ratios, were both greater

than 1, indicating tumor uptake was not mediated by blood pooling and was also tissue specific. SPECT imaging of the radiolabeled peptide revealed high uptake in the region surrounding the tumor, consistent with radiolabeled RGD peptide and an anti-VEGF antibody specific for tumor vasculature antigens (56, 92). Vasculature targeting peptides have been selected by *in vivo* and *in vitro* phage display previously, and it is known that a sequence as short as 3 amino acids, such as RGD, is sufficient to endow tumor vasculature targeting properties to a peptide (45). The highly similar uptake pattern between peptide 51 and other tumor vasculature imaging agents suggested that the peptide may have similar targeting properties. Upon a detailed inspection of vasculature targeting peptide sequences in the literature, it was discovered that peptide 51 resembled a Nrp1-targeted peptide selected previously by phage display (135). The displayed peptide of Clone 51, ATWLPVPVVGYFMASA, was identical in its 5 N-terminal residues to the Nrp-1 targeted V1 peptide, which has the sequence ATWLPPR. Nrp-1 has been demonstrated to be expressed in breast cancer, and its expression has been confirmed in BT-474 cells (138). It was possible therefore, that the binding of Clone 51 was mediated by the N-terminal residues homologous to V1. In order to test this, 51 and V1 were examined for similar targeting characteristics *in vitro* and *in vivo* and several truncated versions of 51 were examined to determine the sequence that mediated BT-474 binding.

*In vitro* cell binding studies revealed that 51 bound both BT-474 and HUVEC cells, while V1 only targeted HUVEC cells. Although BT-474 cells express Nrp1, it has been shown that they express the receptor at lower levels than HUVEC cells, which may explain the difference in binding of V1 to BT-474 and HUVEC cells (138). In fact, a

monoclonal antibody targeting Nrp1 failed to elicit anti-proliferative effects with BT-474 cells *in vitro*, consistent with the observed results of V1 binding to BT-474 cells (139). However, this does not account for the difference in cell binding between 51 and V1. Although it was initially thought that the target of 51 may be Nrp1, the data presented here and previous analysis of V1 indicate this is not likely. In an earlier study examining the critical amino acids necessary for V1 binding, it was determined that the C-terminal LPPR of V1 was the crucial sequence, as demonstrated by binding assays using alanine scanning and truncation variants, and nuclear magnetic resonance spectrometry (140). Since peptide 51 does not contain the critical LPPR domain, the similarity between the 51 and V1 peptides may only be coincidental, or the ATWLP sequence by itself may not be enough to contribute to the binding properties of the peptide. Finally, truncated peptides were examined to determine the role of shorter sequences, including ATWLP, on the binding of full length 51. It was determined that the full length peptide was required for optimal target affinity and specificity.

In addition to comparison of V1 and 51 *in vitro*, the *in vivo* data of this study was compared to previously published V1 *in vivo* data for pharmacokinetics and imaging comparison. Unfortunately, V1 has only been tested as a $^{99m}$Tc radiolabeled peptide, and it was used with a different tumor model (141). Nevertheless, the *in vivo* analysis of V1 revealed higher tumor uptake (~2% ID/g) than 51, but its tumor to muscle ratio was 0.22, significantly lower than 51. Although blood levels of the peptide were not given, it was reported that blood levels of the V1 peptide prevented detection of tumors by SPECT imaging. Though not directly comparable, the stark differences in pharmacokinetic and

SPECT imaging properties suggest that 51 and V1 do have different properties and targets.

# Conclusion

The data presented here provide evidence that $^{111}$In-DOTA-51 is a potential candidate for imaging BT-474 human breast tumor xenografts. Although the peptide's properties are not mediated by an Nrp1 targeted sequence, the peptide nonetheless appears to target tumor vasculature, as demonstrated both *in vitro* and *in vivo*. In order to progress the peptide further to the clinic, several questions must be addressed. Solid tumor uptake of the peptide is low, however it remains to be seen whether the vasculature uptake of the peptide will be sufficient for imaging in humans. Additionally, although BT-474 cells are a suitable base for developing a peptide targeted at resistance susceptible breast cancer, more in depth models must be used to confirm that the peptide is indeed specific for targeted therapy resistant breast cancer. In that same regard, identification of the target of peptide 51, while not trivial, could provide information for further investigation of proteins that mediate resistance. Regardless, the work here demonstrates that *in vivo* phage display can be used to select peptides, which target a resistance susceptible breast cancer cell line, and the radiolabeled peptides can be used to identify xenografted tumors *in vivo*.

## Acknowledgments

The a uthors w ould l ike to a cknowledge t he c ontributions of Jessica N ewton-Northup, Marie T. Dickerson and the VA Biomolecular Imaging Core. This material is based upon work supported by the Department of Veterans Affairs, Veterans Health Administration, Office o f R esearch and D evelopment, Biomedical Laboratory Research an d Development, C linical S ciences R esearch an d D evelopment i ncluding t he C ooperative Studies Program, Rehabilitation Research and Development Service, and Health Services Research and D evelopment t hrough a V A M erit A ward ( I01BX000964). Additional support provided by an NIBIB Training Grant NIBIB 5 T32 EB004822.

# REFERENCES


1. Siegel R, Naishadham D, Jemal A. Cancer statistics, 2012. CA Cancer J Clin. 2012;62(1):10-29.

2. Bernstein L, Ross RK. Endogenous hormones and breast cancer risk. Epidemiol Rev. 1993;15(1):48-65.

3. Welch H, Schwartz LM, Woloshin S. Are increasing 5-year survival rates evidence of success against cancer? JAMA. 2000;283(22):2975-8.

4. Loft S, Poulsen HE. Cancer risk and oxidative DNA damage in man. J Mol Med. 1996;74(6):297-312.

5. Claus EB. Genetic analysis of breast cancer in the cancer and steroid hormone study. Am J Hum Genet. 1991;48(2):232.

6. Walboomers JMM. Human papillomavirus is a necessary cause of invasive cervical cancer worldwide. The Journal of pathology. 1999;189(1):12.

7. Pim D, Massimi P, Dilworth SM, Banks L. Activation of the protein kinase B pathway by the HPV-16 E7 oncoprotein occurs through a mechanism involving interaction with PP2A. Oncogene. 2005;24(53):7830-8.

8. Elmore S. Apoptosis: A Review of Programmed Cell Death. Toxicol Pathol. 2007;35(4):495-516.

9. Levine AJ. p53, the Cellular Gatekeeper for Growth and Division. Cell. 1997;88(3):323-31.

10. Alroy I. The ErbB signaling network in embryogenesis and oncogenesis: signal diversification through combinatorial ligand-receptor interactions. FEBS Lett. 1997;410(1):83.

11. Folkman J, Long DM, Becker FF. Growth and metastasis of tumor in organ culture. Cancer. 1963;16(4):453-67.

12. Tannock IF. The relation between cell proliferation and the vascular system in a transplanted mouse mammary tumour. Br J Cancer. 1968;22(2):258-73. PMCID: 2008239.

13. Ausprunk DH, Folkman J. Migration and proliferation of endothelial cells in preformed and newly formed blood vessels during tumor angiogenesis. Microvasc Res. 1977;14(1):53-65.

14. Jain RK. Transport of Molecules in the Tumor Interstitium: A Review. Cancer Res. 1987;47(12):3039-51.

15. Liotta LA. Tumor Invasion and Metastases - Role of the Extracellular Matrix: Rhoads Memorial Award Lecture. Cancer Res. 1986;46(1):1-7.

16. Pantel K, Brakenhoff RH, Brandt B. Detection, clinical relevance and specific biological properties of disseminating tumour cells. Nat Rev Cancer. 2008;8(5):329-40.

17. Hagemeister FB, Buzdar AU, Luna MA, Blumenschein GR. Causes of death in breast cancer a clinicopathologic study. Cancer. 1980;46(1):162-7.

18. Paget S. The distribution of secondary growths in cancer of the breast. The Lancet. 1889;133(3421):571-3.

19. Schottenfeld D, Fraumeni Jr JF. Cancer epidemiology and prevention: Eastbourne, UK; WB Saunders Co; 1982.

20. Poola I, Abraham J, Marshalleck JJ, Yue Q, Fu SW, Viswanath L, et al. Molecular constitution of breast but not other reproductive tissues is rich in growth promoting molecules: A possible link to highest incidence of tumor growths. FEBS Lett. 2009;583(18):3069-75.

21. Fisher CJ. Histopathology of breast cancer in relation to age. Br J Cancer. 1997;75(4):593.

22. Clemons M, Danson S, Howell A. Tamoxifen ('Nolvadex'): a review: Antitumour treatment. Cancer Treat Rev. 2002;28(4):165-80.

23. Holbro T, Hynes NE. ERBB RECEPTORS: Directing Key Signaling Networks Throughout Life. Annu Rev Pharmacol Toxicol. 2004;44(1):195-217.

24. Olayioye MA, Neve RM, Lane HA, Hynes NE. The ErbB signaling network: receptor heterodimerization in development and cancer. EMBO J. 2000;19(13):3159-67.

25. Hynes NE, Stern DF. The biology of erbB-2/neu/HER-2 and its role in cancer. Biochim Biophys Acta. 1994;1198(2-3):165-84.

26. Baselga J, Tripathy D, Mendelsohn J, Baughman S, Benz CC, Dantis L, et al. Phase II study of weekly intravenous recombinant humanized anti-p185HER2 monoclonal antibody in patients with HER2/neu-overexpressing metastatic breast cancer. J Clin Oncol. 1996;14(3):737-44.

27. Howlader N, Noone A, Krapcho M, Neyman N, Aminou R, Waldron W, et al. SEER cancer statistics review, 1975-2008. Bethesda, MD: National Cancer Institute. 2011;19.

28. Moss SM, Cuckle H, Evans A, Johns L, Waller M, Bobrow L. Effect of mammographic screening from age 40 years on breast cancer mortality at 10 years' follow-up: a randomised controlled trial. The Lancet. 2006;368(9552):2053-60.

29. Dang CV, Semenza GL. Oncogenic alterations of metabolism. Trends Biochem Sci. 1999;24(2):68-72.

30. Fischman AJ, Babich JW, Strauss HW. A Ticket to Ride: Peptide Radiopharmaceuticals. J Nucl Med. 1993;34(12):2253-63.

31. Schottelius M, Wester H-J. Molecular imaging targeting peptide receptors. Methods. 2009;48(2):161-77.

32. Weissleder R. Molecular Imaging in Cancer. Science. 2006;312(5777):1168-71.

33. Witton CJ, Reeves JR, Going JJ, Cooke TG, Bartlett JMS. Expression of the HER1–4 family of receptor tyrosine kinases in breast cancer. The Journal of pathology. 2003;200(3):290-7.

34. Yarden Y. Untangling the ErbB signalling network. Nature reviews Molecular cell biology. 2001;2(2):127.

35. Cho H-S, Mason K, Ramyar KX, Stanley AM, Gabelli SB, Denney DW, et al. Structure of the extracellular region of HER2 alone and in complex with the Herceptin Fab. Nature. 2003;421(6924):756-60.

36. Graus-Porta D, Beerli RR, Daly JM, Hynes NE. ErbB-2, the preferred heterodimerization partner of all ErbB receptors, is a mediator of lateral signaling. EMBO J. 1997;16(7):1647-55.

37. Baselga J, Gelmon KA, Verma S, Wardley A, Conte P, Miles D, et al. Phase II trial of pertuzumab and trastuzumab in patients with human epidermal growth factor receptor 2–positive metastatic breast cancer that progressed during prior trastuzumab therapy. J Clin Oncol. 2010;28(7):1138-44.

38. Franklin MC, Carey KD, Vajdos FF, Leahy DJ, de Vos AM, Sliwkowski MX. Insights into ErbB signaling from the structure of the ErbB2-pertuzumab complex. Cancer Cell. 2004;5(4):317-28.

39. Cavaliere A, Sidoni A, Scheibel M, Bellezza G, Brachelente G, Vitali R, et al. Biopathologic profile of breast cancer core biopsy: is it always a valid method? Cancer Lett. 2005;218(1):117-21.

40. Smith GP. Filamentous fusion phage: novel expression vectors that display cloned antigens on the virion surface. Science. 1985;228(4705):1315-7.

41. Thomas WD, Golomb M, Smith GP. Corruption of phage display libraries by target-unrelated clones: diagnosis and countermeasures. Anal Biochem. 2010;407(2):237-40.

42. Zou J, Glinsky VV, Landon LA, Matthews L, Deutscher SL. Peptides specific to the galectin-3 carbohydrate recognition domain inhibit metastasis-associated cancer cell adhesion. Carcinogenesis. 2005;26(2):309-18.

43. Karasseva NG, Glinsky VV, Chen NX, Komatireddy R, Quinn TP. Identification and Characterization of Peptides That Bind Human ErbB-2 Selected from a Bacteriophage Display Library. J Protein Chem. 2002;21(4):287-96.

44. Peletskaya E, Glinsky G, Deutscher S, Quinn T. Identification of peptide sequences that bind the Thomsen-Friedenreich cancer-associated glycoantigen from bacteriophage peptide display libraries. Mol Divers. 1996;2(1):13-8.

45. Ruoslahti E. RGD AND OTHER RECOGNITION SEQUENCES FOR INTEGRINS. Annu Rev Cell Dev Biol. 1996;12(1):697-715.

46. Day JW, Kim CH, Smider VV, Schultz PG. Identification of metal ion binding peptides containing unnatural amino acids by phage display. Bioorg Med Chem Lett. 2013(0).

47. Kumar SR, Deutscher SL. 111In-Labeled Galectin-3–Targeting Peptide as a SPECT Agent for Imaging Breast Tumors. J Nucl Med. 2008;49(5):796-803.

48. Kumar SR, Quinn TP, Deutscher SL. Evaluation of an 111In-Radiolabeled Peptide as a Targeting and Imaging Agent for ErbB-2 Receptor-Expressing Breast Carcinomas. Clin Cancer Res. 2007;13(20):6070-9.

49. Arap W, Kolonin MG, Trepel M, Lahdenranta J, Cardo-Vila M, Giordano RJ, et al. Steps toward mapping the human vasculature by phage display. Nat Med. 2002;8(2):121-7.

50. Newton JR, Kelly KA, Mahmood U, Weissleder R, Deutscher SL. In vivo selection of phage for the optical imaging of PC-3 human prostate carcinoma in mice. Neoplasia. 2006;8(9):772-80. PMCID: 1584300.

51. Lobo ED, Hansen RJ, Balthasar JP. Antibody pharmacokinetics and pharmacodynamics. J Pharm Sci. 2004;93(11):2645-68.

52. Yeh ET, Tong AT, Lenihan DJ, Yusuf SW, Swafford J, Champion C, et al. Cardiovascular complications of cancer therapy diagnosis, pathogenesis, and management. Circulation. 2004;109(25):3122-31.

53. Chen J, Cheng Z, Miao Y, Jurisson SS, Quinn TP. α–melanocyte-stimulating hormone peptide analogs labeled with technetium-99m and indium-111 for malignant melanoma targeting. Cancer. 2002;94(S4):1196-201.

54. Hoffman TJ, Gali H, Smith CJ, Sieckman GL, Hayes DL, Owen NK, et al. Novel Series of 111In-Labeled Bombesin Analogs as Potential Radiopharmaceuticals for Specific Targeting of Gastrin-Releasing Peptide Receptors Expressed on Human Prostate Cancer Cells. J Nucl Med. 2003;44(5):823-31.

55. Olsen JO, Pozderac RV, Hinkle G, Hill T, O'Dorisio TM, Schirmer WJ, et al. Somatostatin receptor imaging of neuroendocrine tumors with indium-111 pentetreotide (Octreoscan). Semin Nucl Med. 1995;25(3):251-61.

56. McDonald DM, Choyke PL. Imaging of angiogenesis: from microscope to clinic. Nat Med. 2003;9(6):713-25.

57. Koivunen E, Gay DA, Ruoslahti E. Selection of peptides binding to the alpha 5 beta 1 integrin from phage display library. J Biol Chem. 1993;268(27):20205-10.

58. Bausch D, Thomas S, Mino-Kenudson M, Fernández-del CC, Bauer TW, Williams M, et al. Plectin-1 as a Novel Biomarker for Pancreatic Cancer. Clin Cancer Res. 2011;17(2):302-9.

59. Maecke HR, Riesen A, Ritter W. The molecular structure of indium-DTPA. Journal of nuclear medicine: official publication, Society of Nuclear Medicine. 1989;30(7):1235-9.

60. Harris TD, Sworin M, Williams N, Rajopadhye M, Damphousse PR, Glowacka D, et al. Synthesis of Stable Hydrazones of a Hydrazinonicotinyl-Modified Peptide for the Preparation of 99mTc-Labeled Radiopharmaceuticals. Bioconjug Chem. 1999;10(5):808-14.

61. Prasanphanich AF, Nanda PK, Rold TL, Ma L, Lewis MR, Garrison JC, et al. [64Cu-NOTA-8-Aoc-BBN (7-14) NH2] targeting vector for positron-emission

tomography imaging of gastrin-releasing peptide receptor-expressing tissues. Proceedings of the National Academy of Sciences. 2007;104(30):12462-7.

62. Sun X, Wuest M, Weisman GR, Wong EH, Reed DP, Boswell CA, et al. Radiolabeling and In Vivo Behavior of Copper-64-Labeled Cross-Bridged Cyclam Ligands. J Med Chem. 2001;45(2):469-77.

63. De Leon-Rodriguez LM, Kovacs Z. The Synthesis and Chelation Chemistry of DOTA-Peptide Conjugates. Bioconjug Chem. 2007;19(2):391-402.

64. Mariani G, Bruselli L, Kuwert T, Kim EE, Flotats A, Israel O, et al. A review on the clinical uses of SPECT/CT. Eur J Nucl Med Mol Imaging. 2010;37(10):1959-85.

65. Liu S, Edwards DS. 99mTc-labeled small peptides as diagnostic radiopharmaceuticals. Chem Rev. 1999;99(9):2235-68.

66. Zeglis BM, Lewis JS. A practical guide to the construction of radiometallated bioconjugates for positron emission tomography. Dalton Transactions. 2011;40(23):6168-95.

67. Bar-Shalom R, Yefremov N, Guralnik L, Gaitini D, Frenkel A, Kuten A, et al. Clinical performance of PET/CT in evaluation of cancer: additional value for diagnostic imaging and patient management. J Nucl Med. 2003;44(8):1200-9.

68. Milenic DE, Yokota T, Filpula DR, Finkelman MAJ, Dodd SW, Wood JF, et al. Construction, Binding Properties, Metabolism, and Tumor Targeting of a Single-Chain Fv Derived from the Pancarcinoma Monoclonal Antibody CC49. Cancer Res. 1991;51(23 Part 1):6363-71.

69. Fujimori K. A modeling analysis of monoclonal antibody percolation through tumors: a binding-site barrier. J Nucl Med. 1990;31(7):1191.

70. Landon LA, Zou J, Deutscher SL. Is Phage Display Technology on Target for Developing Peptide-Based Cancer Drugs? Current Drug Discovery Technologies. 2004;1(2):113-32.

71. Landon LA, Deutscher SL. Combinatorial discovery of tumor targeting peptides using phage display. J Cell Biochem. 2003;90(3):509-17.

72. Ruoslahti E. Targeting tumor vasculature with homing peptides from phage display. Semin Cancer Biol. 2000;10(6):435-42.

73. Deutscher SL, Figueroa SD, Kumar SR. 111In-labeled KCCYSL peptide as an imaging probe for ErbB-2-expressing ovarian carcinomas. Journal of Labelled Compounds and Radiopharmaceuticals. 2009;52(14):583-90.

74. Kocks C, Rajewsky K. Stepwise intraclonal maturation of antibody affinity through somatic hypermutation. Proc Natl Acad Sci U S A. 1988;85(21):8206-10.

75. Landon LA, Peletskaya EN, Glinsky VV, Karasseva N, Quinn TP, Deutscher SL. Combinatorial Evolution of High-Affinity Peptides That Bind to the Thomsen-Friedenreich Carcinoma Antigen. J Protein Chem. 2003;22(2):193-204.

76. Smith GP. G.P. Smith Phage Display Website. 2006 [updated 2006 3/5/2006; cited]; Available from: http://www.biosci.missouri.edu/smithGP/PhageDisplayWebsite/PhageDisplayWebsiteIndex.html.

77. Altschul SF, Gish W, Miller W, Myers EW, Lipman DJ. Basic local alignment search tool. J Mol Biol. 1990;215(3):403-10.

78. Huang J, Ru B, Li S, Lin H, Guo F-B. SAROTUP: scanner and reporter of target-unrelated peptides. BioMed Research International. 2010;2010.

79. Molina MA, Codony-Servat J, Albanell J, Rojo F, Arribas J, Baselga J. Trastuzumab (Herceptin), a humanized anti-HER2 receptor monoclonal antibody, inhibits basal and activated HER2 ectodomain cleavage in breast cancer cells. Cancer Res. 2001;61(12):4744-9.

80. Zhang X, Cabral P, Bates M, Pablo Gambini J, Fernandez M, Calzada V, et al. In Vitro and In Vivo Evaluation of [99mTc (CO) 3]-Radiolabeled ErbB-2-Targeting Peptides for Breast Carcinoma Imaging. Current Radiopharmaceuticals. 2010;3(4):308-21.

81. Vegt E, de Jong M, Wetzels JFM, Masereeuw R, Melis M, Oyen WJG, et al. Renal Toxicity of Radiolabeled Peptides and Antibody Fragments: Mechanisms, Impact on Radionuclide Therapy, and Strategies for Prevention. J Nucl Med. 2010;51(7):1049-58.

82. Miao Y, Fisher DR, Quinn TP. Reducing renal uptake of 90Y- and 177Lu-labeled alpha-melanocyte stimulating hormone peptide analogues. Nucl Med Biol. 2006;33(6):723-33.

83. Froidevaux S, Eberle AN, Christe M, Sumanovski L, Heppeler A, Schmitt JS, et al. Neuroendocrine tumor targeting: Study of novel gallium-labeled somatostatin radiopeptides in a rat pancreatic tumor model. Int J Cancer. 2002;98(6):930-7.

84. Good S, Walter MA, Waser B, Wang X, Müller-Brand J, Béhé MP, et al. Macrocyclic chelator-coupled gastrin-based radiopharmaceuticals for targeting of gastrin receptor-expressing tumours. Eur J Nucl Med. 2008;35(10):1868-77.

85. Chen J, Cheng Z, Owen NK, Hoffman TJ, Miao Y, Jurisson SS, et al. Evaluation of an 111In-DOTA–Rhenium Cyclized α-MSH Analog: A Novel Cyclic-Peptide Analog with Improved Tumor-Targeting Properties. J Nucl Med. 2001;42(12):1847-55.

86. Deutscher SL. Phage display in molecular imaging and diagnosis of cancer. Chem Rev. 2010;110(5):3196-211.

87. Derda R, Tang S, Li SC, Ng S, Matochko W, Jafari M. Diversity of Phage-Displayed Libraries of Peptides during Panning and Amplification. Molecules. 2011;16(2):1776-803.

88. Yu D, Hung M-C. Overexpression of ErbB2 in cancer and ErbB2-targeting strategies. Oncogene. 2000;19(53):6115.

89. Krenning EP, Kwekkeboom DJ, Bakker WH, Breeman WAP, Kooij PPM, Oei HY, et al. Somatostatin receptor scintigraphy with [111In-DTPA-d-Phe1]- and [123I-Tyr3]-octreotide: the Rotterdam experience with more than 1000 patients. Eur J Nucl Med. 1993;20(8):716-31.

90. Béhé M, Becker W, Gotthardt M, Angerstein C, Behr T. Improved kinetic stability of DTPA-dGlu as compared with conventional monofunctional DTPA in

chelating indium and yttrium: preclinical and initial clinical evaluation of radiometal labelled minigastrin derivatives. Eur J Nucl Med Mol Imaging. 2003;30(8):1140-6.

91. Ferro-Flores G, de Murphy CA, Rodr`guez-Corte`s J, Pedraza-Lo`pez M, Ram`rez-Iglesias MaT. Preparation and evaluation of 99mTc-EDDA/HYNIC-[Lys3]-bombesin for imaging gastrin-releasing peptide receptor-positive tumours. Nucl Med Commun. 2006;27(4):371-6

92. Thakur ML, Aruva MR, Gariepy J, Acton P, Rattan S, Prasad S, et al. PET Imaging of Oncogene Overexpression Using 64Cu-Vasoactive Intestinal Peptide (VIP) Analog: Comparison with 99mTc-VIP Analog. J Nucl Med. 2004;45(8):1381-9.

93. Rolleman E, Valkema R, de Jong M, Kooij P, Krenning E. Safe and effective inhibition of renal uptake of radiolabelled octreotide by a combination of lysine and arginine. Eur J Nucl Med Mol Imaging. 2003;30(1):9-15.

94. Vegt E, van Eerd JEM, Eek A, Oyen WJG, Wetzels JFM, de Jong M, et al. Reducing Renal Uptake of Radiolabeled Peptides Using Albumin Fragments. J Nucl Med. 2008;49(9):1506-11.

95. Shojaei F. Anti-angiogenesis therapy in cancer: Current challenges and future perspectives. Cancer Lett. 2012;320(2):130-7.

96. Folkman J. Tumor angiogenesis: therapeutic implications. N Engl J Med. 1971;285(21):1182-6.

97. Ruoslahti E, Rajotte D. An address system in the vasculature of normal tissues and tumors. Annu Rev Immunol. 2000;18(1):813-27.

98. Jain RK. The Eugene M. Landis Award Lecture 1996. Delivery of molecular and cellular medicine to solid tumors. Microcirculation (New York, NY : 1994). 1997;4(1):1-23.

99. Weis SM, Cheresh DA. Tumor angiogenesis: molecular pathways and therapeutic targets. Nat Med. 2011;17(11):1359-70.

100. Coukos G. Novel surface targets and serum biomarkers from the ovarian cancer vasculature. Cancer biology & therapy. 2011;12(3):1.

101. DeRisi J, Penland L, Brown PO, Bittner ML, Meltzer PS, Ray M, et al. Use of a cDNA microarray to analyse gene expression patterns in human cancer. Nat Genet. 1996;14(4):457-60.

102. Li J-L, Harris AL. The Potential of New Tumor Endothelium-Specific Markers for the Development of Antivascular Therapy. Cancer Cell. 2007;11(6):478-81.

103. Bild AH, Yao G, Chang JT, Wang Q, Potti A, Chasse D, et al. Oncogenic pathway signatures in human cancers as a guide to targeted therapies. Nature. 2006;439(7074):353-7.

104. Yeung G, Mulero JJ, Berntsen RP, Loeb DB, Drmanac R, Ford JE. Cloning of a Novel Epidermal Growth Factor Repeat Containing Gene EGFL6: Expressed in Tumor and Fetal Tissues. Genomics. 1999;62(2):304-7.

105. Buckanovich RJ, Sasaroli D, O'Brien-Jenkins A, Botbyl J, Hammond R, Katsaros D, et al. Tumor Vascular Proteins As Biomarkers in Ovarian Cancer. J Clin Oncol. 2007;25(7):852-61.

106. Wang X, Gong Y, Wang D, Xie Q, Zheng M, Zhou Y, et al. Analysis of gene expression profiling in meningioma: deregulated signaling pathways associated with meningioma and egfl6 overexpression in benign meningioma tissue and serum. PLoS ONE. 2012;7(12):e52707.

107. Chim SM, Qin A, Tickner J, Pavlos N, Davey T, Wang H, et al. EGFL6 Promotes Endothelial Cell Migration and Angiogenesis through the Activation of Extracellular Signal-regulated Kinase. J Biol Chem. 2011;286(25):22035-46.

108. Jung E, Lee N, Kang S-K, Choi S-H, Kim D, Park K, et al. Identification of tissue-specific targeting peptide. J Comput Aided Mol Des. 2012:1-9.

109. Presta LG, Chen H, O'Connor SJ, Chisholm V, Meng YG, Krummen L, et al. Humanization of an anti-vascular endothelial growth factor monoclonal antibody for the therapy of solid tumors and other disorders. Cancer Res. 1997;57(20):4593-9.

110. Holash J, Davis S, Papadopoulos N, Croll SD, Ho L, Russell M, et al. VEGF-Trap: A VEGF blocker with potent antitumor effects. Proc Natl Acad Sci U S A. 2002;99(17):11393-8.

111. O'Farrell AM, Abrams TJ, Yuen HA, Ngai TJ, Louie SG, Yee KWH, et al. SU11248 is a novel FLT3 tyrosine kinase inhibitor with potent activity in vitro and in vivo. Blood. 2003;101(9):3597-605.

112. Langmuir PB, Yver A. Vandetanib for the treatment of thyroid cancer. Clin Pharmacol Ther. 2012;91(1):71-80.

113. Kerbel RS. Tumor Angiogenesis. N Engl J Med. 2008;358(19):2039-49.

114. Cascone T, Herynk MH, Xu L, Du Z, Kadara H, Nilsson MB, et al. Upregulated stromal EGFR and vascular remodeling in mouse xenograft models of angiogenesis inhibitor-resistant human lung adenocarcinoma. J Clin Invest. 2011;121(4):1313-28.

115. Shojaei F, Wu X, Malik AK, Zhong C, Baldwin ME, Schanz S, et al. Tumor refractoriness to anti-VEGF treatment is mediated by CD11b +Gr1+ myeloid cells. Nat Biotechnol. 2007;25(8):911-20.

116. Sánchez-Martín D, Martínez-Torrecuadrada J, Teesalu T, Sugahara KN, Alvarez-Cienfuegos A, Ximénez-Embún P, et al. Proteasome activator complex PA28 identified as an accessible target in prostate cancer by in vivo selection of human antibodies. Proceedings of the National Academy of Sciences. 2013.

117. Bjornsti M-A, Houghton PJ. Lost in translation: Dysregulation of cap-dependent translation and cancer. Cancer Cell. 2004;5(6):519-23.

118. Koumenis C, Naczki C, Koritzinsky M, Rastani S, Diehl A, Sonenberg N, et al. Regulation of Protein Synthesis by Hypoxia via Activation of the Endoplasmic Reticulum Kinase PERK and Phosphorylation of the Translation Initiation Factor eIF2α. Mol Cell Biol. 2002;22(21):7405-16.

119. Carmeliet P, Jain RK. Angiogenesis in cancer and other diseases. Nature. 2000;407(6801):249-57.

120. Haubner R, Beer A, Wang H, Chen X. Positron emission tomography tracers for imaging angiogenesis. Eur J Nucl Med Mol Imaging. 2010;37(1):86-103.

121. Slamon DJ, Leyland-Jones B, Shak S, Fuchs H, Paton V, Bajamonde A, et al. Use of Chemotherapy plus a Monoclonal Antibody against HER2 for Metastatic Breast Cancer That Overexpresses HER2. N Engl J Med. 2001;344(11):783-92.

122. Abe O, Abe R, Enomoto Kt, Kikuchi K, Koyama H, Nomura Y, et al. Tamoxifen for early breast cancer: an overview of the randomised trials. Lancet. 1998;351(9114):1451-67.

123. Borg Å, Baldetorp B, Fernö M, Killander D, Olsson H, Ryden S, et al. ERBB2 amplification is associated with tamoxifen resistance in steroid-receptor positive breast cancer. Cancer Lett. 1994;81(2):137-44.

124. Berns K, Horlings HM, Hennessy BT, Madiredjo M, Hijmans EM, Beelen K, et al. A Functional Genetic Approach Identifies the PI3K Pathway as a Major Determinant of Trastuzumab Resistance in Breast Cancer. Cancer Cell. 2007;12(4):395-402.

125. Doane AS, Danso M, Lal P, Donaton M, Zhang L, Hudis C, et al. An estrogen receptor-negative breast cancer subset characterized by a hormonally regulated transcriptional program and response to androgen. Oncogene. 2006;25(28):3994-4008.

126. Charafe-Jauffret E, Ginestier C, Monville F, Finetti P, Adelaide J, Cervera N, et al. Gene expression profiling of breast cell lines identifies potential new basal markers. Oncogene. 2005;25(15):2273-84.

127. Tang Y, Wang J, Scollard DA, Mondal H, Holloway C, Kahn HJ, et al. Imaging of HER2/neu-positive BT-474 human breast cancer xenografts in athymic mice using< sup> 111</sup> In-trastuzumab (Herceptin) Fab fragments. Nucl Med Biol. 2005;32(1):51-8.

128. van Slooten HJ, Bonsing BA, Hiller AJ, Colbern GT, van Dierendonck JH, Cornelisse CJ, et al. Outgrowth of BT-474 human breast cancer cells in immune-deficient mice: a new in vivo model for hormone-dependent breast cancer. Br J Cancer. 1995;72(1):22-30.

129. Chung YL, Sheu ML, Yang SC, Lin CH, Yen SH. Resistance to tamoxifen-induced apoptosis is associated with direct interaction between Her2/neu and cell membrane estrogen receptor in breast cancer. Int J Cancer. 2002;97(3):306-12.

130. Scott J, Smith G. Searching for peptide ligands with an epitope library. Science. 1990;249(4967):386-90.

131. Larimer B, Thomas W, Smith G, Deutscher S. Affinity Maturation of an ERBB2-Targeted SPECT Imaging Peptide by In Vivo Phage Display. Mol Imaging Biol. 2014:1-10.

132. Rooy I, Cakir-Tascioglu S, Couraud P-O, Romero I, Weksler B, Storm G, et al. Identification of Peptide Ligands for Targeting to the Blood-Brain Barrier. Pharm Res. 2010;27(4):673-82.

133. Matsubara T, Onishi A, Saito T, Shimada A, Inoue H, Taki T, et al. Sialic Acid-Mimic Peptides As Hemagglutinin Inhibitors for Anti-Influenza Therapy. J Med Chem. 2010;53(11):4441-9.

134. Yao Z-J, Kao MC, Chung MC. Epitope identification by polyclonal antibody from phage-displayed random peptide library. J Protein Chem. 1995;14(3):161-6.

135. Binetruy-Tournaire R, Demangel C, Malavaud B, Vassy R, Rouyre S, Kraemer M, et al. Identification of a peptide blocking vascular endothelial growth factor (VEGF)-mediated angiogenesis. EMBO J. 2000;19(7):1525-33.

136. Barr M, Byrne A, Duffy A, Condron C, Devocelle M, Harriott P, et al. A peptide corresponding to the neuropilin-1-binding site on VEGF165 induces apoptosis of neuropilin-1-expressing breast tumour cells. Br J Cancer. 2005;92(2):328-33.

137. Kute T, Lack CM, Willingham M, Bishwokama B, Williams H, Barrett K, et al. Development of Herceptin resistance in breast cancer cells. Cytometry Part A. 2004;57A(2):86-93.

138. Glinka Y, Mohammed N, Subramaniam V, Jothy S, Prud'homme GJ. Neuropilin-1 is expressed by breast cancer stem-like cells and is linked to NF-κB activation and tumor sphere formation. Biochem Biophys Res Commun. 2012;425(4):775-80.

139. Pan Q, Chanthery Y, Liang W-C, Stawicki S, Mak J, Rathore N, et al. Blocking Neuropilin-1 Function Has an Additive Effect with Anti-VEGF to Inhibit Tumor Growth. Cancer Cell. 2007;11(1):53-67.

140. Starzec A, Ladam P, Vassy R, Badache S, Bouchemal N, Navaza A, et al. Structure–function analysis of the antiangiogenic ATWLPPR peptide inhibiting VEGF165 binding to neuropilin-1 and molecular dynamics simulations of the ATWLPPR/neuropilin-1 complex. Peptides. 2007;28(12):2397-402.

141. Perret GY, Starzec A, Hauet N, Vergote J, Le Pecheur M, Vassy R, et al. In vitro evaluation and biodistribution of a 99mTc-labeled anti-VEGF peptide targeting neuropilin-1. Nucl Med Biol. 2004;31(5):575-81.

# VITA

Ben Larimer was born September 26th, 1986, in Normal, Illinois. In May 2005, he graduated from O'Fallon Township High School in O'Fallon, Illinois. He received his Bachelor of Science degree in Biochemistry from the University of Missouri in May 2009. He will complete his Ph.D. in Biochemistry in May 2014 from the University of Missouri.